Numerical Simulation of Exciton Dynamics in Cuprous Oxide at Ultra Low Temperatures

Dissertation
for the degree of
doctor rerum naturalium (Dr. rer. nat.)
submitted to
the
Faculty for the Natural Sciences and for Mathematics
of the Rostock University
Germany

presented by
Sunipa Som
born in Arambagh, India

Rostock 2012

urn:nbn:de:gbv:28-diss2015-0135-2

Reviewers:

1. Reviewer: Prof. Dr. Heinrich Stolz,
   Institute of Physics, University of Rostock.
2. Reviewer: Prof. Dr. Wolf Dietrich Kraeft,
   Institute of Physics, University of Rostock.
3. Reviewer: Prof. Dr. Manfred Bayer,
   Physics Department,TU Dortmund University.

Date of Submission: 25.07.2012

Date of Defense: 29.06.2015

Numerical Simulation of Exciton Dynamics in Cuprous Oxide at Ultra Low Temperatures

Dissertation
zur
Erlangung des akademischen Grades
doctor rerum naturalium (Dr. rer. nat.)
der Mathematischen-Naturwissenschaftlichen Fakultät
der Universität Rostock

vorgelegt von
Sunipa Som
aus Arambagh, India

Rostock 2012

Gutachter:

4. Gutachter: Prof. Dr. Heinrich Stolz,
   Institute of Physics, University of Rostock.
5. Gutachter: Prof. Dr. Wolf Dietrich Kraeft,
   Institute of Physics, University of Rostock.
6. Gutachter: Prof. Dr. Manfred Bayer,
   Physics Department,TU Dortmund University.

Datum der Einreichung: 25.07.2012

Datum der Verteidigung: 29.06.2015

"There is only one good, which is knowledge, and one evil, which is ignorance."

Plato (c. 427 BC - 347 BC)

"In nature's infinite book of secrecy, A little I can read."

William Shakespeare (1605-1606)

Contents

Chapter 1

Introduction and Fundamentals

This chapter contains introduction of our work, overview of this thesis and few fundamental things. We have discussed about the previous works in this field. General properties of exciton, band structure of cuprous oxide (Cu_2O), the optical properties of exciton in Cu_2O and the possibility of Bose-Einstein condensation (BEC) of exciton in Cu_2O are discussed.

1.1 Introduction

This thesis is a theoretical investigation of the relaxation behaviour of excitons in Cu_2O at ultra low temperatures when excitons are confined within a potential trap and also in a homogeneous system. Excitons are in particular interest because in the low density limit they are bosons, and therefore obey Bose-Einstein statistics. The possibility of BEC of excitons in semiconductors was an interesting topic for many years [1,2]. Cuprous oxide is a well known semiconductor as a good host for BEC for excitons [3,4]. Due to special band structure, the exciton in cuprous oxide is a model system for kinetic studies.

In all physical systems, in which BEC has been demonstrated up to now, excitons should be confined in a potential trap. This has the advantage that the diffusion process, which reduce the exciton density is suppressed and the critical number of excitons

$$N_c = \varsigma(3)\left(\frac{k_B T}{\hbar\Omega}\right)^3 \tag{1}$$

with ς the Riemann Zeta function and Ω the average oscillator frequency of the trapping potential , required for the phase transition from exciton gas to BEC decreases much faster with temperature than in free space [5].

Several works have been done in this field [6-23]. But all of these studies have been undertaken for temperature above 1 K. In contrast, in our work we have studied excitons inside the potential trap and for the temperatures in the millikelvin range. Excitons behaviour under various conditions has been analyzed theoretically.

In typical experiment excitons are created with the kinetic energy of the order of meV and then drift down to the potential trap. Now two questions arise: first, how long time excitons take to thermalize and second, when does a BEC occurs.

We have studied theoretically the relaxation behavior of excitons in Cu_2O in the temperature range from 0.05 K to 5 K. It has been done numerically by solving the Boltzmann equation [24] that describes the statistical distribution of particles in a fluid. The Boltzmann equation has been solved by finite difference method and the method of lines [25], using MATLAB. We assumed that the excitons are confined in a stress induced parabolic potential trap with potential energy $V(\vec{r}) = a\vec{r}^2$ with a the steepness

constant and $\vec{r}$ the radius. The relation between steepness constant a and oscillator frequency Ω is $a = \frac{1}{2} M_x \Omega^2$, where M_x is the exciton mass. As relaxation processes, we have included deformation potential phonon scattering, radiative, non-radiative decay, Auger decay and elastic scattering.

First we have included the deformation potential LA phonon-scattering but no other collisions of excitons. We find that the exciton exhibits a quasiequilibrium within the potential trap due to the long lifetime of the order of microseconds. An important point is that excitons can thermalize locally within their lifetime for all cases over 0.5 K but below 0.5 K a non thermal distribution remains. In contrast, globally the excitons don't reach equilibrium with the lattice even at temperatures of 5 K, but show always a higher effective global temperature. When we add radiative, non-radiative and Auger decay, we find that both locally and globally the effective temperature is not coming down to the bath temperature even after long times. If we include elastic and phonon-scattering together, then the local cooling behaviour is same like the local cooling behaviour with the phonon-scattering only. The global effective temperature is not coming down to the bath temperature but coming down more closes towards the bath temperature in comparison with the case of phonon scattering only.

In the first case we find a Bose-Einstein condensation (BEC) occurs for all temperatures in the investigated range. Comparing our results with the thermal equilibrium case, we find that BEC occurs for significantly higher number of excitons in the trap. In the case of Auger decay, we do not find at any temperature a BEC due to the heating of the exciton gas. In the case of elastic and phonon-scattering together, if the excitons number is over the critical number of excitons, then excitons number at zero energy state increasing with a high rate, which is an indication of BEC. In this case BEC occurs for all observed temperatures.

1.2 Overview

The first chapter 'Introduction and fundamentals' contains introduction, previous works in this field and the background information of the work presented in this thesis. General

properties of exciton, band structure of Cu_2O, the optical properties of exciton in Cu_2O and the possibility of BEC of exciton in Cu_2O are discussed.

Chapter 2 is entitled 'Boltzmann Equation with Drift and Force terms'. The first part of this chapter contains the theory of Boltzmann equation with drift and force terms. The next part contains about numerical modeling of the Boltzmann equation with drift and force terms, initial condition, boundary conditions, and results.

Chapter 3 is entitled 'Phonon Scattering'. The first part of this chapter contains the theory of phonon scattering. The second part of this chapter contains about numerical modeling of phonon scattering. The next part contains the results of phonon scattering in the homogeneous system and within the potential trap. The last part is short summary of this chapter.

Chapter 4 is entitled 'Auger Recombination and Radiative and Non Radiative Decay'. The first part of this chapter contains the theory of Auger recombination, radiative and non-radiative Decay. The second part is about previous works on Auger decay and the estimations of the Auger decay rate. The next part contains the results of the Boltzmann equation including phonon scattering, Auger recombination, radiative and non radiative decay. The last part is short summary of this chapter.

Chapter 5 is entitled 'Elastic Scattering'. The first part of this chapter contains the theory of elastic scattering. The second part of this chapter contains about numerical modeling of elastic scattering. The next part contains the results of elastic scattering in homogeneous system and within a potential trap. The last part is short summary of this chapter.

General conclusions of the main results are discussed in chapter 6.

1.3 Previous works in this field

Several groups have been reported the observation of Bose distributions of excitons in Cu_2O when using intense photo excitation [6-16]. The thermodynamics of long-lived paraexcitons confined to a parabolic potential well in Cu_2O was studied in reference [17]. The possibility of BEC of paraexcitons was examined both theoretically and experimentally. They concluded that there are two barriers to achieve BEC of long-lived

paraexcitons in Cu_2O. First one was the limitation of exciton density due to Auger collisions and second one was the rather slow thermalization of excitons in the well.

The Boltzmann kinetics for both of para and ortho excitons in Cuprous oxide specially for a homogeneous gas have been analyzed numerically and within certain approximations analytically in reference [18,19]. In reference [18] the thermalization of the both optically quadrupole-allowed ortho and para excitons has been analyzed for temperatures above and below the critical temperature T_c for a BEC. They concluded that the polariton effect prevents a steady-state BEC of ortho excitons in Cu_2O. For paraexcitons, a slow nonexponential occupation kinetics of the ground-state mode at temperature $T \leq T_c$ prevents the development of a steady state BEC within the optical phonon assisted radiative lifetime. The effects of radiative recombination have been added in reference [19].

The effects of optical-phonon emission, exciton interconversion and Auger decay have been included in reference [20], but it has been assumed that the exciton gas is continuously in internal equilibrium, and followed only the density and temperature of the gas. They concluded that the para excitons condense while the ortho excitons fail to do so. Finally, they remark that their analysis presents no fundamental reason why the ortho excitons cannot condense, however, their multiplicity, their faster Auger decay, and their conversion to para excitons make their condensation much more difficult than for para excitons.

The relaxation of a spatially homogeneous gas of long-lived excitons under the influence of elastic scattering and LA-phonon emission only has been investigated in reference [21]. They reported that at low density a gas of bosons achieves a classical equlibrium distribution of energies within just few characteristic scattering times but at high densities, due to stimulated emission, the rate of scattering increases into low energy states. they concluded that BEC may take place within the particle lifetime, and the exciton-phonon interactions will not significantly increase the rate of approach to condensation.

The relaxation kinetics of excitons in Cu_2O due to scattering by LA-phonons have been showed that the long living excitons in Cu_2O can reach the critical values of a BEC [3,9,10,13,16,21].

The relaxation kinetics of excitons in Cu_2O was studied in reference [22] and [23]. They included all of the known kinetics effects like optical and acoustic phonon emission, Auger decay, elastic scattering and ortho-para-conversion, but not within a potential trap. They concluded that due to the strong Auger decay process it is difficult to get a thermodynamic condensation of excitons in Cu_2O.

Reference [26] studied on quasi-two-dimensional excitons in an in-plane potential trap. The photo luminescence measurements show that the quasi-two-dimensional excitons indeed condense at the bottom of the traps, giving rise to a statistically degenerate Bose gas.

To study about BEC, various systems have been examined in bulk [11, 13, 27] and two-dimensional semiconductors [28, 29] and also in exciton–photon hybrid systems [30–32]. Recently BEC of excitons has been studies experimentally at sub-kelvin temperatures [33]. They demonstrated that it is nevertheless possible to achieve BEC by cooling paraexcitons to sub-kelvin temperatures in a cold phonon bath. Emission spectra from paraexcitons in a three dimensional trap show an anomalous distribution in a threshold-like manner at the critical number of BEC expected for ideal bosons.

In our work we have studied the relaxation kinetics of excitons inside the potential trap and for temperature in the millikelvin range.

1.4 Excitons

The concept of excitons was first proposed by Yakov Frenkel in 1931. He proposed that this excited state would be able to travel in a particle-like fashion through the lattice without the net transfer of charge [34, 35].

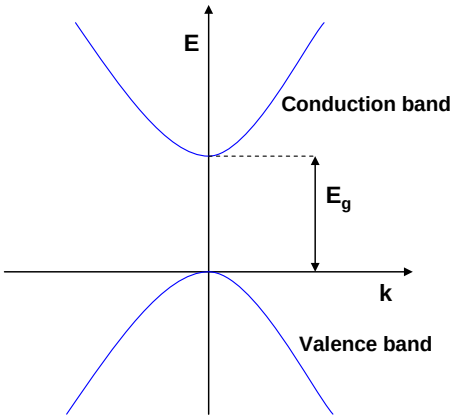

Figure 1.1: Direct band gap semiconductor with band gap energy E_g

The creation of exciton can be described in terms of band theory. A pure semiconductor has no mobile charge carriers at zero temperature. So, all valence bands are completely filled with electrons and all conduction bands are completely empty. In a direct band gap semiconductor, excitons can be created in two ways: (i) by the absorption of a photon with an energy $h\nu$ that is less than the band gap energy *Eg* but sufficient to excite an electron from the valence band to the excitonic bound state, or (ii) by the absorption of a photon with an energy equal to or larger than the band gap energy, which creates a free electron in the conduction band and a free hole in the valence band. This free electron and free hole can bind into exciton. The free electrons then relax in energy usually by the emission of phonons. In a direct band gap semiconductor, the minimum energy needed to create a free electron and a free hole is *Eg*, see Fig. 1.1.

The binding energy of the exciton follows the same type of series as observed in hydrogen, but is modified by the parameter ε, which takes into account the screening effect of the ions in the lattice.

$$E_b = \frac{e^4 \mu_{ex}}{2\hbar^2 \varepsilon^2 n^2} \qquad n = 1, 2, 3..... \tag{2}$$

Where e is the electronic charge, ε is the static dielectric constant and μ_{ex} is the exciton reduced mass. $\varepsilon = 4\pi\varepsilon_0\varepsilon_r$, where $\varepsilon_0 = 8.85419\times10^{-12}$ $A^2s^4kg^{-1}m^{-3}$ is the dielectric constant and ε_r is the dielectric number of the material. $\mu_{ex} = m_e m_h / (m_e + m_h)$, where m_e and m_h are the electron and hole effective mass respectively. Due to spin orbit coupling, the paraexciton has slightly larger binding energy than orthoexciton.

The electron and the hole can be treated as two interacting particles with masses m_e and m_h respectively. The Hamiltonian can be written as [36, 37]:

$$H = -\frac{\hbar^2\nabla_e^2}{2m_e} - \frac{\hbar^2\nabla_h^2}{2m_h} - \frac{e^2}{\varepsilon|r_e - r_h|} + \frac{\hbar^2}{2\mu_{ex}}\cdot\frac{l(l+1)}{r^2} \tag{3}$$

where ε is the lattice dielectric constant, l is the angular momentum quantum number and r_e and r_h are the positions of the electron and the hole, respectively. The corresponding eigen values form a series of exciton energies, given by:

$$E_n = E_g - \frac{\mu_{ex}\left(e^2/\varepsilon\right)^2}{2\hbar^2 n^2} + \frac{\hbar^2k^2}{2M} + \frac{\hbar^2}{2\mu_{ex}}\cdot\frac{l(l+1)}{r^2} \tag{4}$$

Here E_g is the band-gap energy, the second term is the exciton binding energy and the third term is the kinetic energy of exciton of a wave vector k.

Exciton may make themselves visible by emission of photons. The radiative recombination of the electron and hole back to the ground state by emitting a photon with an energy:

$$h\nu = E_g - E_b + E_k \tag{5}$$

The recombination may also takes place together with the emission of phonon with an energy:

$$h\nu = E_g - E_b + E_k \pm E_p \tag{6}$$

where E_k is the exciton kinetic energy and E_p is the energy of the phonon and "+" and "-" corresponds to anti-stokes and stokes processes respectively. Momentum conservation

requires that only two types of processes are possible: $k = k_{photon}$ for direct transitions and $k = k_{photon} + k_{phonon}$ for phonon-assisted transitions.

There are two types of excitons, Frenkel exciton and Wannier-Mott exciton (see figure 1.2). The radius of the excitonic entity (half of the distance between the electron and hole) is given by

$$a_B = a_0 \frac{m_e}{\mu_{ex}} \varepsilon$$

$$\text{or, } a_B = \frac{\hbar^2}{\mu_{ex}\left(\frac{e^2}{\varepsilon}\right)} \tag{7}$$

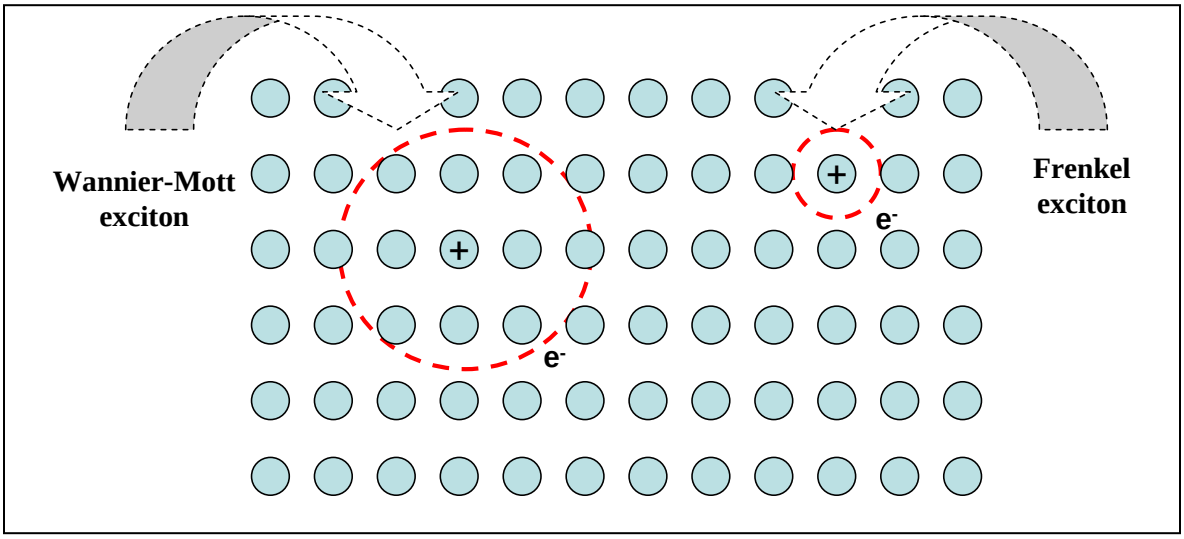

Figure 1.2: A schematic diagram of Frenkel exciton and Wannier-Mott exciton, not to scale.

Where a_0 is the Bohr radius and m_e is the electron rest mass. When a_B is large (a_B >lattice constant) then excitons are weakly bound. So the attraction between the electron and hole is small in comparison with E_g. These excitos are called Wannier-Mott exciton. When a_B is smaller or on the order of the lattice constant, excitons are strongly bound are called Frenkel exciton. Wannier-Mott excitons are mainly found in

semiconductors like in gallium arsenide (GaAs), zinc selenide (ZnSe), copper chloride (CuCl) and cuprous oxide (Cu_2O). In this thesis the exciton radius is much larger than the inter atomic distance, therefore it is a Wannier-Mott exciton.

1.5 Cuprous Oxide

Copper(I) oxide or cuprous oxide is one of the principal oxides of copper with the formula Cu_2O. Copper(I) oxide may be produced by several methods. Most straightforwardly, it arises via the oxidation of copper metal:

$4\ Cu + O_2 \rightarrow 2\ Cu_2O$

(8)

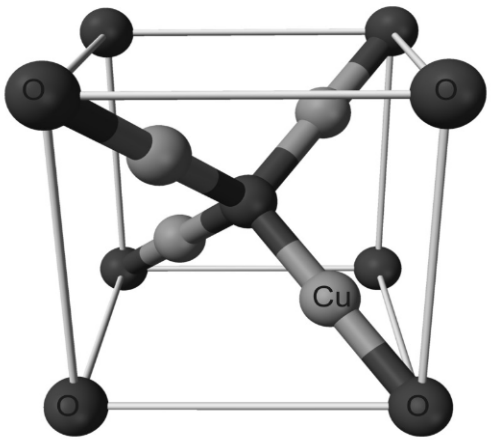

Figure 1.3: Crystal structure of Cu_2O. Light grey balls represent copper and dark grey balls represent oxygen.

The crystal structure of Cu2O (see figure 1.3) can be described by two interpenetrating BCC (O atom in the center) and FCC (Cu atom in the center) sublattices. The Bravais lattice is a simple cubic with a lattice constant 4.27 Å. The unit cell contains 4 Cu atoms and 2 O atoms.

The copper ion's electronic structure [38] ends with $3d^{10}4s^0$, where the 4s levels has slightly higher energy than 3d levels. The Cu 3d levels form the valence band and Cu 4s

levels form the conduction band in Cu_2O. The lowest state in the conduction band ${}^2\Gamma_6^+$ and highest state in the valence band ${}^2\Gamma_7^+$ are at the center of the Brillouin zone, means both state has the full periodicity of the lattice. So, Cu_2O has direct band gap. Both states have a positive parity at zone center, causing a dipole-forbidden gap of *Eg*=2.173 eV. The second highest valence ${}^4\Gamma_8^+$ band lies 131 meV lower than highest valence band ${}^2\Gamma_7^+$ due to spin-orbit interaction.

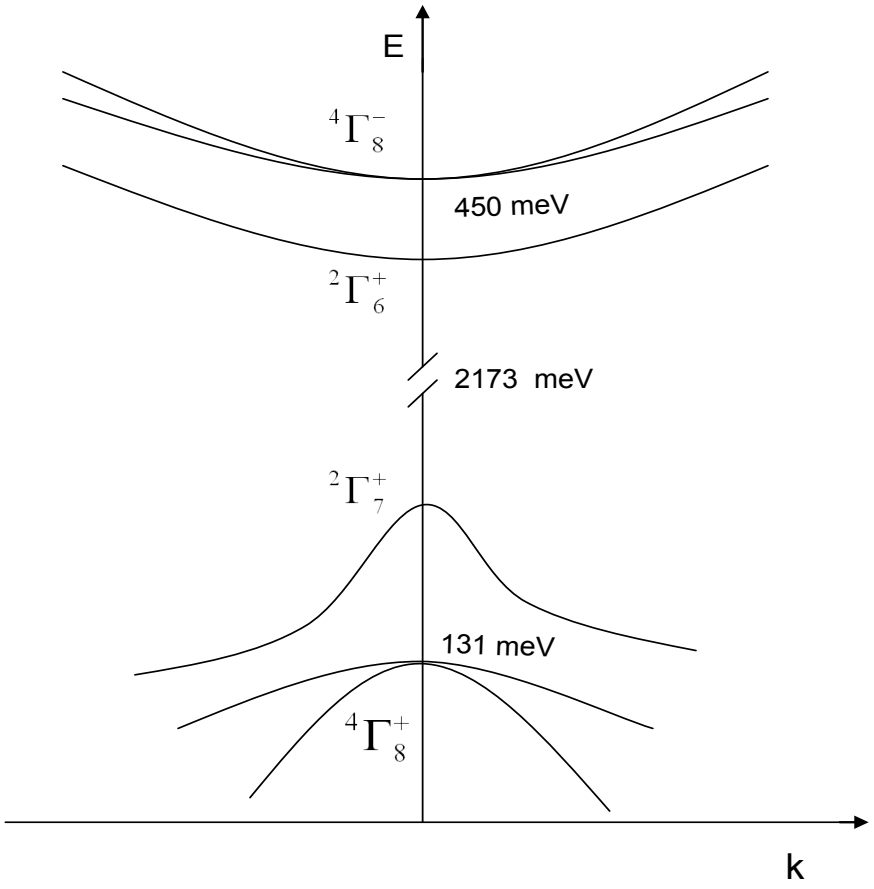

Figure 1.4: Band structure of Cu_2O near the zone center.

The second lowest conduction band ${}^4\Gamma_8^-$ lies 450 meV above the lowest conduction band ${}^2\Gamma_6^+$ which serves as intermediate state for the optical phonon-assisted radiative recombination and non-radiative Auger recombination processes. Cu_2O has all ten valence bands and four conduction bands. Figure (1.4) shows band structure of Cu_2O considering only two conduction bands and two valence bands which forms the visible exciton series.

1.6 Exciton in Cuprous Oxide

Cuprous oxide is a favorite semiconductor among many physicist because all classes of transition predicted by theory of exciton spectra are observed in different part of energy region of Cu_2O. The exciton in cuprous oxide is a model system for kinetic studies due to its special band structure.

The yellow exciton series is formed from the ${}^2\Gamma_6^+$ conduction band and ${}^2\Gamma_7^+$ valence band, (see figure 1.4) green exciton series formed from the ${}^2\Gamma_6^+$ conduction band and ${}^4\Gamma_8^+$ valence band, blue exciton series formed from the ${}^4\Gamma_8^-$ conduction band and ${}^2\Gamma_7^+$ valence band and indigo series formed from the ${}^4\Gamma_8^-$ conduction band and ${}^4\Gamma_8^+$ valence band. The ground excitonic state, formed from the ${}^2\Gamma_6^+$ conduction band and ${}^2\Gamma_7^+$ valence band, is split into J=0 the singlet paraexciton (${}^1\Gamma_2^+$) band and J=1 the triplet orthoexciton (${}^3\Gamma_{25}^+$) band. Paraexciton lies 12 meV lower than orthoexciton.

Since both valence and conduction bands have a positive parity, the total parity is determined by the parity of the exciton level. For an excitonic s-state, the parity is positive, and the transition to the ground state is dipole forbidden, but quadrupole allowed. For a p-state, the parity is negative, and the transition to the ground state is dipole allowed.

Ortho and paraexciton are not simple product forms of the pure electron $\left(\left|\uparrow e\right\rangle,\left|\downarrow e\right\rangle\right)$ and hole spin states $\left(\left|\uparrow h\right\rangle,\left|\downarrow h\right\rangle\right)$. Spin orbit coupling causes complicated hole states. Wannier functions for yellow excitons in Cu_2O [39, 40] are φ_s^c for the

conduction band and φ_{xy}^{v}, φ_{yz}^{v} and φ_{zx}^{v} for the valence band. The ${}^{2}\Gamma_{7}^{+}$ hole states $\left(\left|\uparrow H\right\rangle,\left|\downarrow H\right\rangle\right)$ are linear combination of $\left|\uparrow h\right\rangle$ and $\left|\downarrow h\right\rangle$:

$$\left|\uparrow H\right\rangle = -\frac{i}{\sqrt{3}}[(\varphi_{yz}^{v} + i\varphi_{zx}^{v})\left|\downarrow h\right\rangle + \varphi_{xy}^{v}\left|\uparrow h\right\rangle] \tag{9}$$

$$\left|\downarrow H\right\rangle = -\frac{i}{\sqrt{3}}[(\varphi_{yz}^{v} - i\varphi_{zx}^{v})\left|\uparrow h\right\rangle - \varphi_{xy}^{v}\left|\downarrow h\right\rangle] \tag{10}$$

The singlet paraexciton and the triplet orthoexciton states can be written as follows:

$$\left|S\right\rangle = \frac{1}{\sqrt{2}}\left(\left|\uparrow e\downarrow h\right\rangle - \left|\downarrow e\uparrow h\right\rangle\right) \tag{11}$$

$$\left|T_{+1}\right\rangle = \left|\uparrow e\uparrow h\right\rangle \tag{12}$$

$$\left|T_{0}\right\rangle = \frac{1}{\sqrt{2}}\left(\left|\uparrow e\downarrow h\right\rangle + \left|\downarrow e\uparrow h\right\rangle\right) \tag{13}$$

$$\left|T_{-1}\right\rangle = \left|\downarrow e\downarrow h\right\rangle \tag{14}$$

If we say

$\left|T_{X}\right\rangle = \frac{1}{\sqrt{2}}(\left|T_{-1}\right\rangle - \left|T_{+1}\right\rangle)$ and $\left|T_{Y}\right\rangle = \frac{1}{\sqrt{2}}(\left|T_{-1}\right\rangle + \left|T_{+1}\right\rangle)$ then we can write one paraexciton state and three orthoexciton states in the following way

$$\left|P\right\rangle = \frac{i}{\sqrt{3}}\varphi_{s}^{c}(\left|T_{X}\right\rangle\varphi_{yz}^{v} + i\left|T_{Y}\right\rangle\varphi_{zx}^{v} + \left|T_{0}\right\rangle\varphi_{xy}^{v}) \tag{15}$$

$$\left|O_{xy}\right\rangle = \frac{-1}{\sqrt{3}}\varphi_{s}^{c}(\left|T_{Y}\right\rangle\varphi_{yz}^{v} + i\left|T_{X}\right\rangle\varphi_{zx}^{v} - \left|S\right\rangle\varphi_{xy}^{v}) \tag{16}$$

$$\left|O_{yz}\right\rangle = \frac{1}{\sqrt{3}}\varphi_{s}^{c}(\left|S\right\rangle\varphi_{yz}^{v} + i\left|T_{0}\right\rangle\varphi_{zx}^{v} - \left|T_{Y}\right\rangle\varphi_{xy}^{v}) \tag{17}$$

$$\left|O_{zx}\right\rangle = \frac{-i}{\sqrt{3}}\varphi_{s}^{c}(\left|T_{0}\right\rangle\varphi_{yz}^{v} + i\left|S\right\rangle\varphi_{zx}^{v} - \left|T_{X}\right\rangle\varphi_{xy}^{v}) \tag{18}$$

1.7 Possibility of the Bose-Einstein condensation

Bose-Einstein condensation (BEC) is a macroscopic occupation of the lowest energy state, at zero energy. When a liquid or gas of bosons cooled below critical temperature

$T_{c,}$ then a Bose-Einstein condensate forms. It was first predicted by Bose and Einstein theoretically in 1924 [41, 42, 43] and it was first observed in 1995 in a remarkable series of experiments on vapors of rubidium [44] and sodium [45] in which the atoms were confined in magnetic traps and cooled down to extremely low temperatures, of the order of fractions of microkelvins.

The possibility of Bose-Einstein condensation (BEC) of excitons in semiconductors was an interesting topic for many years [1, 2]. The exciton, being composed of two fermions, namely an electron and an hole, is the basic electronic excited state of an intrinsic semiconductor. Its low effective mass is a favorable factor for the occurrence of BEC at moderate particle densities.

Cuprous oxide is a well known semiconductor as a good host for Bose-Einstein condensation for excitons [3, 4]. Due to special band structure, the exciton in cuprous oxide is a model system for kinetic studies. The excitons in Cuprous oxide showed transient kinetic energy distributions which matched those expected for a Bose gas near the critical density for Bose-Einstein condensation. The high binding energy (150 meV) of excitons in Cu_2O corresponds to a small Bohr radius of 7 $\mathring{A}$.

At low densities ($na_B^D << 1$, where a_B is the exciton Bohr radius, n the density and D the dimensionality) excitons are hydrogen like Bose particles. Because the exciton mass is small even smaller than the free electron mass, then exciton BEC is expected to occure at relatively high temperatures, about 1 K.

For a gas of bosons of mass m and concentration n_{3D}, the phase transition to a Bose-Einstein condensed phase occurs when their thermal de-Broglie wavelength becomes comparable to their inter-particle distance [46-48]. For example, BEC takes place when $n_{3D}\lambda_{dB}^3 = 2.612$ in 3D systems, where λ_{dB} is the de Broglie wavelength and is given by $\lambda_{dB} = \sqrt{2\pi\hbar^2/(mk_BT)}$. This is of the order of $n_{3D} \sim 10^{17} cm^{-3}$ for $T_c \sim 1\,\mathrm{K}$ and m of the order of the electron mass e.g. excitons in bulk Cu_2O.

The exciton, is a Boson because it is a composition of two fermions, is an integral spin particle. The probability of boson of being scattered into state of wave-vector $\vec{k}$ is proportional to $1+ f_{\vec{k}}$ according to the quantum statistical rules for boson where $f_{\vec{k}}$ is the

occupation number of the state. Assuming that the system is in thermal equilibrium at a temperature T and chemical potential μ, then the total number of particles in a box N is equal to the sum of the occupation numbers [49, 50]

$$N = \sum_{\vec{k}} f_{\vec{k}} = \sum_{E=0}^{\infty} N_E \tag{19}$$

where $E = \frac{\hbar^2 k^2}{2M_x}$ is the kinetic energy of an exciton. Occupation number is given by the Bose- Einstein distribution function,

$$f_{\vec{k}} = N_E = \frac{1}{e^{(E-\mu)/k_B T} - 1} \tag{20}$$

The total number of particles can be replaced by an integral

$$N = \int_0^{\infty} D_E \cdot N_E \cdot dE \tag{21}$$

where D_E is the density of states, $D_E = CE^{1/2}$. If the exciton number *N* occupy a volume *V*, then we can write C as

$$C = \frac{gV}{4\pi^2}\left(\frac{2M_x}{\hbar}\right)^{3/2} \tag{22}$$

where g is the spin degeneracy. In terms of the gas density, $n=N/V$, we can finally write

$$n = \frac{g}{4\pi^2}\left(\frac{2M_x}{\hbar}\right)^{3/2} \int_0^{\infty} \frac{E^{1/2}}{e^{E-\mu/k_B T} - 1} dE \tag{23}$$

In this case, the integral is finite and approaches a finite value as μ approaches zero. This implies a critical concentration above which no more particles can be added to the excited states, so that any additional particles must then go into the zero energy state; this is Bose-Einstein condensation.

To study on BEC various systems have been examined in bulk [11, 13, 27] and two-dimensional semiconductors [28, 29] and also in exciton–photon hybrid systems [30–32]. Recently BEC of excitons has been studies at sub-kelvin temperatures [33]. Among them, the 1s paraexciton state in a single crystal of Cu_2O has been a prime candidate for BEC. Due to the long life time [6, 51] and the large binding energy it is possible to prepare the cold excitons in thermal equlibrium with the lattice. The 1s paraexciton is a pure spin

triplet state, so it is decoupled from the radiation field. Paraexcitons are light quasi-particles with effective mass $M_x = 2.6m_e$ (m_e is the electron rest mass) [52], therefore BEC has been believed to be attainable at moderate density $n \sim 10^{17} cm^{-3}$ at the temperature of superfluid helium 2 K [11, 13, 27]. In this thesis we work on excitons which are actually paraexcitons.

References

[1] Blatt J M, Boer K W, and Brandt W, 1962, *Phys. Rev.* **126**, 1691-1692, "Bose–Einstein condensation of excitons".

[2] Moskalenko S A, 1962, *Fiz. Tverd. Tela (Sov. Phys. Solid State)* **4**, 276.

[3] Griffin A, Snoke D W, and Stringari S, 1995, "Bose-Einstein Condensation" (Cambridge: Cambridge University Press) Chaps. 13 and 14.

[4] Snoke D W, 2002, *Science* **298**, 1368-1372, "Spontaneous Bose Coherence of Excitons and Polaritons".

[5] Pethick C J and Smith H, 2002, "Bose-Einstein Condensation in Dilute Gases" (Cambridge, UK: Cambridge University Press).

[6] Mysyrowicz A, Hulin D, and Antonetti A, 1979, *Phys. Rev. Lett.* **43**, 1123-1126, "Long Exciton Lifetime in Cu_2O".

[7] O'Hara K E, Gullingsrud J R, and Wolfe J P, 1999, *Phys. Rev. B* **60**, 10872-10885, "Auger decay of excitons in Cu_2O".

[8] Beg M M and Shapiro S M, 1976, *Phys. Rev. B* **13**, 1728-1734, "Study of phonon dispersion relations in cuprous oxide by inelastic neutron scattering".

[9] Hulin D, Mysyrowicz A, and Benoit a´ la Guillaume C., 1980, *Phys.Rev. Lett.* **45**, 1970-1973, "Evidence for Bose-Einstein Statistics in an Exciton Gas".

[10] Snoke D W, Wolfe J P, and Mysyrowicz A, 1987, *Phys. Rev. Lett.* **59**, 827-830, "Quantum saturation of a Bose gas: Excitons in Cu_2O".

[11] Snoke D W, Wolfe J P, and Mysyrowicz A, 1990, *Phys. Rev. B* **41**, 11171-11184, " Evidence for Bose-Einstein condensation of excitons in Cu_2O".

[12] Snoke D W and Wolfe J P, 1990, *Phys. Rev. B* **42**, 7876-7884, "Picosecond dynamics of degenerate orthoexcitons in Cu_2O".

[13] Lin J L and Wolfe J P, 1993, *Phys. Rev. Lett.* **71**, 1222-1225, "Bose-Einstein condensation of paraexcitons in stressed Cu_2O".

[14] Naka N, Kono S, Hasuo M., and Nagasawa N, 1996, *Prog. Cryst. Growth Charact. Mater.* **33**, 89-92.

[15] Goto T, Shen M Y, Koyama S, and Yokuochi T, 1997, *Phys. Rev. B* **55**, 7609-7614, "Bose-Einstein statistics of orthoexcitons generated by two-photon resonant absorption in cuprous oxide".

- - Goto T, Shen M Y, Koyama S, and Yokuochi T, 1997, *Phys. Rev. B* **56**, 4284-4284, "Erratum: Theory of arbitrarily polarized quantum Hall states: Filling fractions and wave functions".

[16] Shen M Y, Yokouchi T, Koyama S, and Goto T, 1997, *Phys. Rev. B* **56**, 13 066-072, "Dynamics associated with Bose-Einstein statistics of orthoexcitons generated by resonant excitations in cuprous oxide".

[17] Trauernicht D P, Wolfe J P, and Mysyrowicz A, 1986, *Phys. Rev. B* **34**, 2561-2575, "Thermodynamics of strain-confined paraexcitons in Cu_2O".

[18] Ell C, Ivanov A L, and Haug H, 1998, *Phys. Rev. B* **57**, 9663-73, "Relaxation kinetics of a low-density exciton gas in Cu_2O".

[19] Ivanov A L, Ell C, and Haug H, 1997, *Phys. Rev. E* **55**, 6363-6369, "Phonon-assisted Boltzmann kinetics of a Bose gas: Generic solution for $T \leq T_c$ ".

- - Ivanov A L, Ell C, and Haug H, 1998, *Phys. Status Solidi B* **206**, 235-247, "Phonon-assisted Relaxation Kinetics of a Degenerate Bose gas".

[20] Kavoulakis G M, Baym G, and Wolfe J P, 1996, *Phys. Rev. B* **53**, 7227-7243, "Quantum saturation and condensation of excitons in Cu2O: A theoretical study".

[21] Snoke D W and Wolfe J P, 1989, *Phys. Rev. B* **39**, 4030-4037, "Population dynamics of a Bose gas near saturation".

[22] O'Hara K E and Wolfe J P, 2000, *Phys. Rev. B* **62**, 12 909-921, "Relaxation kinetics of excitons in cuprous oxide".

[23] O'Hara K E, 1999, "Relaxation Kinetics of Excitons in Cuprous Oxide", Ph.D. Thesis (University of Illinois, Urbana, Illinois, USA).

[24] Ashcroft N W and Mermin N D, 1976, "Solid State Physics" (Fortworth: Harcourt Brace).

[25] William E. Schiesser and Graham W. Griffiths, 2009, "A Compendium of Partial Differential Equation Models" (Cambridge University Press).

[26] Butov L V, Lai C W, Ivanov A L, Gossard A C, and Chemla D S, 2002, *Nature* **417**, 47-51, "Towards Bose–Einstein condensation of excitons in potential traps".

[27] Naka N and Nagasawa N, 2005, *J. Lumin.* **112**, 11–16, "Bosonic stimulation of cold excitons in a harmonic potential trap in Cu_2O".

[28] Butov L V, Gossard A C, and Chemla D S, 2002, *Nature* **418**, 751–754, "Macroscopically ordered state in an exciton system".

[29] Snoke D, Denev S, Liu Y, Pfeiffer L, and West K, 2002, *Nature* **418**, 754–757, "Long-range transport in excitonic dark states in coupled quantum wells".

[30] Deng H, Weihs G, Santori C, Bloch J, and Yamamoto Y, 2002, Science 298, 199–202, "Condensation of semiconductor microcavity exciton polaritons".

[31] Kasprzak J et al., 2006, Nature 443, 409–414, "Bose-Einstein condensation of exciton polaritons".

[32] Balili R, Hartwell V, Snoke D, Pfeiffer L, and West K, 2007, *Science* **316**, 1007–1010, "Bose-Einstein condensation of microcavity polaritons in a trap".

[33] Yoshioka K, Chae E, and Kuwata-Gonokami M, 2011, *Nature Communications*, **2**, 328, "Transition to a Bose-Einstein condensate and relaxation explosion of excitons at sub-Kelvin temperatures".

[34] Frenkel J, 1931, Phys. Rev. 37, 1276, "On the Transformation of light into Heat in Solids. I".

[35] Frenkel J, 1936, *Soviet Experimental and Theoretical Physics*, **6**, 647.

[36] Karpinska K et al., 2005, *J. of Luminescence*, **112**, 17-20, "Para-excitons in Cu_2O a new approach".

[37] Libo R L, 2003, "Introductory quantum mechanics" (Addison Wesley).

[38] French M, Schwartz R, Stolz H, and Redmer R, 2009, J. Phys. Cond. Matter **21**, 015502, "Electronic band structure of Cu_2O by spin density functional theory".

[39] Kavoulakis G M, Chang Y C, and Baym G, 1997, *Phys. Rev. B* **55**, 7593, "Fine structure of excitons in Cu_2O".

[40] Dasbach G, Frohlich D, Klieber R, Suter D, Bayer M, and Stolz H, 2004, *Phys. Rev. B* **70**, 045206, " Wave-vector-dependent exchange interaction and its relevance for the effective exciton mass in Cu_2O".

[41] Bose S, 1924, *Z. phys*. **26**, 178, "Plancks Gesetz und Lichtquantenhypothese".

[42] Einstein, A, 1924, *Sitzber. Kgl. Preuss. Akad. Wiss.*, **261**.

[43] Einstein, A, 1925, *Sitzber. Kgl. Preuss. Akad. Wiss.*, **3**.

[44] Anderson M H, Ensher J R, Matthews M R, Wieman C E, and Cornell E A, 1995, *Science* **269**, 198, "Observation of Bose-Einstein Condensation in a Dilute Atomic Vapor".

[45] Davis, K. B., M.-O. Mewes, M. R. Andrews, N. J. van Druten, D. S. Durfee, D. M. Kurn, and W. Ketterle, 1995, *Phys. Rev. Lett*. **75**, 3969.

[46] Ketterle W, 2002, *Rev. Mod. Phys*., **74**, 1131, Nobel lecture: "When atoms behave as waves: Bose-Einstein condensation and the atom laser".

[47] Cornell E A and Wieman C E, 2002, *Rev. Mod. Phys*., **74**, 875, Nobel Lecture: "Bose-Einstein condensation in a dilute gas, the first 70 years and some recent experiments".

[48] Kavoulakis G M, 2003, *J. Low Temp. Phys*., **132**, 297, "Bose-Einstein condensation of indirect excitons in coupled quantum wells".

[49] Kim J C and Wolfe J P, 1998, *Phys. Rev. B*, **57**, 9861, "Bose-Einstein statistics of an excitonic gas in two dimensions: Excitons and biexcitons in a GaAs quantum well".

[50] Swarup A and Cowan B, 2004, *J. Low Temp. Phys*., **134**, 881, "Fermi-Bose correspondence and Bose-Einstein con-densation in the two-dimensional ideal gas".

[51] Yoshioka K, Ideguchi T, Mysyrowicz A, and Kuwata-Gonokami M, 2010, *Phys. Rev. B* **82**, 041201(R), "Quantum inelastic collisions between paraexcitons in Cu_2O".

[52] Brandt J, Fröhlich D, Sandfort C, Bayer M, Stolz H, and Naka N, 2007, *Phys. Rev. Lett*. **99**, 217403, "Ultranarrow optical absorption and two-phonon excitation spectroscopy of Cu_2O paraexcitons in a high magnetic field".

Chapter 2

Boltzmann Equation with Drift and Force Terms

The Boltzmann equation [1], also often known as the Boltzmann transport equation, devised by Ludwig Boltzmann, describes the statistical distribution of particles in a fluid. First we discretize the Boltzmann equation by finite difference method and then by method of lines [2] we solve it numerically by using MATLAB. The Boltzmann equation contains the drift, force, collision and interaction terms. In this chapter the Boltzmann equation with Drift and force terms, initial condition and boundary conditions, which we have used in our numerical simulation are discussed. We will discuss about the collision and interaction terms in the next few chapters.

2.1 Boltzmann equation

The Boltzmann equation describes the particle's occupation number $N(\vec{r},\vec{k},t)$ as a function of radius $\vec{r}$, momentum $\hbar\vec{k}$ and time t. The Boltzmann equation is

$$\frac{\partial N}{\partial t}+\vec{v}\cdot\overrightarrow{\nabla_r}N+\vec{F}\cdot\frac{1}{\hbar}\overrightarrow{\nabla_k}N=\left(\frac{\partial N}{\partial t}\right)_{\text{collision+interaction}} \tag{1}$$

with $\vec{v}$ is the velocity, $\vec{F}$ is the force and ∇_r and ∇_k are the nabla operator in r and k space respectively. The terms on the left hand side are often referred to as the drift terms, and the term on the right hand side as collision and interaction term. Collision and interaction terms are phonon scattering, Auger decay, radiative and non-radiative decay and elastic scattering. For starting the calculation, we have created the excitons that are actually paraexcitons, which after phonon scattering, Auger decay, radiative and non-radiative decay and elastic scattering excitons cool down to the bottom of the trap.

2.2 Drift and force terms of the Boltzmann equation

Drift and force terms of the Boltzmann equation (1) is are given by

$$\left(\frac{\partial N}{\partial t}\right)_{Drift\ \&\ force}=-\vec{v}\cdot\vec{\nabla}_r N-\vec{F}\cdot\frac{1}{\hbar}\cdot\vec{\nabla}_k N \tag{2}$$

where N is the exciton occupation number, t is the time, $\vec{v}$ is the velocity and $\vec{F}$ is the force. As we know, $\vec{P}=\hbar\vec{k}=M_x\vec{v}$ so, $\vec{v}=\frac{\hbar}{M_x}\vec{k}$

And $\vec{F}=-\vec{\nabla}V(\vec{r})$, Where $V(\vec{r})=a\vec{r}^{\,2}$ So, $\vec{F}=-2a\vec{r}$, a is the steepness constant. Using the potential $V(\vec{r})$ in the force term we have created a potential trap (see figure 2.1).

By putting values of $\vec{v}$ and $\vec{F}$ in equation (2), we get

$$\left(\frac{\partial N}{\partial t}\right)_{Drift\ \&\ force}=-\frac{\hbar k}{M_x}\cdot\frac{\partial N}{\partial r}-\frac{-2ar}{\hbar}\cdot\frac{\partial N}{\partial k} \tag{3}$$

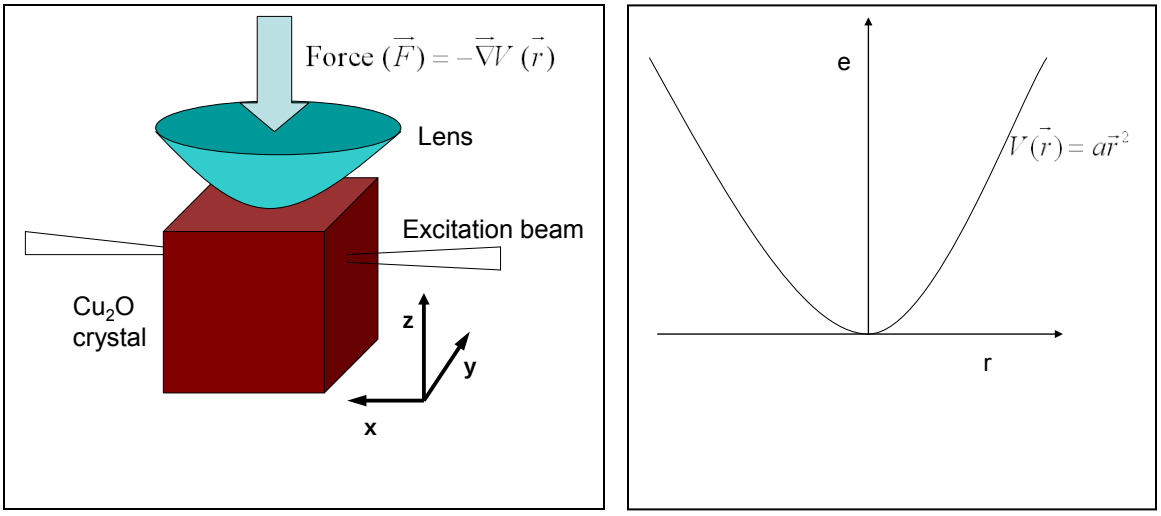

Figure 2.1: In the left hand side, potential trap is formed by potential $V(\vec{r})$ in the force term in the numerical simulation. Generally in experiment it has been formed by pressing the crystal by glass lens. In the right hand side, the potential trap which we have used in our numerical simulation.

2.3 Numerical modeling

First we discretize the Boltzmann equation by finite difference method and then by method of lines we solve it numerically by using MATLAB [2-4]. By using finite difference method, we can write

$$\frac{\Delta N}{\Delta r} = \frac{N_i - N_{i-1}}{\Delta r} \text{ Where } r = r_0 .....r_i \text{ and } r_i = i\Delta r$$

$$\frac{\Delta N}{\Delta k} = \frac{N_{j+1} - N_j}{\Delta k_j} \text{ Where } k = k_0 .....k_j \text{ and } k_j = j\Delta k_j \text{, with } \Delta k_j = \frac{\Delta e\sqrt{M_x}}{\hbar\sqrt{2e_j}}.$$

So, equation (3) can be written as

$$\left(\frac{\partial N}{\partial t}\right)_{Drift\ \&\ force} = -\frac{\hbar k}{M_x \Delta r}\{N(i,j) - N(i-1,j)\} + \frac{2ar}{\hbar\Delta k}\{N(i,j+1) - N(i,j)\} \quad (4)$$

But, we know $e = \frac{\hbar^2 k^2}{2M_x}$, $e = \frac{e_0 j}{M}$, $\Delta e = \frac{e_0}{M}$ and $e_0 = 2M_x v_s^2$

So, $\frac{\hbar k}{M_x} = \frac{2v_s}{\sqrt{M}}\sqrt{j}$ (5)

Now, $\Delta k = \frac{dk}{de}\Delta e = \frac{\Delta e}{\hbar\sqrt{\frac{2e}{M_x}}}$

So, $\frac{2ar}{\hbar\Delta k} = \frac{2a\Delta r.i\hbar\sqrt{\frac{2e}{M_x}}}{\hbar\Delta e} = \frac{2a\Delta r\sqrt{M}}{M_x v_s} i\sqrt{j}$ (6)

But with $\Delta e = \frac{e_0}{M}$, we can write

$$\left(\frac{\partial N}{\partial t}\right)_{Drift\ \&\ force} = -\frac{2v_s}{\sqrt{M}\Delta r}\sqrt{j}\{N(i,j) - N(i-1,j)\}$$

$$+\frac{2a\Delta r\sqrt{M}}{M_x v_s} i\sqrt{j}\{N(i,j+1) - N(i,j)\} \quad (7)$$

2.4 Initial condition

We have used laser excitement which is representative for actual experimental studies [5]. Here the laser beam at energy e_L crosses the trap centrally and leads to exciton creation at $e = e_L - a\vec{r}^2$. If σ is the spectral width, then the initial exciton occupation number distribution can be formulated as

$$N_0(\vec{r}, e) = n_0 \exp\left(\frac{-\left(e - \left(e_L - a\vec{r}^2\right)\right)^2}{2\sigma^2}\right)\Theta\left(\vec{r}_{\max} - \vec{r}\right)\Theta\left(\vec{r}\right) \quad (8)$$

where $r_{\max} = \sqrt{\frac{2e_L}{a}}$.

From these two step function, we get two conditions

First, from $\Theta\left(\vec{r}\right)$ we get $\vec{r} \geq 0$ and

Second, from $\Theta(\vec{r}_{\max} - \vec{r})$ we get $\vec{r}_{\max} - \vec{r} \geq 0$ or $\vec{r} \leq \vec{r}_{\max}$

So, we can write

$$N_0(i, j) = n_0 \exp\left(\frac{-\left(j - \left(j_0 - a(r(i))^2 \right) \right)^2}{2\sigma_1^2} \right) \text{Where } \vec{r}_{\max} \geq \vec{r} \geq 0 \qquad (9)$$

Here $\sigma_1 = \dfrac{\sigma M}{e_0}$

Initial distribution is like figure 2.2.

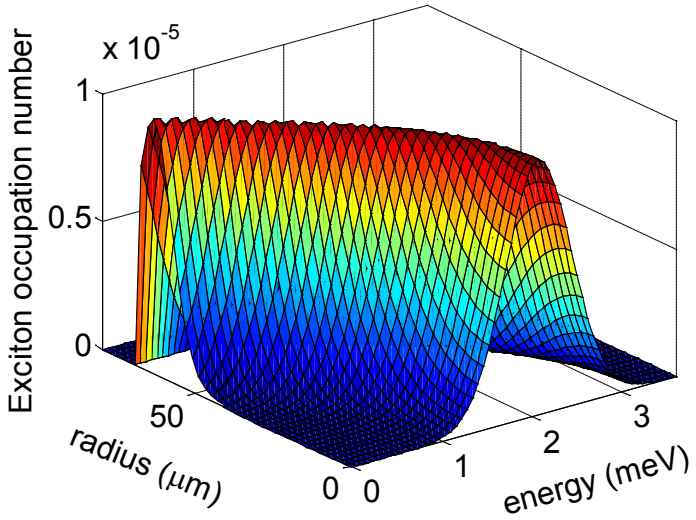

Figure 2.2: Initial distribution where excitons number within the trap is 4×10^6. The parameters, which we have used, are $\sigma = 0.36$ meV and $e_L = 2.1$ meV.

2.5 Boundary conditions

The boundary conditions are derived from the fact that no exciton flows takes place outside the trap. Therefore

(1) The derivative of exciton occupation number with respect to radius

(i) $\frac{\partial N}{\partial r} = 0$ at $r < 0$, for all values of e.

(ii) $\frac{\partial N}{\partial r} = 0$ at $r > r_{max}$, for all values of e.

(iii) $\frac{\partial N}{\partial r} = 0$ at $e > e_{max}$, for all values of r.

(2) The derivative of exciton occupation number with respect to energy

(i) $\frac{\partial N}{\partial e} = 0$ at $e < 0$, for all values of r.

(ii) $\frac{\partial N}{\partial e} = 0$ at $e > e_{max}$, for all values of r.

(iii) $\frac{\partial N}{\partial e} = 0$ at $r > r_{max}$, for all values of e.

In our case the maximum radius $r_{max} = 200$ μm and the maximum energy $e_{max} = 6$ meV .

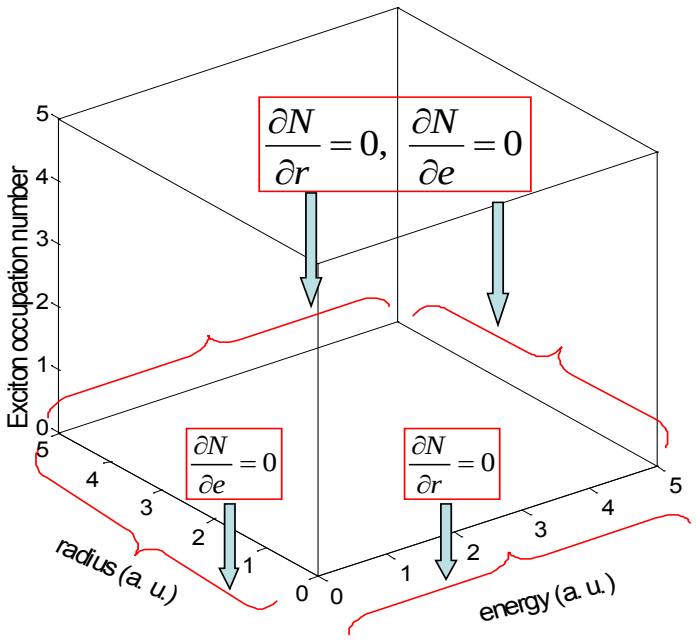

Figure 2.3: Boundary conditions which we have used in our numerical simulation.

2.6 Results

After solving the equation (7) we are getting exciton occupation number $N(\vec{r},e,t)$ as a function of energy *e*, radius $\vec{r}$ and time t (see figure 2.4). Figure 2.4 represents exciton distribution after solving Boltzmann equation without source term, at 5 ns. After 5 ns, the distribution is stable like figure 2.4.

We have calculated total number of exciton by the equation

$$N_{total} = \frac{1}{(2\pi)^3} \iint 4\pi \vec{r}^{\,2} dr \cdot 4\pi \vec{k}^{\,2} dk \cdot N(\vec{r},\vec{k}) \qquad (10)$$

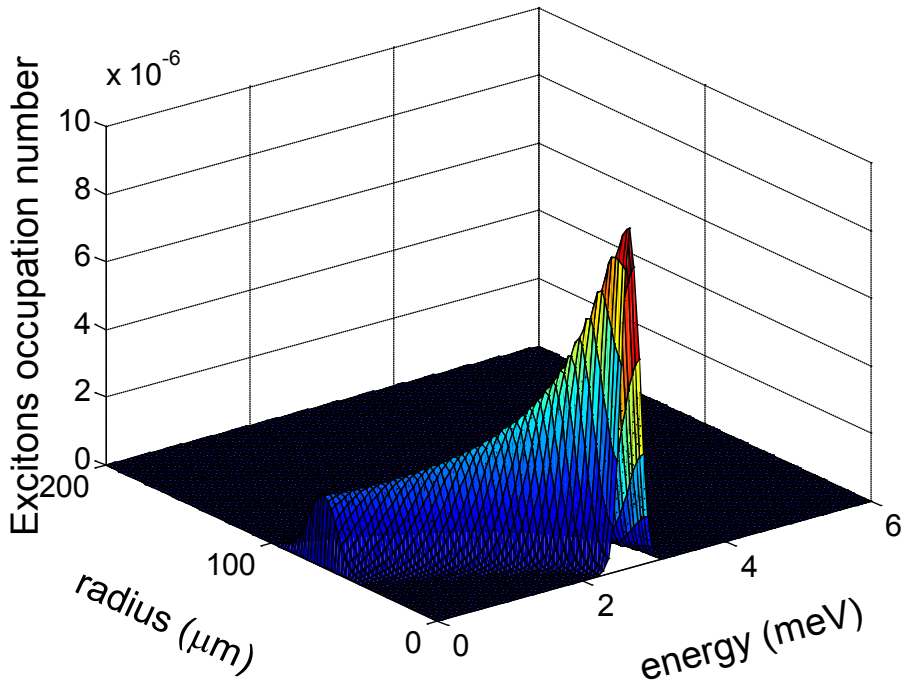

Figure 2.4: Exciton distribution after solving Boltzmann equation without source term, at 5 ns. When initially the excitons number within the trap is 1.98×10^{6}. The parameters, which we have used, are M_x=2.61 m_e, $m_e = 9.109\times10^{-31}$ *kg* is the electron rest mass, v_s=4.5×10^{3} m/s, $a = 0.5\cdot \mu eV \cdot \mu m^{-2}$.

the summation of exciton number along $\vec{r}$ direction by the equation

$$n_r(e) = \int_0^\infty 4\pi \vec{r}^2 \cdot N(\vec{r}, e) \cdot dr \tag{11}$$

and the summation of exciton number along the direction of energy by the equation

$$n_e(\vec{r}) = \int_0^\infty \frac{1}{(2\pi)^3} \cdot 4\pi k^2 dk N(\vec{r}, \vec{k}) \tag{12}$$

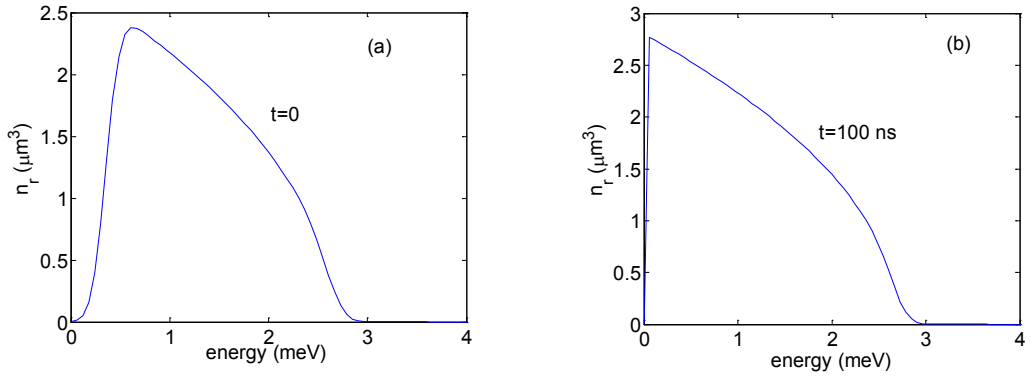

Figure 2.5: The distribution of summation of exciton number in $\vec{r}$ direction n_r vs. energy for different times. When initially the excitons number within the trap is 1.98×10^6.

Figure 2.5 shows the distribution of summation of exciton number in $\vec{r}$ direction n_r vs. energy for different times. To check the boundary conditions, we have checked that the total numbers of excitons are almost constant with increasing time (see figure 2.6).

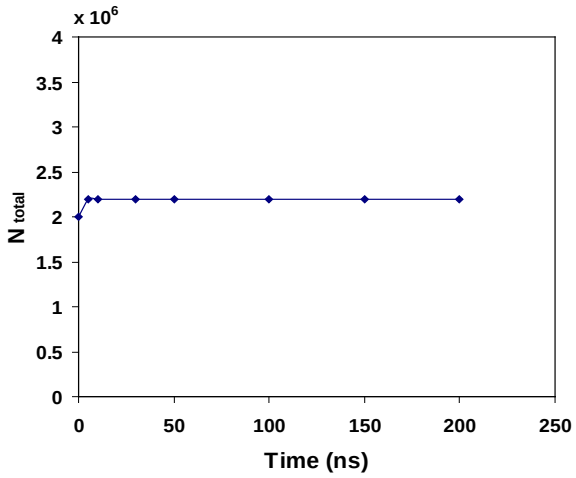

Figure 2.6: The total number of excitons vs. time without including any source term. The curve shows that the total numbers of excitons are almost constant with increasing time.

References:

[1] Ashcroft N W and Mermin N D, 1976, "Solid State Physics" (Fortworth: Harcourt Brace).

[2] William E Schiesser and Graham W Griffiths, 2009, "A Compendium of Partial Differential Equation Models" (Cambridge University Press).

[3] Coleman, Matthew P, 2005, "An introduction to partial differential equation with MATLAB" (Chapman and Hall/CRC).

[4] Otto S R and Denier J P, 2005, "An Introduction to Programming and numerical methods in MATLAB" (Springer).

[5] Schwartz R, Naka N, Kieseling F, and Stolz H, 2011, *New Journal of Physics* **14**, 023054, "Dynamics of excitons in a potential trap at ultra-low temperatures: paraexcitons in Cu_2O".

Chapter 3

Phonon Scattering

In this chapter we have discussed about the phonon scattering, the results of the phonon scattering in homogeneous system and the results of the Boltzmann equation with the phonon scattering within the potential trap. The possibility of Bose-Einstein condensation of exciton in Cu_2O, within the potential trap is discussed.

3.1 Theory

3.11 General equation for the phonon scattering

Phonon scattering term, which describes the kinetics of a specially homogeneous system of excitons. We use local approximation and neglect any phonon induced diffusion. The phonon scattering term with decay term of the Boltzmann equation [1] is then given by

$$\begin{aligned}\frac{\partial N_{\vec{k}}}{\partial t} = -\frac{2\pi}{\hbar}\sum_{\vec{p}}\left|M_{x-ph}(\vec{p}-\vec{k})\right|^2 \{[N_{\vec{k}}(1+n^{ph}_{\vec{k}-\vec{p}})(1+N_{\vec{p}}) \\ -(1+N_{\vec{k}})n^{ph}_{\vec{k}-\vec{p}}N_{\vec{p}}]\delta(e_{\vec{k}}-e_{\vec{p}}-\hbar\omega_{\vec{k}-\vec{p}}) \\ +[N_{\vec{k}}n^{ph}_{\vec{p}-\vec{k}}(1+N_{\vec{p}})-(1+N_{\vec{k}})(1+n^{ph}_{\vec{p}-\vec{k}})N_{\vec{p}}] \\ \times\delta(e_{\vec{k}}-e_{\vec{p}}+\hbar\omega_{\vec{p}-\vec{k}})\} - N_{\vec{k}}/\tau_{opt}\end{aligned} \quad (1)$$

Where $e_{\vec{k}} = \hbar^2k^2/2M_x$, $e_{\vec{p}} = \hbar^2p^2/2M_x$ and $\hbar\omega_{\vec{p}-\vec{k}} = \hbar v_s\left|\vec{p}-\vec{k}\right|$ are the exciton energy in wavevector $\vec{k}$ state, exciton energy in wavevector $\vec{p}$ state and phonon energy, respectively. $N_{\vec{k}}$, $N_{\vec{p}}$ and $n^{ph}_{\vec{p}-\vec{k}} = 1/[\exp(\hbar\omega_{\vec{p}-\vec{k}}/k_BT_b)-1]$ are the exciton occupation number in $\vec{k}$ state, exciton occupation number in $\vec{p}$ state and phonon occupation number, respectively. $M_{x-ph}\left(\vec{p}-\vec{k}\right)$ is the matrix element of the exciton-phonon deformation potential interaction, and τ_{opt} is the radiative lifetime of excitons. The exciton-phonon coupling is given by $\left|M_{x-ph}(\vec{p}-\vec{k})\right|^2 = \hbar D^2\left|\vec{p}-\vec{k}\right|/(2V\rho v_s)$, where D is the deformation potential energy, V is the crystal volume, ρ is the crystal density, v_s is the longitudinal acoustic sound velocity and M_x is the exciton mass and δ is the Dirac distribution. The first term in the square brackets on the right-hand side of equation (1) is due to the Stokes scattering and the second term is for anti-Stokes scattering of excitons.

3.12 Transfer momentum terms to energy terms

Then we transfer all $N_{\vec{k}}$ terms in momentum space to N_e terms in the one dimensional energy space by

$$\frac{\partial N_{e_{\vec{k}}}}{\partial t} = \frac{V}{(2\pi)^3}\int_0^{\pi}\sin\theta d\theta\int_0^{2\pi} d\varphi\int_0^{\infty}\vec{k}^2\frac{\partial N_{\vec{k}}}{\partial t}dk \tag{2}$$

where $k,\ \theta,\ \varphi$ are the spherical coordinates of wave vector $\vec{k}$. Then we put the value of $\frac{\partial N_{\vec{k}}}{\partial t}$ in equation (2) and transfer all $\vec{k}$ terms into e terms where $e_{\vec{k}} = \hbar^2 k^2 / 2M_x$ and $e_{\vec{p}} = \hbar^2 p^2 / 2M_x$.

$$\frac{\partial N_{e_{\vec{k}}}}{\partial t} = -\frac{2\pi}{\hbar}\cdot\frac{V}{(2\pi)^3}\int_0^{\pi}\sin\theta d\theta\int_0^{2\pi} d\varphi\int \vec{p}^2 dp\left|M_{x-ph}(\vec{p}-\vec{k})\right|^2$$
$$\times\{I_S\delta(e_{\vec{k}}-e_{\vec{p}}-\hbar\omega_{\vec{k}-\vec{p}})+I_{AS}\delta(e_{\vec{k}}-e_{\vec{p}}+\hbar\omega_{\vec{p}-\vec{k}})\}-\left(N_{e_{\vec{k}}}/\tau_{opt}\right) \tag{3}$$

where $I_S = [N_{\vec{k}}(1+n^{ph}_{\vec{k}-\vec{p}})(1+N_{\vec{p}})-(1+N_{\vec{k}})n^{ph}_{\vec{k}-\vec{p}}N_{\vec{p}}]$ and

$I_{AS} = [N_{\vec{k}}n^{ph}_{\vec{p}-\vec{k}}(1+N_{\vec{p}})-(1+N_{\vec{k}})(1+n^{ph}_{\vec{p}-\vec{k}})N_{\vec{p}}]$

$$\frac{\partial N_{e_{\vec{k}}}}{\partial t} = -\frac{D^2}{4\pi\rho v_s}\int_0^{\pi}\sin\theta d\theta\int \vec{p}^2 dp\cdot\left|\vec{p}-\vec{k}\right|$$
$$\times\{I_S\delta(e_{\vec{k}}-e_{\vec{p}}-\hbar\omega_{\vec{k}-\vec{p}})+I_{AS}\delta(e_{\vec{k}}-e_{\vec{p}}+\hbar\omega_{\vec{p}-\vec{k}})\}-\left(N_{e_{\vec{k}}}/\tau_{opt}\right) \tag{4}$$

Now let $\left|\vec{p}-\vec{k}\right| = |\vec{u}|$

or, $\sqrt{\vec{k}^2+\vec{p}^2-2\vec{k}\vec{p}\cos\theta} = |\vec{u}|$

or, $\sin\theta d\theta = \frac{u\ du}{k\ p}$

By using the relation $\sin\theta d\theta = \frac{u\ du}{k\ p}$ we get

$$\frac{\partial N_{e_{\vec{k}}}}{\partial t} = -\frac{D^2}{4\pi\rho v_s}\int_p\int_u \frac{\vec{u}^2\ du}{\vec{k}\ \vec{p}}\cdot \vec{p}^2 dp\cdot\{(I_S + I_{AS})\cdot\delta(e_{\vec{k}} - e_{\vec{p}} \pm \hbar v_s\left|\vec{k}-\vec{p}\right|)\} - \left(N_{e_{\vec{k}}}/\tau_{opt}\right) \tag{5}$$

$$\text{or, } \frac{\partial N_{e_{\vec{k}}}}{\partial t} = -\frac{D^2}{4\pi\rho\hbar v_s^{\ 2}}\int_p\int_u \frac{\vec{u}^2\ du}{\vec{k}\ \vec{p}}\cdot \vec{p}^2 dp\cdot\left\{(I_S + I_{AS})\cdot\delta\left(\frac{e_{\vec{k}} - e_{\vec{p}}}{\hbar v_s} \pm \left|\vec{u}\right|\right)\right\} - N_{e_{\vec{k}}}/\tau_{opt} \tag{6}$$

$$\begin{aligned}\text{or, } \frac{\partial N_{e_{\vec{k}}}}{\partial t} = &-\frac{D^2}{4\pi\rho\hbar v_s^{\ 2}}\int_p \frac{\vec{p}\ dp}{\vec{k}}\cdot\left(\frac{e_{\vec{k}} - e_{\vec{p}}}{\hbar v_s}\right)^2\cdot\{I_S\cdot\Theta\left(q_s - \sqrt{e_{\vec{k}}} + \sqrt{e_{\vec{p}}}\right)\Theta\left(-q_s + \sqrt{e_{\vec{k}}} + \sqrt{e_{\vec{p}}}\right)\\ &\times\Theta\left(e_{\vec{k}} - e_{\vec{p}}\right) + I_{AS}\cdot\Theta\left(q_{as} - \sqrt{e_{\vec{p}}} + \sqrt{e_{\vec{k}}}\right)\\ &\times\Theta\left(-q_{as} + \sqrt{e_{\vec{p}}} + \sqrt{e_{\vec{k}}}\right)\Theta\left(e_{\vec{p}} - e_{\vec{k}}\right)\} - N_{e_{\vec{k}}}/\tau_{opt}\end{aligned} \tag{7}$$

We have calculated step functions from delta functions which is in detail in the appendix.

Using the relations $\vec{p}^2 = \frac{2M_x e_{\vec{p}}}{\hbar^2}$ or, $p\ dp = \frac{M_x}{\hbar^2}de_p$ and $\left|\vec{k}\right| = \sqrt{\frac{2M_x e_{\vec{k}}}{\hbar^2}}$ we get

$$\begin{aligned}\frac{\partial N_{e_{\vec{k}}}}{\partial t} = &-\frac{D^2}{4\pi\rho\hbar v_s^{\ 2}}\cdot\frac{\sqrt{M_x}}{\sqrt{2}\hbar}\cdot\int_{e_{\vec{p}}}\frac{de_{\vec{p}}}{\sqrt{e_{\vec{k}}}}\cdot\left(\frac{e_{\vec{k}} - e_{\vec{p}}}{\hbar v_s}\right)^2\cdot\{I_S\cdot\Theta\left(q_s - \sqrt{e_{\vec{k}}} + \sqrt{e_{\vec{p}}}\right)\\ &\times\Theta\left(-q_s + \sqrt{e_{\vec{k}}} + \sqrt{e_{\vec{p}}}\right)\Theta\left(e_{\vec{k}} - e_{\vec{p}}\right) + I_{AS}\cdot\Theta\left(q_{as} - \sqrt{e_{\vec{p}}} + \sqrt{e_{\vec{k}}}\right)\\ &\times\Theta\left(-q_{as} + \sqrt{e_{\vec{p}}} + \sqrt{e_{\vec{k}}}\right)\Theta\left(e_{\vec{p}} - e_{\vec{k}}\right)\} - N_{e_{\vec{k}}}/\tau_{opt}\end{aligned} \tag{8}$$

Now we say $e_{\vec{k}} = e$ and $e_{\vec{p}} = e_1$. Therefore, we get

$$\begin{aligned}\frac{\partial N_e}{\partial t} = &-\left(\frac{D^2\sqrt{M_x}}{4\sqrt{2}\pi\hbar^4 v_s^4\rho\sqrt{e}}\right)\int de_1\left(e - e_1\right)^2\\ &\times\{[N_e\left(1 + n_{e-e_1}^{ph}\right)\left(1 + N_{e_1}\right) - \left(1 + N_e\right)n_{e-e_1}^{ph}N_{e_1}]\Theta\left(q_s - \sqrt{e} + \sqrt{e_1}\right)\\ &\times\Theta\left(-q_s + \sqrt{e} + \sqrt{e_1}\right)\Theta\left(e - e_1\right)\end{aligned}$$

$$+[N_e n^{ph}_{e_1-e}\left(1+N_{e_1}\right)-\left(1+N_e\right)\left(1+n^{ph}_{e_1-e}\right)N_{e_1}]$$
$$\times\Theta\left(q_{as}-\sqrt{e_1}+\sqrt{e}\right)\Theta\left(-q_{as}+\sqrt{e_1}+\sqrt{e}\right)\Theta\left(e_1-e\right)\}-N_e/\tau_{opt}\ . \quad (9)$$

3.13 Equation for zero energy state

At k=0 Stokes scattering is not allowed. Therefore, the phonon scattering term only with anti-Stokes part [1] is given by

$$\frac{\partial N_{\vec{k}}}{\partial t}=-\frac{2\pi}{\hbar}\sum_{\vec{p}}\left|M_{x-ph}(\vec{p}-\vec{k})\right|^2\cdot\{[N_{\vec{k}}n^{ph}_{\vec{p}-\vec{k}}(1+N_{\vec{p}})-(1+N_{\vec{k}})(1+n^{ph}_{\vec{p}-\vec{k}})N_{\vec{p}}]$$
$$\times\delta(e_{\vec{k}}-e_{\vec{p}}+\hbar\omega_{\vec{p}-\vec{k}})\}-N_{\vec{k}}/\tau_{opt} \quad (10)$$

In terms of $e_{\vec{k}}$

$$\frac{\partial N_{e_{\vec{k}}}}{\partial t}=-\frac{2\pi}{\hbar}\cdot\frac{V}{(2\pi)^3}\cdot 2\pi\int_0^{\pi}\sin\theta d\theta\int\vec{p}^{\,2}dp\left|M_{x-ph}(\vec{p}-\vec{k})\right|^2$$
$$\times\{[N_{e_{\vec{k}}}n^{ph}_{e_{\vec{p}}-e_{\vec{k}}}(1+N_{e_{\vec{p}}})-(1+N_{e_{\vec{k}}})(1+n^{ph}_{e_{\vec{p}}-e_{\vec{k}}})N_{e_{\vec{p}}}]$$
$$\times\delta(e_{\vec{k}}-e_{\vec{p}}+\hbar\omega_{\vec{p}-\vec{k}})\}-N_{e_{\vec{k}}}/\tau_{opt} \quad (11)$$

But with $e_{\vec{k}}=0$, we get

$$\frac{\partial N_{e_{\vec{k}}=0}}{\partial t}=-\frac{8\pi^2}{\hbar}\cdot\frac{V}{(2\pi)^3}\cdot\frac{\hbar D^2}{2V\rho v_s}\int|\vec{p}|^3dp$$
$$\times\{[N_{e_{\vec{k}}=0}n^{ph}_{e_{\vec{p}}}(1+N_{e_{\vec{p}}})-(1+N_{e_{\vec{k}}=0})(1+n^{ph}_{e_{\vec{p}}})N_{e_{\vec{p}}}]\delta(\hbar v_s\vec{p}-e_{\vec{p}})\}-N_{e_{\vec{k}}=0}/\tau_{opt} \quad (12)$$

or, $$\frac{\partial N_{e_{\vec{k}}=0}}{\partial t}=-\frac{D^2M_x^2}{\pi\rho v_s\hbar^4}\int e_p\ de_p$$
$$\times\{[N_{e_{\vec{k}}=0}n^{ph}_{e_{\vec{p}}}(1+N_{e_{\vec{p}}})-(1+N_{e_{\vec{k}}=0})(1+n^{ph}_{e_{\vec{p}}})N_{e_{\vec{p}}}]\delta(\hbar v_s\vec{p}-e_{\vec{p}})\}-N_{e_{\vec{k}}=0}/\tau_{opt} \quad (13)$$

or, $$\frac{\partial N_{e_{\vec{k}}=0}}{\partial t}=-\frac{D^2M_x^2}{\pi\rho v_s\hbar^4}\cdot 2e_0\cdot[N_{e_{\vec{k}}=0}n^{ph}_{e_0}(1+N_{e_0})-(1+N_{e_{\vec{k}}=0})(1+n^{ph}_{e_0})N_{e_0}]$$
$$-\left(N_{e_{\vec{k}}=0}/\tau_{opt}\right) \quad (14)$$

or, $$\frac{\partial N_{e_{\vec{k}}=0}}{\partial t} = -\frac{4D^2 M_x^3 v_s}{\pi\rho\hbar^4} \cdot [N_{e_{\vec{k}}=0} n_{e_0}^{ph}(1+N_{e_0}) - (1+N_{e_{\vec{k}}=0})(1+n_{e_0}^{ph})N_{e_0}] - N_{e_{\vec{k}}=0}/\tau_{opt} \quad (15)$$

If we say $e_{\vec{k}} = e$

$$\frac{\partial N_{e=0}}{\partial t} = \left(\frac{4D^2 M_x^3 v_s}{\pi\hbar^4\rho}\right)\left[N_{e_0}\left(1+n_{e_0}^{ph}\right) - N_{e=0}\left(n_{e_0}^{ph} - N_{e_0}\right)\right] - (N_{e=0}/\tau_{opt}) \quad (16)$$

3.2 Numerical modeling

We discretize the energy $e_j = (j-1)\Delta e$ where $j = 1.....ne$ and $\Delta e = \frac{e_0}{M}$ with M is an integer. Analogously we discretize the energy $e_{1q} = (q-1)\Delta e$. We know that $N_{j-q}^{ph} = 1/[\exp(e_0(j-q)/(k_B TM)) - 1]$. So we can write the equation (9) in the form

$$\frac{\partial N_j}{\partial t} = -\frac{C}{M^{5/2}\sqrt{j-1}} \sum_{q_{\min}}^{q_{\max}} (j-q)^2 \times [\{N_j(1+N_{j-q}^{ph})(1+N_q) - (1+N_j)N_{j-q}^{ph}N_q\}$$
$$+\{N_j N_{q-j}^{ph}(1+N_q) - (1+N_j)(1+N_{q-j}^{ph})N_q\}] - N_j/\tau_{opt} \quad (17)$$

where, $C = \frac{D^2 M_x^3 v_s}{\pi\hbar^4\rho}$.

For Stokes scattering q_{max}=j-1 and $q_{\min} = \left(\sqrt{j-1} - \sqrt{M}\right)^2$ and for anti-Stokes scattering q_{min} is the maximum of $q1_{min}$ and $q2_{min}$, where $q1_{min}$=j-1 and $q2_{\min} = \left(\sqrt{j-1} - \sqrt{M}\right)^2$ and $q_{\max} = \left(\sqrt{j-1} + \sqrt{M}\right)^2$. Here j=2.....ne. We get these values of q_{max} and q_{min} for Stokes and anti-Stokes scattering from the Dirac distribution in equation (3) .

We can write the equation (16), for j=1 in the form

$$\frac{\partial N_{j=1}}{\partial t} = \left(\frac{4D^2 M_x^3 v_s}{\pi\hbar^4\rho}\right)\left[N_{e_0}\left(1+n_{e_0}^{ph}\right) - N_{j=1}\left(n_{e_0}^{ph} - N_{e_0}\right)\right] - (N_{j=1}/\tau_{opt}) \quad (18)$$

3.3 Results in homogeneous system including phonon scattering

As we have discussed in chapter 1, the relaxation kinetics of excitons in Cu_2O due to phonon scattering have been investigated in references [1-8]. We have also investigated the Boltzmann kinetics of paraexcitons in Cu_2O in homogeneous system and also within the potential trap.

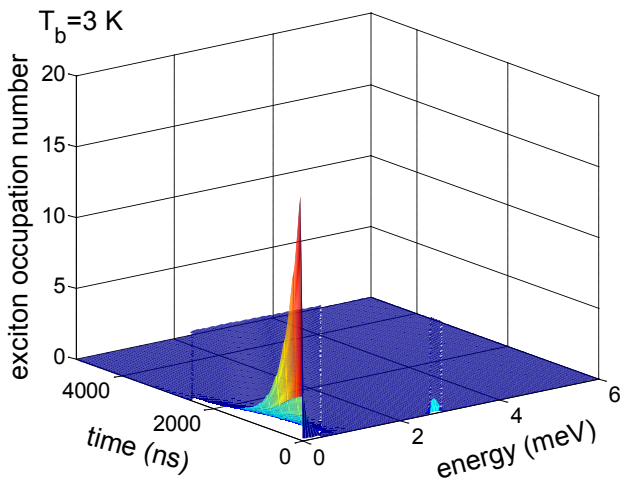

Figure 3.1: The result of the phonon scattering with decay term in homogeneous system at 3 K when the exciton density is $1.5\times10^5\ \mu m^{-3}$ and lifetime is 650 ns. The figure shows that with increasing time exciton number is increasing near zero energy and then it is decreasing with time.

After solving the phonon scattering term of the Boltzmann equation we are getting the exciton occupation number as a function of energy *e*, and time *t* (see figure 3.1 and 3.2). In figure 3.1 we have plotted simulation result of phonon scattering with decay term and in figure 3.2 we have plotted simulation result of phonon scattering without decay term.

Here the initial distribution [1] is given by the Gaussian $N_e(t=0)=N_{\tilde{e}}\exp[-(e-\tilde{e})^2/(\Delta e)^2]$ with the central energy $\tilde{e}$ and the width Δe. The parameters, which we have used, are the exciton mass M_x=2.61 m_e, $m_e=9.109\times10^{-31}\ kg$ is the electron rest mass, the longitudinal acoustic sound velocity

v_s =4.5×10^3 m/s, the deformation potential energy D=1.68 eV and the crystal density $\rho = 6.11\times10^3\ kg/m^3$.

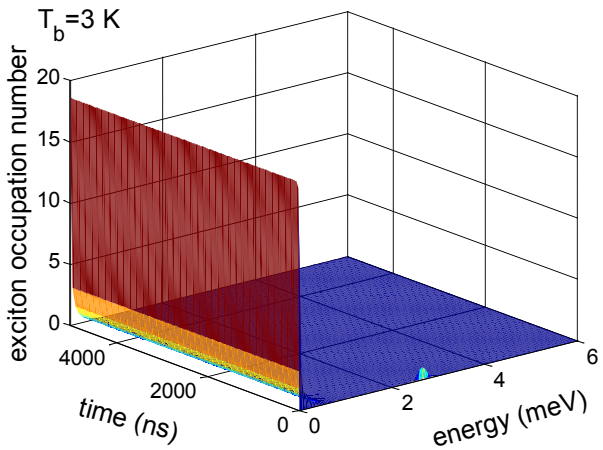

Figure 3.2: The result of the phonon scattering in homogeneous system at 3 K when the exciton density is $1.5\times10^5\ \mu m^{-3}$. The figure shows that with increasing time exciton number stays constant.

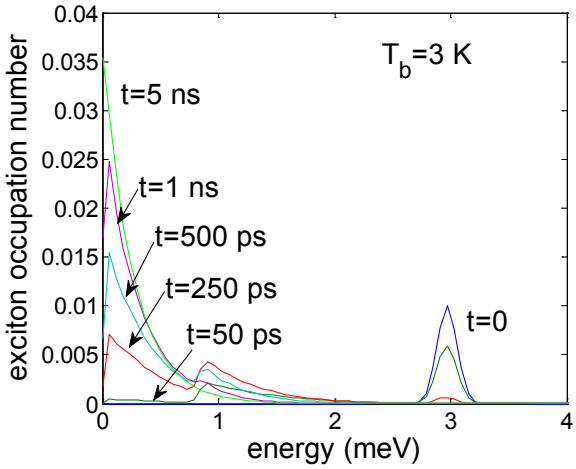

Figure 3.3: Exciton distribution in homogeneous system from zero to 5 ns for 3 K. In this case exciton density is $1.7\times10^3\ \mu m^{-3}$.

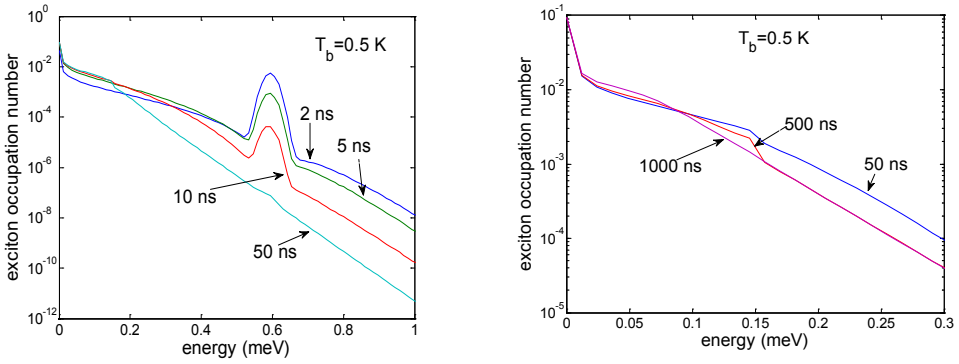

Figure 3.4: Exciton distribution in homogeneous system for 0.5 K. Left hand side's figure is for 2 ns to 50 ns and right hand side's figure is for 50 ns to 1000 ns. Exciton density is $1.5\times10^{2}\ \mu m^{-3}$.

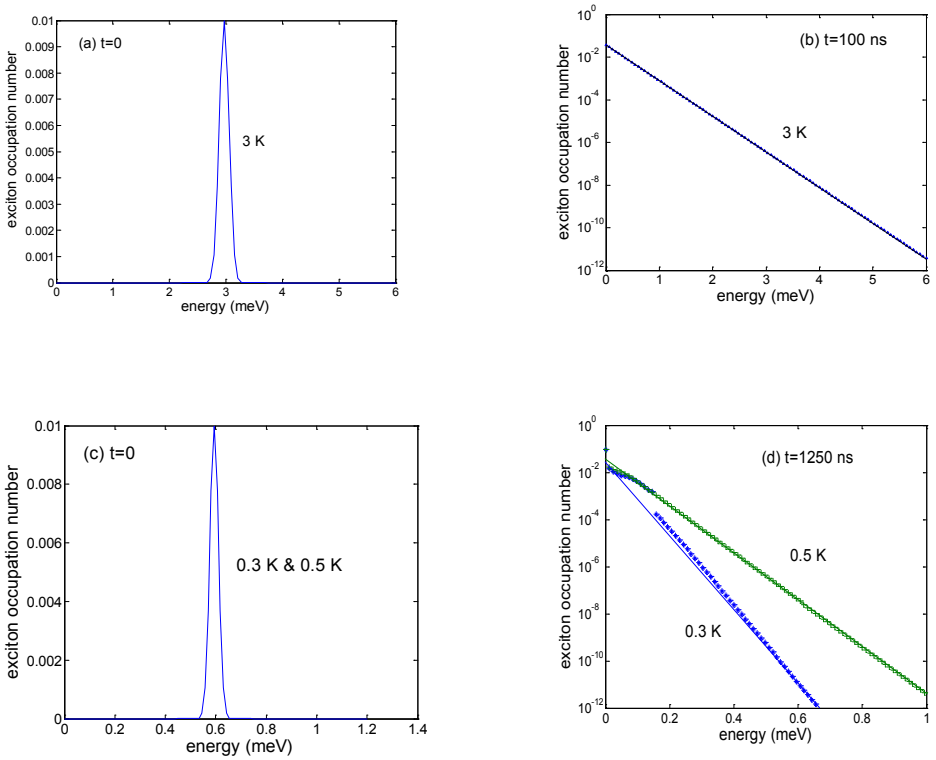

Figure 3.5: Initial [3.5a, 3.5c] and final [3.5b, 3.5d] exciton distributions vs. energy for different temperatures. Final distributions are taken, at 100 ns for 3 K and at 1250 ns for 0.3 K and 0.5 K. For 3 K, exciton density is $1.7\times10^{3}\ \mu m^{-3}$, and for 0.3 K and 0.5 K exciton density is $1.5\times10^{2}\ \mu m^{-3}$. Markers represent the results of the numerical simulation and solid lines are for the thermal equilibrium case.

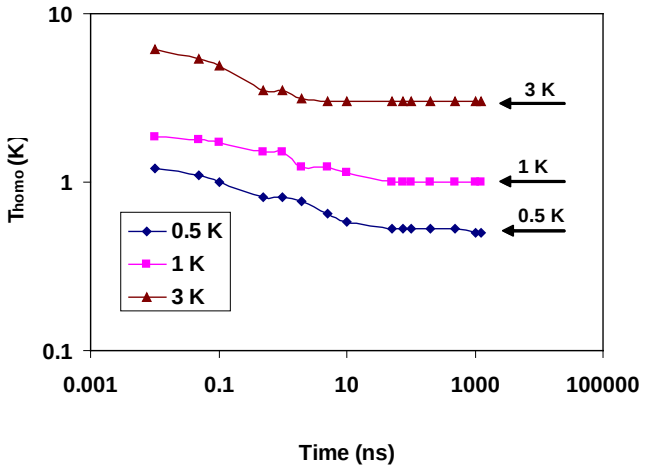

Figure 3.6: Local exciton temperature T_{homo} vs. time for different bath temperatures in homogeneous system. Here we see that the effective temperature is decreasing with time for different bath temperatures. The arrows on the right hand side indicate the effective temperatures. For 0.5 K, 1 K and 3 K exciton densities are $1.5\times10^{2}\ \mu m^{-3}$, $1.5\times10^{2}\ \mu m^{-3}$ and $1.7\times10^{3}\ \mu m^{-3}$, respectively. The curves serve as a guide to the eye.

We have calculated the total number of excitons by the equation

$$N_{total} = \frac{V}{(2\pi)^3}\int_0^\infty 4\pi k^2 dk \cdot N(\vec{k}) \tag{19}$$

In figure 3.3 we have plotted exciton distribution for 3 K from zero to 5 ns. We see with increasing time distribution is coming close to zero energy. In figure 3.4 we have plotted exciton distribution for 0.5 K from 2 ns to 1000 ns. In figure 3.5 we have plotted initial and final exciton distribution for different bath temperatures. For 0.5 K it is thermalizing but taking long time to thermalize. For 0.3 K in the beginning it is not straight but then it is coming straight (see figure 3.5d) and there is some deviation between numerical result and thermal equilibrium case. Therefore, it is not thermalizing. Below 0.3 K, same thing happening like 0.3 K. We have calculated the local effective temperature T_{homo} (see figure 3.6) by fitting the long energy tail of the exciton distribution, using the equation

$e^{-e/k_B T_{homo}}$. This Boltzman distribution $f(e) = e^{-e/k_B T}$ is an approximation which is derived from Bose-Einstein distribution $f(e) = \frac{1}{e^{-e/k_B T} - 1}$ for $e >> k_B T$. We see over 1 K it takes 10 ns to come down to bath temperature in contrast below 1 K it takes around 100 ns to come down to bath temperature.

We know for constant potential energy, the critical density is given by

$$n_c = \left(\frac{M_x k_B T}{2\pi\hbar^2} \right)^{3/2} \tag{20}$$

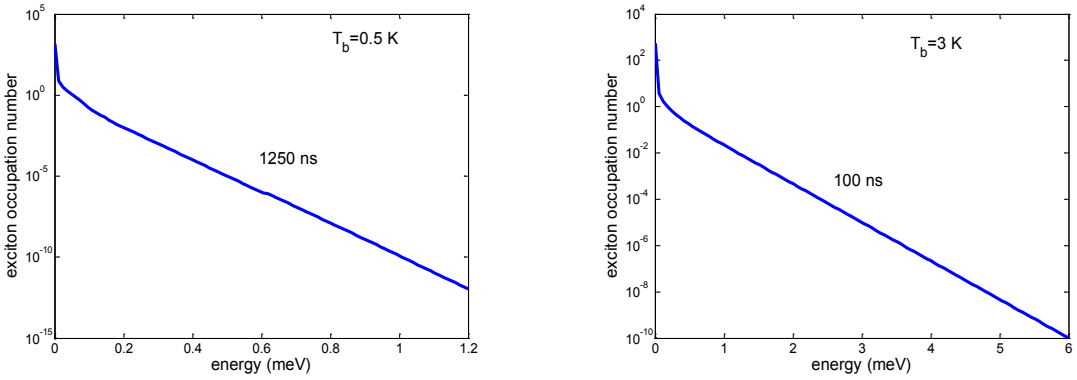

Figure 3.7: Exciton distribution in homogeneous system for 0.5 K and 3 K. For 0.5 K and 3 K exciton densities are $1.5\times10^5\ \mu m^{-3}$ and $1.7\times10^6\ \mu m^{-3}$ respectively. The critical densities of exciton for 0.5 K and 3 K are $1\times10^4\ \mu m^{-3}$ and $1.4\times10^5\ \mu m^{-3}$ respectively. Here the exciton densities are higher than the critical densities and high peak at zero energy indicates BEC.

In our numerical simulation, if we increase exciton density over the critical density, we see high peak at zero energy in the exciton distribution (see figure 3.7). In the figure 3.7 represents exciton occupation vs. energy curves for 0.5 K and 3 K. Where for 0.5 K and 3 K exciton densities are $1.5\times10^5\ \mu m^{-3}$ and $1.7\times10^6\ \mu m^{-3}$ respectively but the critical densities of exciton for 0.5 K and 3 K are $1\times10^4\ \mu m^{-3}$ and $1.4\times10^5\ \mu m^{-3}$ respectively. Here the exciton densities are higher than the critical densities and we see high peak at zero energy which indicates BEC.

3.4 Results within a trap including phonon scattering

After solving the Boltzmann equation with phonon scattering term we are getting the exciton occupation number as a function of energy *e*, radius $\vec{r}$ and time *t* (see Figure 3.8). We see that for a particular temperature, the excitons are going towards the bottom of the trap with increasing time, and after some time they are accumulated in a place near the bottom of the trap. In this case total exciton number within the trap is 1.7×10^4 .

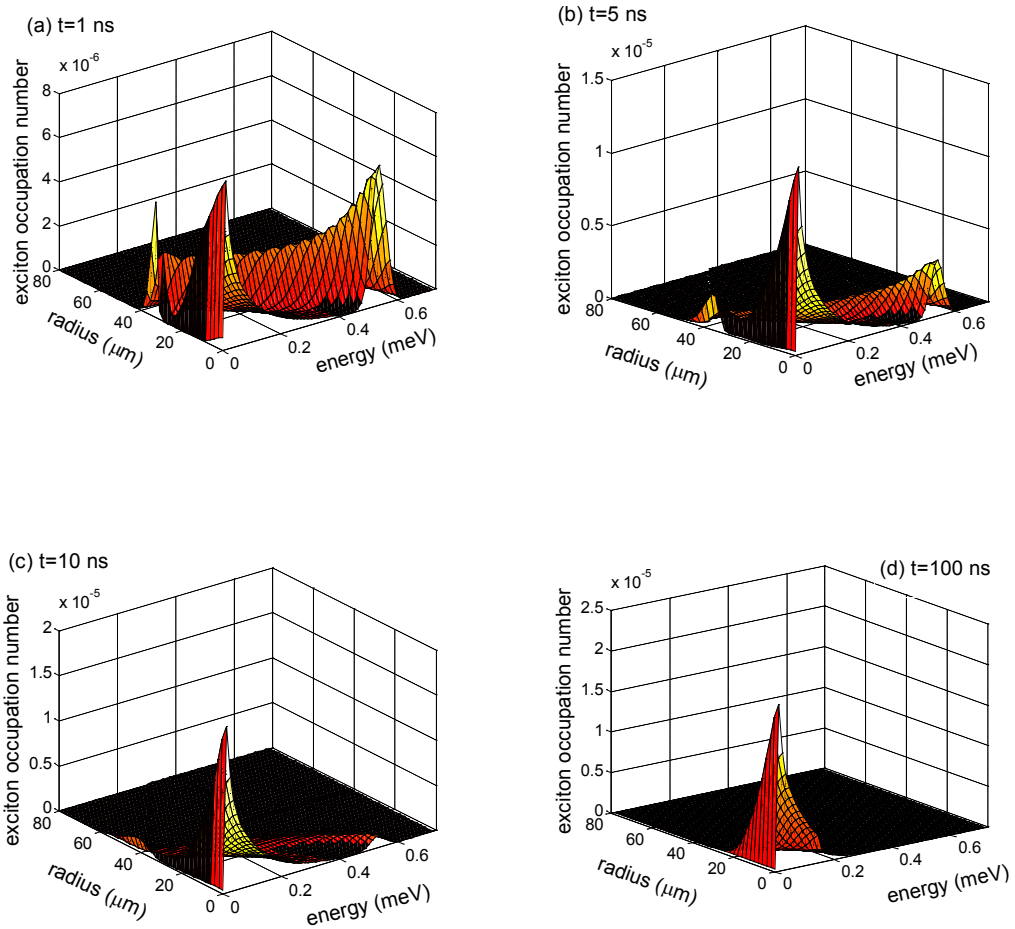

Figure 3.8: The results of the simulation with phonon scattering at different times for 0.5 K when the initial exciton number within the trap is 1.7×10^4 . The parameters, which we have used, are M_x=2.61 m_e, $m_e = 9.109\times10^{-31}\ kg$ is the electron rest mass, v_s=4.5×10^3 m/s, $a = 0.5\cdot\mu eV\cdot\mu m^{-2}$, D=1.68 eV and $\rho = 6.11\times10^3\ kg/m^3$. The series of figures shows that excitons are accumulated at the bottom of the trap within 100 ns at 0.5 K.

We have calculated the total number of excitons by the equation

$$N_{total} = \frac{1}{(2\pi)^3} \int_0^\infty \int_0^\infty 4\pi \vec{r}^{\,2} dr \cdot 4\pi \vec{k}^{\,2} dk \cdot N(\vec{r}, \vec{k}) \tag{21}$$

the summation of exciton number along *r* direction by the equation

$$n_r(e) = \int_0^\infty 4\pi \vec{r}^{\,2} dr \cdot N_e(\vec{r}, e) \tag{22}$$

we call it exciton occupation, and the summation of exciton number along the direction of energy by the equation

$$n_e(\vec{r}) = \frac{1}{(2\pi)^3} \int_0^\infty 4\pi k^2 dk \cdot N(\vec{r}, \vec{k}) \tag{23}$$

From $n_r(e)$, we get the total number of exciton by the equation

$$N_{total} = \frac{1}{(2\pi)^2} \cdot \left(\frac{2M_x}{\hbar^2} \right)^{3/2} \int_e \sqrt{e} \cdot de \cdot n_r(e) \tag{24}$$

The critical number of excitons N_c at condensate for the BEC for the thermal equilibrium case

$$N_c = 1.202 \left(\frac{k_B T}{\hbar \Omega} \right)^3 \tag{25}$$

with the frequency $\Omega = \sqrt{\frac{2a}{M_x}}$, the exciton mass $M_x = 2.61 m_e$, the steepness constant $a = 0.5 \mu eV \cdot \mu m^{-2}$ and the temperature T.

The kinetics of bosonic excitons in a potential trap was studied in reference [9] by rate equation in the basis of the single-particle eigenfunctions, in contrast in our work we have solved the Boltzmann equation. The thermodynamics of long-lived paraexcitons confined to a parabolic potential well in Cu_2O was studied in reference [10].

3.41 Low number of excitons

First we discuss about the results with low number of excitons within the trap. Figure 3.9 represents exciton occupation n_r at 3 K by summation of total exciton number of non

degenerate exciton in r direction vs. energy for zero to 1 ns. We see with increasing time exciton distribution is coming close to zero energy and at 1 ns it has the boltzmann distribution.

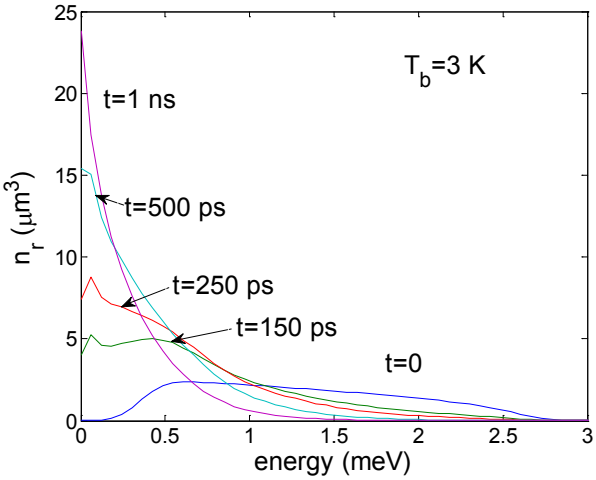

Figure 3.9: Exciton occupation n_r at 3 K by summation of exciton number of non-degenerate exciton gas in $\vec{r}$ direction vs. energy for different times. Initially total number of excitons are 1.98×10^6.

In figure 3.10 we have plotted exciton occupation n_r at t=0 and at 100 ns by summation of total exciton number of non degenerate exciton in r direction vs. energy for different bath temperatures. For 0.3 K at 100 ns we see there is deviation between our simulation result and thermal equilibrium case therefore, in this case we do not get the thermal equilibrium.

In figure 3.11 we have plotted the total number of excitons N_{tot} vs. time for different bath temperatures with including phonon scattering. We see that in the beginning for all temperatures the exciton number decreases very little with time and then it stays almost constant. As the origin of this initial decay we found that the excitons are scattered of the finite energy space due to the somewhat singular initial distribution.

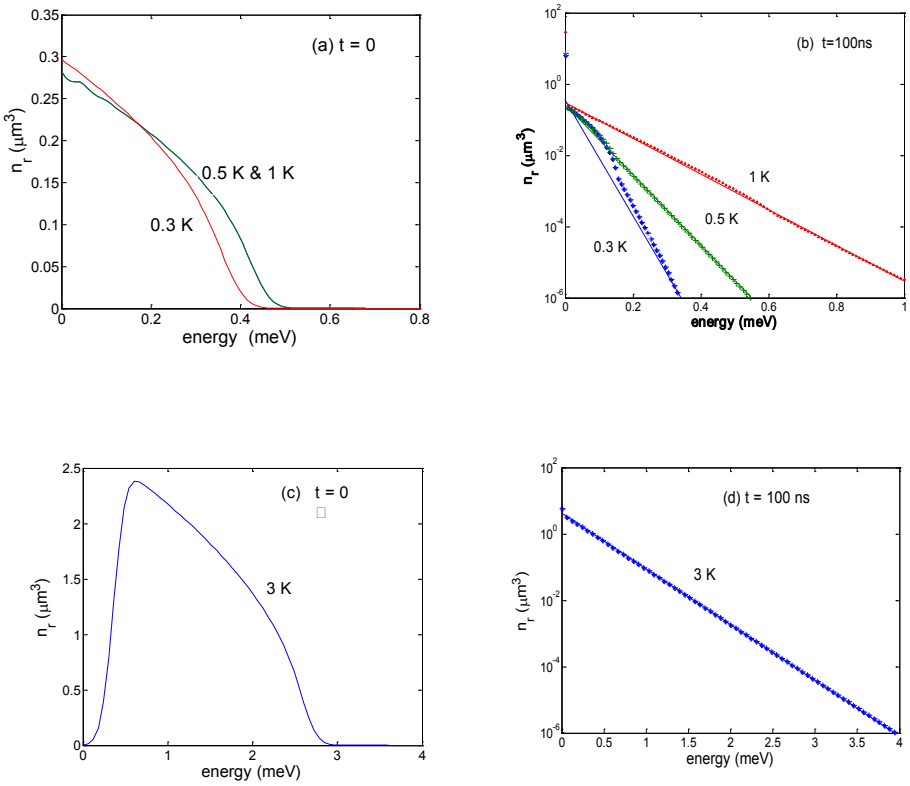

Figure 3.10: Exciton occupation n_r at t=0 [3.10a, 3.10c] and final [3.10b, 3.10d] distribution n_r at 100 ns by summation of exciton number of non-degenerate exciton gas in $\vec{r}$ direction vs. energy for different temperatures. For 0.3 K, 0.5 K, 1 K and 3 K, initially total number of excitons are 1.3×10^4, 1.5×10^4, 1.5×10^4 and 1.98×10^6, respectively. Markers represent the results of the numerical simulation and solid lines are for the thermal equilibrium case.

Reference [11] reported about the same problem and therefore renormalized the exciton number at each time step. To get rid of this numerical artifact, we always considered in our numerical simulations the results for the actual number of excitons at each time. Therefore, our conclusions do not depend on the actual initial number of excitons.

As we say in chapter 2, if we do not include any source term then the total number of excitons are almost constant with increasing time (see figure 2.6). That means the boundary conditions are working fine.

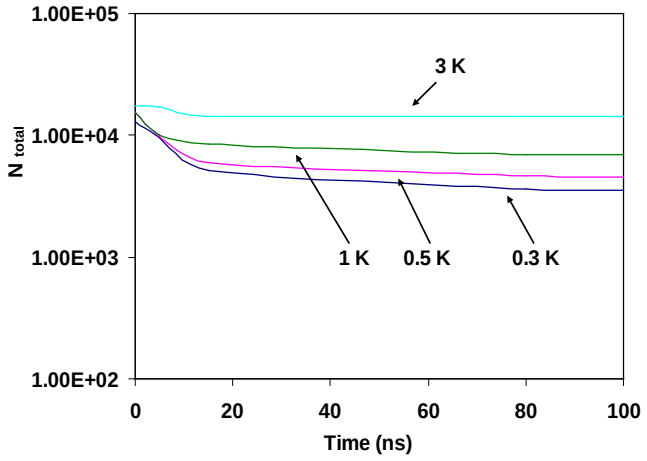

Figure 3.11: Total number of excitons vs. time for different bath temperatures including deformation potential phonon scattering. The curves show that how the total number of excitons is changing with time for different bath temperatures. For 0.3 K, 0.5 K, 1 K and 3 K, initially total number of excitons are 1.3×10^4, 1.5×10^4, 1.5×10^4 and 1.8×10^4, respectively. We see that for all temperatures the exciton number decreases very little with time in the beginning and then it stays almost constant. The origin of this is the excitons are scattering out from the finite energy space due to singular initial distribution. For this reason we consider this as numerical artifact.

Then we have calculated the local effective temperature T_{local} for non degenerate case, by fitting the long energy tail of the exciton distribution by the function $e^{-e/k_BT_{local}}$ and studied how it is changing with time. So, first we have calculated the summation of excitons number n_r along the r direction, plot $\log(n_r)$ vs. energy curves, fit it with the function that is proportional to $e^{-e/k_BT_{local}}$ and get the values of T_{local} for different bath temperatures (see Figure 3.12), We see that for temperatures above 1K the effective temperature is coming down to bath temperature within ten nanoseconds. This is different for temperatures below 1K, where the effective temperature is coming down to bath temperature very slowly in around hundreds of nanoseconds only. Therefore we see cooling time is same for homogeneous system and within the trap.

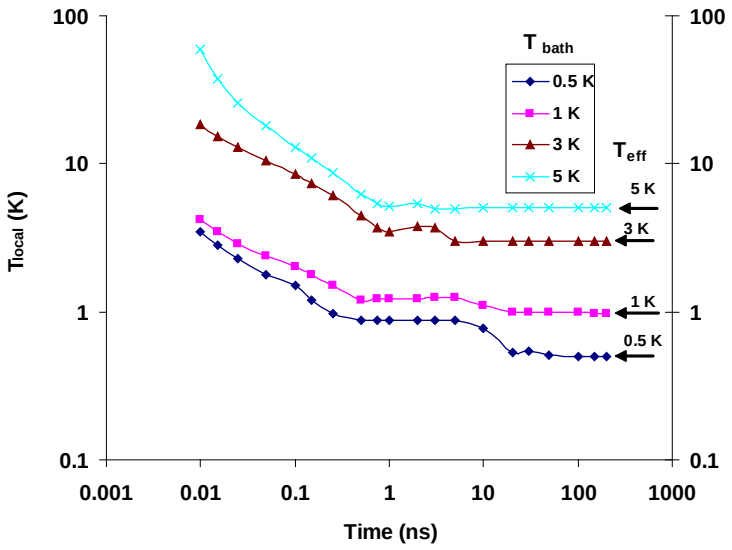

Figure 3.12: Local exciton temperature T_{local} vs. time for different bath temperatures including deformation potential phonon scattering. Here we see that the effective temperature is changing with time for different bath temperatures. The arrows on the right hand side indicate the effective temperatures. For 0.5 K, 1 K, 3 K and 5 K initially total number of excitons are 1.5×10^4, 1.5×10^4, 1.98×10^6 and 1.99×10^6, respectively. The curves serves as a guide to the eye.

We have also calculated global effective temperature for non degenerate case, (see figure 3.13) from the $n_e(r)$ vs. energy curves by using the relation of the exciton distribution $n_e(\vec{r}) \sim e^{-\left(\frac{r}{\xi}\right)^2}$ with $\xi = \sqrt{\frac{k_B T_{global}}{a}}$ and the steepness constant $a = 0.5\mu eV \cdot \mu m^{-2}$.

Therefore, we take the value of $\vec{r}$ at the half maximum of the exciton distribution, and therefore determined the effective temperature. In this case the global effective temperature is not coming down to bath temperature and there is deviation between simulation result and thermal equilibrium curve at 200 ns. In figure 3.14, we see that for the bath temperature 0.5 K, T_{global} is coming down to 0.8 K and for the bath temperature 3 K T_{global} is coming down to 4 K.

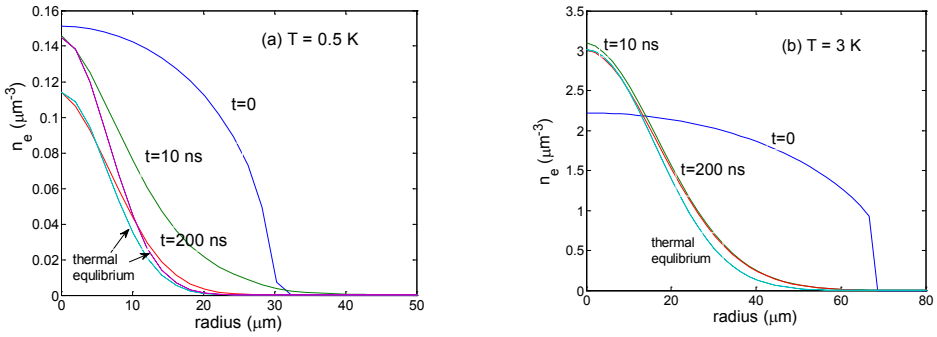

Figure 3.13: Spatial distribution n_e of excitons for different temperature as a function of time for non degenerate case, i.e. the summation of exciton number over the direction of energy vs. radius r, only with phonon scattering for 0.5 K and 3 K at different times. For 0.5 K and 3 K, initially total number of excitons are 1.02×10^4 and 1.98×10^6, respectively. Dotted curve represents n_e vs. r for thermal equilibrium case.

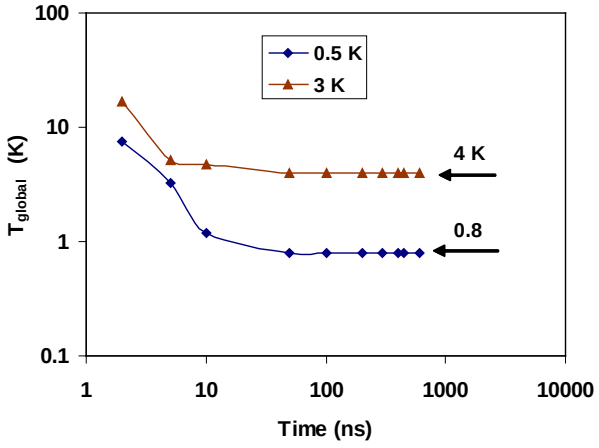

Figure 3.14: T_{global} vs. time for different bath temperatures including deformation potential phonon scattering only. For 0.5 K and 3 K, initially total number of excitons are 1.02×10^4 and 1.98×10^6, respectively. The arrows on the right hand side indicate the effective temperatures.

3.42 High number of excitons and the possibility of the Bose-Einstein Condensation

BEC of excitons has been studied in references [12-18]. Recently BEC of excitons has been studied theoretically [19] and experimentally at sub-Kelvin temperatures [20]. In a real experiment [20] the photoluminescence intensity, which is proportional to the number of excitons, is measured as a function of location z and the spectral position $\hbar\omega = e + e_0$, where e_0 is the minimum energy of the trap. From the Boltzmann equation we get the exciton distribution $N(\vec{r}, e')$ as a function of local energy $e' = \hbar\omega - a\vec{r}^{\,2} - e_0$ and radius $\vec{r}$. Then we transfer $\vec{r}$ to the Cartesian coordinates x, y and z and from the distribution $N(\vec{r}, e')$ we have calculated the distribution $N(z, e')$, where $N(z, e')$ is the exciton occupation number as a function of energy e' and location z. We see only the middle of the trap, therefore in our case x is equal to zero and the distance, that is actually the projected slit width, is Δx. Then by integrating $N(z, e')$ over the location y we get the energy distribution

$$\frac{N(z,e)}{\Delta x} = \int_{-\infty}^{\infty} 4\pi k^2 \cdot \frac{dk}{de} \cdot N(r = \sqrt{y^2 + z^2}, e')dy \tag{26}$$

or,

$$\frac{N(z,e)}{\Delta x} = 2\int_{0}^{\infty} \frac{4\sqrt{2}\pi M_x^{\,3/2}}{\hbar^3} \cdot \sqrt{e} \cdot N\left(r = \sqrt{y^2 + z^2}, e'\right)dy \quad . \tag{27}$$

Then we have integrated $\frac{N(z,e)}{\Delta x}$ over the z direction and got the energy distribution

$$\frac{N(e)}{\Delta x} = \int_{-\infty}^{\infty} N(z,e)dz = 2\int_{0}^{\infty} N(z,e)dz \tag{28}$$

which is proportional to the experimentally measured spectrum.

In figure 3.15, we have plotted $\frac{N(e)}{\Delta x}$ vs. energy curves for the temperature of 0.5 K with different exciton numbers within the trap and for different times. We see that if the initial exciton number within the trap is 1.02×10^9 then no BEC occurs (see figure 3.15a). At 10 ns exciton number is 1.86×10^8. After 10 ns the exciton number and the curve is stable

like 10 ns. In the next two steps we increase the exciton number by factor of 8. If the initial exciton number within the trap is 4.08×10^{9} and at 10 ns exciton number is 3.1×10^{8}, still no BEC occurs (see figure 3.15b), but finally if the initial exciton number within the trap is 8.16×10^{9}, then at 10 ns the BEC occurs (see figure 3.15c) and it is stable over a long time. At 10 ns exciton number is 4.6×10^{8} and a high peak near zero energy indicates BEC. To find the BEC we have changed excitons number in the trap. By changing n_0 in the initial distribution we have changed exciton number.

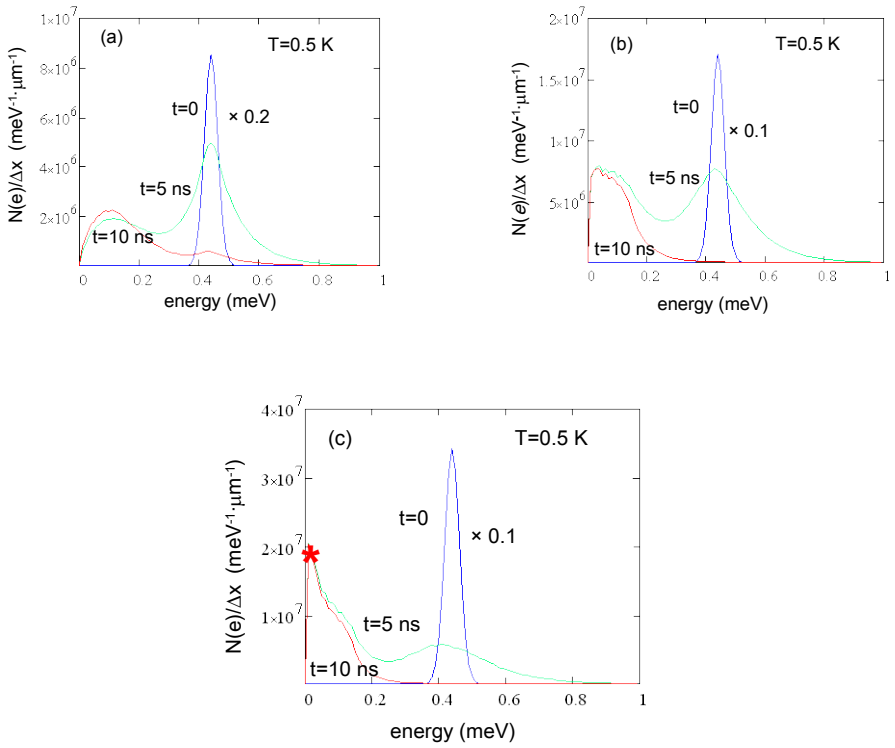

Figure 3.15: The spectral distribution $N(e)/\Delta x$ of excitons as a function of time vs. energy at 0.5 K for a non degenerate case. Figure 3.15a represents number of excitons within the trap vs. energy for 0.5 K at different times when initial exciton number within the trap is 1.02×10^{9}, at 10 ns exciton number is 1.86×10^{8} and $\Delta x = 1\ \mu$m. Figure 3.15b represents $N(e)/\Delta x$ vs. energy spectrum for 0.5 K at different times when initial exciton number within the trap is 4.08×10^{9} and at 10 ns exciton number is 3.05×10^{8}. In both cases we can not see any BEC. Figure 3.15c represents $N(e)/\Delta x$ vs. energy for 0.5 K at different times when initial exciton number within the trap is 8.16×10^{9} at 10 ns exciton number is 4.61×10^{8}. In figure 3.15c at 10 ns a high peak near zero energy (indicated by star) indicates the occurrence of BEC.

3.43 Comparison with the thermal equilibrium case

The table 1 shows (see Table 1.) a comparison between $N_c(T_{Bath})$, $N_c(T_{global})$, and N_{total}. N_{total} is the total number of excitons within the trap from our numerical simulations for which for the first time the BEC appears. $N_c(T_{Bath})$ is the critical number of excitons at thermal equilibrium for the bath temperature. $N_c(T_{global})$ is the critical number of the excitons at thermal equilibrium for the global effective temperature. From our numerical simulations, we see that the BEC occurs for all observed temperatures over and below the bath temperature of 1K. From the table we see that from our numerical simulations the values of N_{total} at the BEC are always one order of magnitude higher than $N_c(T_{Bath})$ for all temperatures.

Table 1. comparison between $N_c(T_{bath})$, $N_c(T_{eff})$ and N_{total}.

T_{bath} (K)	T_{global} (K)	$N_c(T_{bath})$	$N_c(T_{global})$	N_{total}
0.5	0.9	5.45×10^{7}	3.16×10^{8}	4.61×10^{8}
1	1.4	4.36×10^{8}	1.2×10^{9}	1.97×10^{9}
3	4.6	1.18×10^{10}	4.21×10^{10}	6.5×10^{10}
5	5.43	5.45×10^{10}	6.93×10^{10}	9.34×10^{10}

Figure 3.16 shows the total number of excitons N_{total} within the trap for which for the first time the BEC appears vs. time curves for the bath temperatures 0.5 K, 1 K, 3 K and 5 K, where we can see that exciton number is decreasing with time and coming to the BEC within the trap.

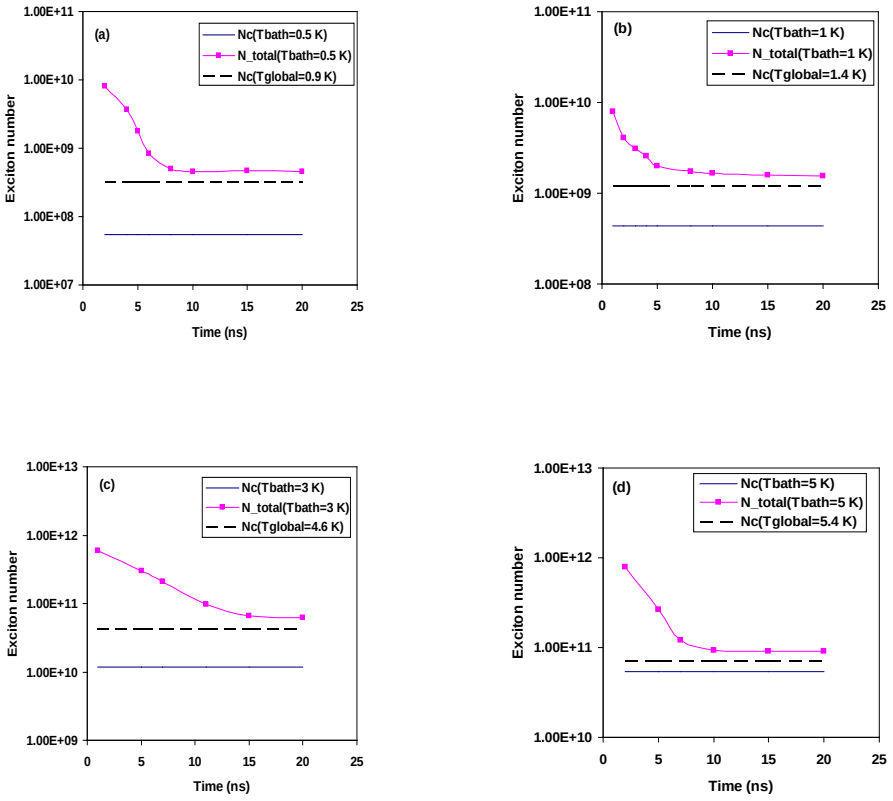

Figure 3.16: Exciton number vs. time curves for different temperatures. Red curves represent total number of excitons within the trap for which first time condensate appears vs. time for 0.5 K, 1 K, 3 K and 5 K. In these cases exciton number is decreasing with time and coming to condensate. Black dotted curves represent critical number of excitons at global effective temperature for the thermal equilibrium case. Blue curves represent critical number of excitons at bath temperature for the thermal equilibrium case.

3.5 Summary

We have seen the relaxation behaviour of excitons between 0.3 K to 5 K in homogeneous system and also within a potential trap. In homogeneous system and within the trap for both cases we see for temperatures between 0.5 K to 3 K excitons are thermalizing but for 0.3 K excitons are not thermalizing within their lifetime.

Within the trap, we see locally, that for the bath temperatures between 1 K to 5 K the local effective temperature T_{local} is coming down to bath temperature very quickly within 10 nanoseconds, but for the bath temperatures below 1 K, the T_{local} is coming down to the bath temperature very slowly within 100 nanoseconds only. Cooling time is same in homogeneous case. This effect can be related to the freezing out of phonons for very low temperatures. On a global scale, exciton effective temperature T_{global} is not coming down to the bath temperature. For low temperatures the global effective temperature is almost a factor of 2 larger than the bath temperatures.

We see from our numerical simulations, that the BEC occurs for all observed temperatures. By comparing our results with the thermal equilibrium case, we see that for all temperatures the BEC comes at a higher number of excitons than in thermal equilibrium case. The effective temperature at the time of BEC has good agreement with the global effective temperature.

References:

[1] Ell C, Ivanov A L, and Haug H, 1998, Phys. Rev. B **57**, 9663-73, "Relaxation kinetics of a low-density exciton gas in Cu2O".

[2] Ivanov A L, Ell C, and Haug H, 1997, *Phys. Rev. E* **55,** 6363-6369, "Phonon-assisted Boltzmann kinetics of a Bose gas: Generic solution for $T \leq T_c$ ".

- - Ivanov A L, Ell C, and Haug H, 1998, *Phys. Status Solidi B* **206,** 235-247, "Phonon-assisted Relaxation Kinetics of a Degenerate Bose gas".

[3] Snoke D W and Wolfe J P, 1989, *Phys. Rev. B* **39,** 4030-4037, "Population dynamics of a Bose gas near saturation".

[4] Griffin A, Snoke D W, and Stringari S, 1995, *Bose-Einstein Condensation* (Cambridge: Cambridge University Press) Chaps. 13 and 14.

[5] Hulin D, Mysyrowicz A, and Benoit a´ la Guillaume C, 1980, *Phys.Rev. Lett.* **45**, 1970-1973, "Evidence for Bose-Einstein Statistics in an Exciton Gas".

[6] Snoke D W, Wolfe J P, and Mysyrowicz A, 1987, *Phys. Rev. Lett.* **59**, 827-830, "Quantum saturation of a Bose gas: Excitons in Cu_2O".

[7] Lin J L and Wolfe J P, 1993, *Phys. Rev. Lett.* **71**, 1222-1225, "Bose-Einstein condensation of paraexcitons in stressed Cu_2O".

[8] Shen M Y, Yokouchi T, Koyama S, and Goto T, 1997, *Phys. Rev. B* **56**, 13 066-072, "Dynamics associated with Bose-Einstein statistics of orthoexcitons generated by resonant excitations in cuprous oxide".

[9] Schmitt A, Banyai L, and Haug H, 2001, Phys. Rev. B 63, 205113, "Trapping kinetics of excitons in a potential well".

[10] Trauernicht D P, Wolfe J P, and Mysyrowicz A, 1986, *Phys. Rev. B* **34**, 2561- 2575, "Thermodynamics of strain-confined paraexcitons in Cu2O".

[11] Snoke D W, Braun D, and Cardona M, 1991, *Phys Rev B* **44**, 2991, Carrier thermalization in Cu2O: Phonon emission by excitons"

[12] Snoke D W , Wolfe J P, and Mysyrowicz A, 1990, *Phys. Rev. B* **41**, 11171, "Evidence for Bose-Einstein condensation of excitons in Cu_2O".

[13] Banyai L, Gartner P, Schmitt O M, and Haug H, 1999, *Phys. Rev. B* **61**, 8823, "Condensation kinetics for bosonic excitons interacting with a thermal phonon bath".

[14] Banyai L A, Bundaru A M, Haug H, 2004, *Phys. Rev. B* **70**, 045201, "Quasiclassical approach to Bose condensation in a finite potential well".

[15] Gerton M G, Strekalov D, Prodan I, and Hulet G R, 2000, *Nature* **408,** 692, "Direct observation of growth and collapse of a Bose–Einstein condensate with attractive interactions".

[16] Butov L V, Lai C W, Ivanov A L, Gossard A C, and Chemla D S, 2002, *Nature* **417**, 47, "Towards Bose-Einstein condensation of excitons in potential traps".

[17] Stolz H and Semkat D, 2010, Phys. Rev. B **81**, 081302, "Unique signatures for Bose-Einstein condensation in the decay luminescence lineshape of weakly interacting excitons in a potential trap".

[18] Haug H, 2005, *Solid State Communications* **134**, 3-9, "Condensation kinetics of excitons".

[19] Naka N and Nagasawa N, 2005, *J. Lumin.* **112**, 11–16 "Bosonic stimulation of cold excitons in a harmonic potential trap in Cu2O".

[20] Yoshioka K, Chae E, and Kuwata-Gonokami M, 2011, *Nature Communications* 2, **328**, 1335, "Transition to a Bose-Einstein condensate and relaxation explosion of excitons at sub-Kelvin temperatures".

[21] Schwartz R, Naka N, Kieseling F, and Stolz H, 2012, *New Journal of Physics* **14**, 023054, "Dynamics of excitons in a potential trap at ultra-low temperatures: paraexcitons in Cu_2O".

Chapter 4

Auger Decay, Radiative and Non-Radiative Decay

This chapter contains the theory of Auger decay, radiative and non-radiative decay and the results of the Boltzmann equation with the phonon scattering, Auger decay, radiative and non-radiative decay within a potential trap. Previous work on Auger decay and the estimation of the Auger decay rate has been discussed.

4.1 Auger decay

In a semiconductor in which the electrons and holes remain unbound, one can observe a process in which one electron-hole pair recombines and giving the band gap energy to the remaining electron or hole. This three body process is called Auger recombination. In Cu_2O at low temperatures, the excitons are the dominant species and the density dependent decay is due to the collision of two excitons. In this case, Auger decay [1] destroys two excitons by recombination of one exciton and ionization the other one. The decay rate of excitons due to this two body decay is An^2 where A is the Auger constant and n is the gas density.

We assume that all of the ionized carriers released by Auger decay rebind to form new excitons, and we distribute these excitons over the whole energy range. Indeed, the electron hole pairs also recombine into orthoexcitons, but these are then converted into paraexcitons. Therefore, only paraexcitons need to be considered. So, in recovery, we are getting back half of the destroyed excitons by Auger decay. The complete effect of Auger decay on the exciton occupation number is [1]

$$\left(\frac{\partial N_{\vec{k}}}{\partial t}\right)_{\text{Auger Decay}} = -A_{pp} n(\vec{r}) N(\vec{r},\vec{k}) + \frac{1}{2} A_{pp} n(\vec{r})^2 \cdot \frac{(2\pi)^3}{\int d^3\vec{k}} \tag{1}$$

or,

$$\left(\frac{\partial N_e}{\partial t}\right)_{\text{Auger Decay}} = -A_{pp} n(\vec{r}) N(\vec{r},e) + \frac{1}{2} A_{pp} n(\vec{r})^2 \cdot \frac{(2\pi)^3}{\int_0^{e_{\max}} \frac{4\sqrt{2}\pi M_x^{3/2}\sqrt{e}}{\hbar^3} de}$$

$$= -A_{pp} n(\vec{r}) N(\vec{r},e) + \frac{1}{2} A_{pp} n(\vec{r})^2 \cdot \frac{3\hbar^3 (2\pi)^3}{8\sqrt{2}\pi M_x^{3/2} e_{\max}^{3/2}} \tag{2}$$

The first term is due to two body decay and the second term is due to recovery. A_{pp} is the Auger constant. $n(\vec{r})$ is the local density obtained by summation of exciton occupation number along the direction of energy.

$$n(\vec{r}) = \frac{1}{(2\pi)^3}\int_k 4\pi k^2 N(\vec{r},\vec{k})dk \tag{3}$$

or,

$$n(\vec{r}) = \frac{1}{(2\pi)^3}\int_e \frac{4\sqrt{2}\pi M_x^{3/2}\sqrt{e}}{\hbar^3}\cdot N(\vec{r},e)de \tag{4}$$

We have used an Auger constant $A_{pp} = 10^{-18}$ cm^3 / ns taken from recent experiments [2].

4.2 Radiative and non-radiative decay

The radiative and non-radiative decay [2] of paraexcitons occurs with the total rate Γ_p, i.e.

$$\left(\frac{\partial N_e}{\partial t}\right)_{\text{R\_NR decay}} = -\Gamma_p N(\vec{r},e) \tag{5}$$

From recent experiment the decay rate is $\Gamma_p = 1/650$ ns^{-1} [2].

4.3 Numerical modeling

By using the relation $e = \frac{e_0 j}{M}$, $\Delta e = \frac{e_0}{M}$ with M is an integer, we can write $n(\vec{r})$ (see equation 4) in the following way

$$n(i) = \frac{1}{(2\pi)^3}\sum_j \frac{4\sqrt{2}\pi M_x^{3/2}\sqrt{j}}{\hbar^3}\cdot\left(\frac{e_0}{M}\right)^{3/2}\cdot N(i,j) \tag{6}$$

Therefore we can write

$$\left(\frac{\partial N_j}{\partial t}\right)_{\text{Auger Decay}} = -A_{pp}n(i)N(i,j) + \frac{1}{2}A_{pp}n(i)^2\cdot\frac{(2\pi\hbar)^3}{\sum_j 4\sqrt{2}\pi M_x^{3/2}\left(\frac{e_0}{M}\right)^{3/2}\sqrt{j}} \tag{7}$$

and $\left(\frac{\partial N_j}{\partial t}\right)_{\text{R\_NR decay}} = -\Gamma_p N(i,j)$ (8)

4.4 Previous works on Auger decay and the estimations of the Auger decay rate

Several groups have been reported about the study on Auger decay process and also Auger decay constant. The first theoretical estimate of the Auger decay rate seems to be that by Culik [3]. From the Fermi's Golden rule he finds the transition rate from a pair of excitons to a free electron and hole. He finds Auger decay constant is zero for 1s excitons and 10^{-14} cm^3/ns for 2p excitons in Cu_2O.

The first experimental measurement of the Auger decay rate of excitons in Cu_2O was by Mysyrowicz et. al. [4]. That measurement was made with the steady state excitation. They extracted an Auger decay constant for the paraexcitons is 2×10^{-19} cm^3/ns. This experiment produces gasses consisting mainly of paraexcitons because the ortho to paraexciton conversion rate is fast on the scale of paraexciton lifetime. The two body decay constant was determined in [5] to be of the order of 1×10^{-20} cm^3/ns.

The first determination of the Auger decay constant through direct observation of the exciton decay rate was made by Snoke and Wolfe [6]. In a crystal at 2 K, Snoke and Wolfe measured the lifetime of the orthoexciton luminescence following an intense 100 ps laser pulse. They reported an Auger decay constant 10^{-18} cm^3/ns for orthoexcitons.

Trauernicht, Wolf and Mysyrowicz [7] reported a rate 0.05/sec for paraexcitons confined to a parabolic strain well.

O'Hara et al. [8] determined the density of excitons by measuring their absolute brightness in a calibrated optical system and measuring the expanding volume occupied by the excitons. The luminescence signal following sub nanosecond laser excitation exhibits a decay rate which is strongly depend on the particle density. They reported that the effective Auger constant is $A = 7\times10^{-17}\,\text{cm}^3/\text{ns}$.

Warren et al. [9] examined the decay of thermalized excitons in Cu_2O and determined their lifetime against two-body decay. They reported that the Auger constant is $A = 0.6 \times 10^{-16} \text{cm}^3/\text{ns}$.

Kavoulakis and Mysyrowicz [10] examined the interconversion between the angular-momentum triplet state excitons and the angular momentum singlet-state excitons by a spin exchange process. They estimated the two-body decay constant is $A \approx 10^{-16} \text{cm}^3/\text{ns}$.

Wolf et al. [11] studied Auger recombination of excitons in Cu_2O by time and space resolved luminescence. Their measured Auger constant range from $A(72K) = 1.8 \times 10^{-16}$ cm^3/ns to $A(212K) = 0.5 \times 10^{-16}$ cm^3/ns respectively.

Kavoulakis and Baym [12] studied the non-radiative Auger decay of excitons in Cu_2O, in which two excitons scatter to an excited electron and hole. They calculated the Auger decay rate for both the direct and phonon assisted mechanisms and they concluded that the rate of the phonon assisted Auger mechanism is much larger than the rate of the direct process. Furthermore, the experimental results differ by at least four orders of magnitude from the theoretical predictions [11, 12].

Recently, Yoshioka et al. [13] studied a density dependent loss of optically inactive paraexcitons as a function of temperature over a wide range of densities in Cu_2O. They reported that the Auger decay rate is 4×10^{-16} cm^3/ns in bulk crystals.
Recently [14], it was suggested that the two-body decay process is actually related to the formation of a biexciton state.
As our aim is to model the experimental work of Ref. [2], we take the Auger constant from this report as $A_{pp} = 10^{-18}$ cm^3/ns.

4.5 Results within a potential trap including phonon scattering, Auger decay, radiative and non-radiative decay

The Boltzmann equation with radiative and non-radiative decay and Auger decay is given by

$$\frac{\partial N}{\partial t} = -\frac{2v_s}{\sqrt{M}\Delta r}\sqrt{j}\{N(i,j) - N(i-1,j)\}$$
$$+\frac{2a\Delta r\sqrt{M}}{M_x v_s} i\sqrt{j}\{N(i,j+1) - N(i,j)\} + \left(\frac{\partial N}{\partial t}\right)_{\text{phonon-scattering}}$$
$$+\left(\frac{\partial N}{\partial t}\right)_{\text{R\_NR\_decay}} + \left(\frac{\partial N}{\partial t}\right)_{\text{Auger\_decay}} \quad (9)$$

4.51 Low number of excitons

After solving the Boltzmann equation with phonon scattering, radiative, non-radiative decay and Auger decay with low number of excitons within the trap we don't see any Auger effect. In section 4.4 we already discussed about previous estimates of Auger decay constant. We have used the Auger constant $A_{pp} = 10^{-18}$ cm^3/ns [2] from recent experimental work.

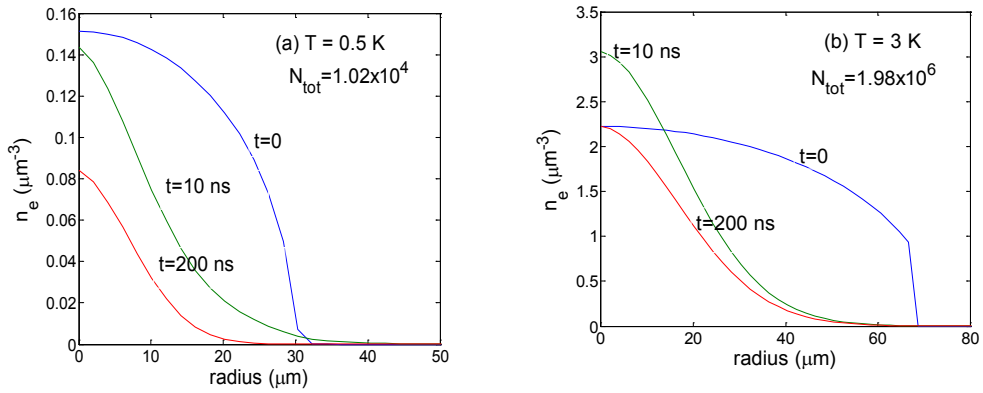

Figure 4.1: Spatial distribution n_e of excitons for different temperatures as a function of time i.e. the summation of exciton number over the direction of energy vs. radius r including Auger decay, radiative and non-radiative recombination with phonon scattering for 0.5 K (figure 4.1a) and 3 K (figure 4.1b) at different times. At 0.5 K and 3 K initial total number of excitons are 1.02×10^4 and 1.98×10^6, respectively.

4.52 High number of excitons and the possibility of the Bose-Einstein condensation

After solving the Boltzmann equation with phonon scattering, radiative, non-radiative decay and Auger decay with the Auger constant $A_{pp} = 10^{-18}$ cm^3 / ns [2], and with high number of excitons within the trap we see that the total number of excitons decreasing with increasing time. Figure 4.2 represents exciton occupation n_r at 3 K by summation of exciton number of non-degenerate exciton gas in r direction vs. energy for different times. We see how exciton distribution is changing with time from 0 to 200 ns.

In figure 4.3, we see locally, that the effective temperatures are not coming down to the bath temperatures even after 600 ns. We have calculated the local effective temperature T_{local} by fitting the long energy tail of the exciton distribution by a function proportional to $e^{-e/k_B T_{local}}$. This Boltzman distribution $f(e) = e^{-e/k_B T}$ is an approximation which is derived from Bose-Einstein distribution $f(e) = \dfrac{1}{e^{-e/k_B T} - 1}$ for $e >> k_B T$.

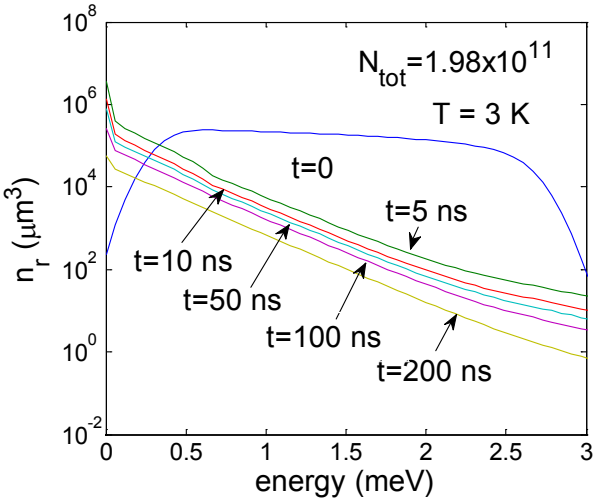

Figure 4.2: Exciton occupation n_r at 3 K by the summation of exciton number of non-degenerate exciton gas in r direction vs. energy at different times. Initially total number of excitons is 1.98×10^{11}.

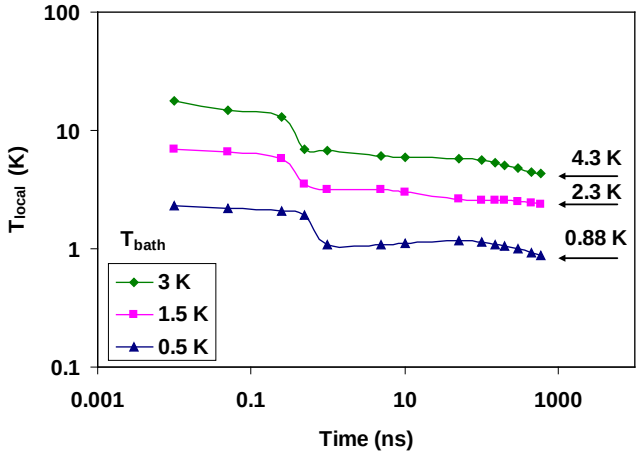

Figure 4.3: Local effective temperature T_{local} vs. time curves for different bath temperatures including deformation potential phonon scattering, radiative, non-radiative decay and Auger decay. The arrows on the right hand side indicate the effective temperatures. We see that the effective temperatures are not coming down to bath temperatures even after 600 ns. At 0.5 K, 1.5 K and 3 K initial exciton number within the trap are 1.02×10^{9}, 2.76×10^{10} and 1.99×10^{11}, respectively. The curves serve as a guide to the eye.

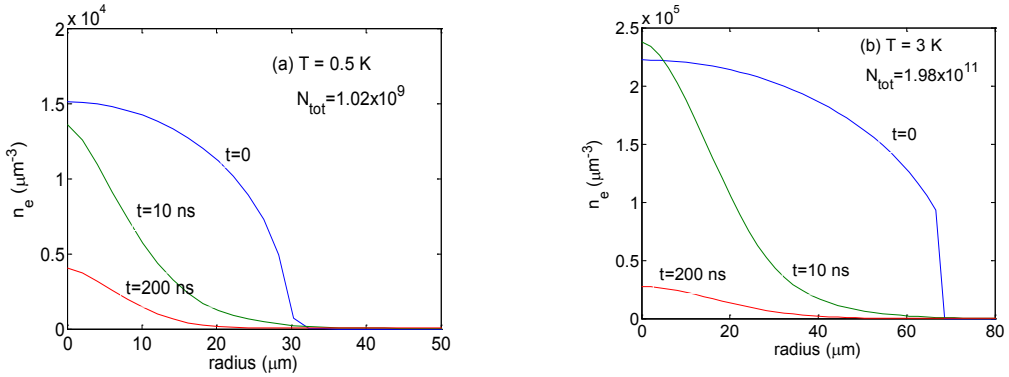

Figure 4.4: Spatial distribution n_e of excitons for different temperatures as a function of time for non degenerate case, i.e. the summation of exciton number over the direction of energy vs. radius r including Auger decay, radiative and non radiative decay with phonon scattering for 0.5 K (figure 4.4a) and 3 K (figure 4.4b) at different times. At 0.5 K and 3 K initial total number of excitons are 1.02×10^{9} and 1.98×10^{11}, respectively.

Figure 4.4 represents exciton distribution n_e vs. radius at different times for 3 K and 0.5 K. We have calculated global effective temperature T_{global} (see figure 4.5) from the $n_e(r)$ vs. energy curves by using the relation of the exciton distribution $n_e(\vec{r}) \sim e^{-\left(\frac{r}{\xi}\right)^2}$, with $\xi = \sqrt{\frac{k_B T_{global}}{a}}$ and the steepness constant $a = 0.5 \mu eV \cdot \mu m^{-2}$. Therefore, we take the value of r at the half maximum of the exciton distribution, and determined the effective temperature. Globally, the effective temperature is also not coming down to the bath temperature.

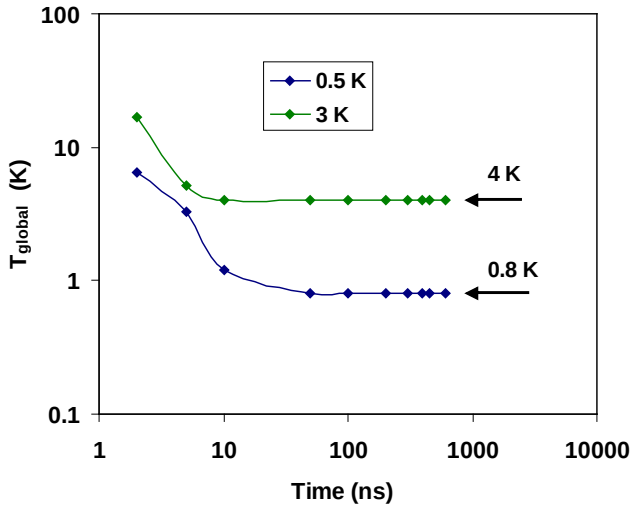

Figure 4.5: Excitons global temperature T_{global} vs. time for different bath temperatures including Auger decay. The arrows on the right hand side indicate the effective temperatures. We see the global effective temperatures are not coming down to the bath temperatures.

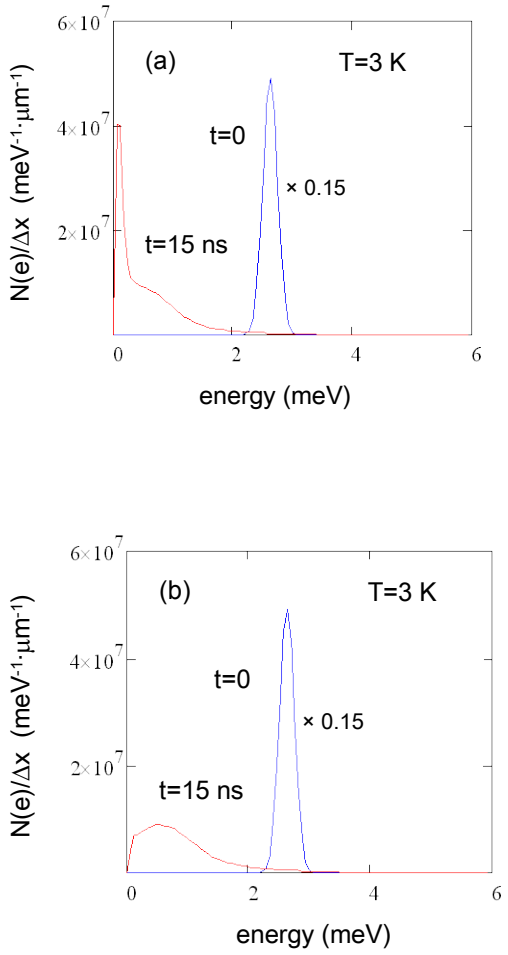

Figure 4.6: The spectrall distribution N(*e*)/ Δx of exciton as a function of time vs. energy at 3 K with and without Auger decay, radiative and non-radiative decay. Figure 4.6a represents the results only with phonon scattering. Here initial exciton number within the trap is 5.97×10^{11} and at 15 ns exciton number is 6.5×10^{10}. At 15 ns, we see that a high peak near zero energy occurs which indicates BEC. Figure 4.6b represents the results including Auger decay, radiative and non-radiative decay with the phonon scattering, and the same exciton number within the trap. In this case we don't see any BEC.

The critical number of excitons N_c at condensate for the BEC for the thermal equilibrium case

$$N_c = 1.202\left(\frac{k_B T}{\hbar\Omega}\right)^3 \tag{10}$$

with the frequency $\Omega = \sqrt{\frac{2a}{M_x}}$, the exciton mass $M_x = 2.61 m_e$, the steepness constant $a = 0.5\mu eV \cdot \mu m^{-2}$ and the temperature T.

To study on BEC in the case of Auger decay, if we increase the exciton number over the critical number we do not see any BEC for any temperature at any time. In figure 4.6 we compare the total number of excitons within the trap vs. energy for the bath temperature of 3 K with and without Auger decay, radiative and non-radiative decay with the same initial exciton numbers within the trap. Here we see that without Auger decay, radiative and non-radiative decay the BEC exist at 15 ns (see figure 4.6a) but with Auger decay, radiative and non-radiative decay no BEC occurs at any time (see figure 4.6b). A similar behaviour was found for other temperatures.

4.6 Summary

After solving the Boltzmann equation with the phonon scattering, radiative, non-radiative decay and Auger decay, we see locally and globally for both cases the effective temperature is not coming down to the bath temperature after long times due to the heating of the exciton gas. In this case, no BEC occurs. Whereas in the case of phonon scattering only, as we discussed in chapter 3, we have seen that locally the effective temperature was coming down to the bath temperature but globally the effective temperature was not coming down to the bath temperature. In that case BEC occurs for all temperatures over and below 1 K. Therefore Auger decay makes a barrier to get the BEC.

References:

[1] O'Hara K E and Wolfe J P, 2000, *Phys. Rev. B* **62,** 12 909-921, "Relaxation kinetics of excitons in cuprous oxide".

[2] Schwartz R, Naka N, Kieseling F, and Stolz H, 2011, *New Journal of Physics* **14**, 023054, "Dynamics of excitons in a potential trap at ultra-low temperatures: paraexcitons in Cu_2O".

[3] Culik F, 1966, *Czech J Phys* **16**, 194, "Exciton-exciton Collisions in crystals".

[4] Mysyrowicz A, D Hulin, and C Benoit a la Guillaume, 1981, *J Luminescence* **24**, 629, "Study of Exciton Luminescence in Cu_2O".

[5] Hulin D, Mysyrowicz A, and Benoit a la Guillaume C, 1980, *Phys. Rev. Lett.*, **45**, 1970, "Evidence for Bose-Einstein Statistics in an Exciton Gas".

[6] Snoke D W and J P Wolfe, 1990, *Phys Rev B* **42**, 7876, "Picosecond dynamics of degenerate orthoexcitons in Cu_2O".

[7] Trauernicht D P, Wolf J P, and Mysyrowicz A, 1986, Phys. Rev. B **34**, 2561, "Thermodynamics of Strain-confined Paraexcitons in Cu_2O".

[8] O'Hara K E, J R Gullingsrud, and J P Wolfe, 1999, Phys Rev B **60**, 10872, "Auger Decay of Excitons in Cu_2O".

[9] Warren J T, O'Hara K E, and Wolfe J P, 1999, Phys Rev B **61**, 8215, "Two-body Decay of Thermalized Excitons in Cu_2O".

[10] Kavoulakis G M and Mysyrowicz A, 2000, Phys Rev B **61**, 16619, "Auger decay, spin exchange, and their connection to Bose-Einstein condensation of excitons in Cu_2O".

[11] Wolfe J P, Jang J I, 2005, Solid State Communications **134**, 143, "New perspectives on kinetics of excitons in Cu_2O".

[12] Kavoulakis G M and Baym G, 1996, Phys. Rev. B **54**, 16625, "Auger decay of degenerate and Bose-condensed excitons in Cu_2O".

[13] Yoshioka K, Ideguchi T, Mysyrowicz A and Kuwata-Gonokami M, 2010, Phys. Rev. B, **82**, 041201, "Quantum inelastic collisions between paraexcitons in Cu_2O".

[14] Jang J I and Wolfe J P, 2006, Phys. Rev. B, **74**, 045211, "Auger recombination and biexcitons in Cu2O: A case for dark excitonic matter".

Chapter 5

Elastic Scattering

In this chapter we have discussed about the elastic scattering, the results of the Boltzmann equation with the elastic scattering and the phonon scattering in the homogeneous system and the results of the Boltzmann equation with the elastic scattering and the phonon scattering within a potential trap. The possibility of Bose-Einstein condensation of exciton in Cu_2O, within the potential trap is discussed.

5.1 Theory

5.11 General equation for the elastic scattering

Elastic scattering term of the Boltzmann equation [1] describes the two-body scattering of boson gas in a homogeneous system. The scattering rate involves all events in which excitons of momentum p and p_2 scatter into k and k_2. There are two initial exciton momenta and two final exciton momenta involved whereas in the case of phonon scattering, one initial exciton momentum and one final exciton momentum involved.

The scattering rate of the exciton into state k is [2, 3]

$$\left(\frac{dN_{\vec{k}}}{dt}\right)_{elastic\_in\_scattering} d^3\vec{k} = \frac{2\pi}{\hbar}\cdot\frac{V^2}{(2\pi)^6}\int d^3\vec{k}\; d^3\vec{p}\; d^3\vec{p}_2\; d^3\vec{k}_2\; M^2_{matrix} \times\{N_{\vec{p}}N_{\vec{p}_2}(1+N_{\vec{k}})(1+N_{\vec{k}_2})\}\delta(\vec{p}+\vec{p}_2-\vec{k}-\vec{k}_2) \times\delta(e_{\vec{p}}+e_{\vec{p}_2}-e_{\vec{k}}-e_{\vec{k}_2}) \quad (1)$$

Where $e_{\vec{k}} = \hbar^2k^2/2M_x$, $e_{\vec{p}} = \hbar^2p^2/2M_x$, $e_{\vec{p}_2} = \hbar^2{p_2}^2/2M_x$ and $e_{\vec{k}_2} = \hbar^2{k_2}^2/2M_x$ are the exciton energy in wavevector $\vec{k}$ state, $\vec{p}$ state, $\vec{p}_2$ state, and $\vec{k}_2$ state, respectively. $N_{\vec{k}}$, $N_{\vec{p}}$, $N_{\vec{p}_2}$ and $N_{\vec{k}_2}$ are the exciton occupation number in $\vec{k}$ state, $\vec{p}$ state, $\vec{p}_2$ state, and $\vec{k}_2$ state, respectively. $M_{matrix} = \dfrac{4\pi\hbar^2a_1}{M_xV}$ is the matrix element [3] with a_1 the scattering length. Here $e_{\vec{k}_2} = e_{\vec{p}} + e_{\vec{p}_2} - e_{\vec{k}}$ or $\vec{k}_2 = \sqrt{\vec{p}^2 + \vec{p}_2^2 - \vec{k}^2}$.

The scattering rate of the exciton out of state k is [2, 3]

$$\left(\frac{dN_{\vec{k}}}{dt}\right)_{elastic\_out\_scattering} d^3\vec{k} = \frac{2\pi}{\hbar}\cdot\frac{V^2}{(2\pi)^6}\int d^3\vec{k}\; d^3\vec{p}\; d^3\vec{p}_2\; d^3\vec{k}_2\; M^2_{matrix} \times\{N_{\vec{k}}N_{\vec{k}_2}(1+N_{\vec{p}})(1+N_{\vec{p}_2})\}\delta(\vec{k}+\vec{k}_2-\vec{p}-\vec{p}_2)$$

$$\times\delta(e_{\vec{k}}+e_{\vec{k}_2}-e_{\vec{p}}-e_{\vec{p}_2}) \tag{2}$$

The net scattering rate of the exciton in and out of the volume of k space $d^3\vec{k}$ is given by

$$\left(\frac{dN_{\vec{k}}}{dt}\right)_{elastic\_scattering}=\left(\frac{dN_{\vec{k}}}{dt}\right)_{elastic\_in\_scattering}-\left(\frac{dN_{\vec{k}}}{dt}\right)_{elastic\_out\_scattering} \tag{3}$$

or,

$$\begin{aligned}\left(\frac{dN_{\vec{k}}}{dt}\right)_{elastic\_scattering}&=\frac{2\pi}{\hbar}\cdot\frac{V^2}{(2\pi)^6}\int d^3\vec{p}\ d^3\vec{p}_2\ d^3\vec{k}_2\ M^2_{matrix}\\&\times[\{N_{\vec{p}}N_{\vec{p}_2}(1+N_{\vec{k}})(1+N_{\vec{k}_2})\}\delta(\vec{p}+\vec{p}_2-\vec{k}-\vec{k}_2)\\&\times\delta(e_{\vec{p}}+e_{\vec{p}_2}-e_{\vec{k}}-e_{\vec{k}_2})-\{N_{\vec{k}}N_{\vec{k}_2}(1+N_{\vec{p}})(1+N_{\vec{p}_2})\}\\&\times\delta(\vec{k}+\vec{k}_2-\vec{p}-\vec{p}_2)\delta(e_{\vec{k}}+e_{\vec{k}_2}-e_{\vec{p}}-e_{\vec{p}_2})]\end{aligned} \tag{4}$$

$$\begin{aligned}\left(\frac{dN_{\vec{k}}}{dt}\right)_{elastic\_scattering}&=\frac{2\pi}{\hbar}\cdot\frac{V^2}{(2\pi)^6}\cdot\left(\frac{4\pi\hbar^2a_1}{M_xV}\right)^2\cdot(2\pi)^2\cdot\frac{2M_x}{\hbar^2}\\&\times\int\vec{p}^2dp\int\vec{p}_2^2dp_2\cdot\min[\vec{p},\vec{p}_2,\vec{k},\vec{k}_2]\cdot\frac{1}{\vec{k}\ \vec{p}\ \vec{p}_2}\\&\times[\{N_{\vec{p}}N_{\vec{p}_2}(1+N_{\vec{k}})(1+N_{\vec{k}_2})\}-\{N_{\vec{k}}N_{\vec{k}_2}(1+N_{\vec{p}})(1+N_{\vec{p}_2})\}]\end{aligned} \tag{5}$$

$$\begin{aligned}\left(\frac{dN_{\vec{k}}}{dt}\right)_{elastic\_scattering}&=\frac{2\pi}{\hbar}\cdot\frac{V^2}{(2\pi)^6}\cdot\left(\frac{4\pi\hbar^2a_1}{M_xV}\right)^2\cdot(2\pi)^2\cdot\frac{2M_x}{\hbar^2}\cdot\frac{1}{\vec{k}}\\&\times\int\vec{p}dp\int\vec{p}_2dp_2\cdot\min[\vec{p},\vec{p}_2,\vec{k},\vec{k}_2]\\&\times[\{N_{\vec{p}}N_{\vec{p}_2}(1+N_{\vec{k}})(1+N_{\vec{k}_2})\}-\{N_{\vec{k}}N_{\vec{k}_2}(1+N_{\vec{p}})(1+N_{\vec{p}_2})\}]\end{aligned} \tag{6}$$

5.12 Transfer momentum terms to energy terms

We know $e_{\vec{k}} = \hbar^2 k^2 / 2M_x$, $e_{\vec{p}} = \hbar^2 p^2 / 2M_x$ and $e_{\vec{p}_2} = \hbar^2 p_2{}^2 / 2M_x$.

Therefore $k = \sqrt{\frac{2M_x e_{\vec{k}}}{\hbar^2}}$, $p\ dp = \frac{1}{2\left(\frac{\hbar^2}{2M_x}\right)} de_p$ and $p_2\ dp_2 = \frac{1}{2\left(\frac{\hbar^2}{2M_x}\right)} de_{p_2}$.

By using these relation we get

$$\left(\frac{dN_{e_{\vec{k}}}}{dt}\right)_{elastic\_scattering} = \frac{2\pi}{\hbar} \cdot \frac{V^2}{(2\pi)^6} \cdot \left(\frac{4\pi\hbar^2 a_1}{M_x V}\right)^2 \cdot \frac{(2\pi)^2}{4} \cdot \left(\frac{2M_x}{\hbar^2}\right)^3 \cdot \frac{1}{\sqrt{\frac{2M_x e_{\vec{k}}}{\hbar^2}}}$$

$$\times \int de_p \int de_{p_2} \cdot \min[\vec{p}, \vec{p}_2, \vec{k}, \vec{k}_2]$$

$$\times [\{N_{e_{\vec{p}}} N_{e_{\vec{p}_2}} (1+N_{e_{\vec{k}}})(1+N_{e_{\vec{k}_2}})\} - \{N_{e_{\vec{k}}} N_{e_{\vec{k}_2}} (1+N_{e_{\vec{p}}})(1+N_{e_{\vec{p}_2}})\}] \qquad (7)$$

$$\left(\frac{dN_{e_{\vec{k}}}}{dt}\right)_{elastic\_scattering} = \frac{4a_1^2 M_x}{\pi\hbar^3} \cdot \frac{1}{\sqrt{e_{\vec{k}}}} \int de_p \int de_{p_2} \cdot \min[\sqrt{e_{\vec{p}}}, \sqrt{e_{\vec{p}_2}}, \sqrt{e_{\vec{k}}}, \sqrt{e_{\vec{k}_2}}]$$

$$\times [\{N_{e_{\vec{p}}} N_{e_{\vec{p}_2}} (1+N_{e_{\vec{k}}})(1+N_{e_{\vec{k}_2}})\} - \{N_{e_{\vec{k}}} N_{e_{\vec{k}_2}} (1+N_{e_{\vec{p}}})(1+N_{e_{\vec{p}_2}})\}] \qquad (8)$$

Now two conditions arise [4, 5], the first one is $e_k > e_p$ and then we can write the equation

$$\left(\frac{dN_{e_{\vec{k}}}}{dt}\right)_{elastic\_scattering} = \frac{4a_1^2 M_x}{\pi\hbar^3} \cdot \frac{1}{\sqrt{e_{\vec{k}}}} \int_0^{e_k} de_p \int_{e_k - e_p}^{\infty} de_{p_2} \cdot \min[\sqrt{e_{\vec{p}}}, \sqrt{e_{\vec{p}_2}}, \sqrt{e_{\vec{k}}}, \sqrt{e_{\vec{k}_2}}]$$

$$\times [\{N_{e_{\vec{p}}} N_{e_{\vec{p}_2}} (1+N_{e_{\vec{k}}})(1+N_{e_{\vec{k}_2}})\} - \{N_{e_{\vec{k}}} N_{e_{\vec{k}_2}} (1+N_{e_{\vec{p}}})(1+N_{e_{\vec{p}_2}})\}] \qquad (9)$$

The second condition is $e_k < e_p$ and then we can write the equation

$$\left(\frac{dN_{e_{\vec{k}}}}{dt}\right)_{elastic\_scattering} = \frac{4a_1^2 M_x}{\pi\hbar^3}\cdot\frac{1}{\sqrt{e_{\vec{k}}}}\int_{e_k}^{\infty} de_p \int_0^{\infty} de_{p_2}\cdot\min[\sqrt{e_{\vec{p}}},\sqrt{e_{\vec{p}_2}},\sqrt{e_{\vec{k}}},\sqrt{e_{\vec{k}_2}}]$$
$$\times[\{N_{e_{\vec{p}}}N_{e_{\vec{p}_2}}(1+N_{e_{\vec{k}}})(1+N_{e_{\vec{k}_2}})\}-\{N_{e_{\vec{k}}}N_{e_{\vec{k}_2}}(1+N_{e_{\vec{p}}})(1+N_{e_{\vec{p}_2}})\}] \quad (10)$$

Therefore the complete equation is

$$\left(\frac{dN_{e_{\vec{k}}}}{dt}\right)_{elastic\_scattering} = \frac{4a_1^2 M_x}{\pi\hbar^3}\cdot\frac{1}{\sqrt{e_{\vec{k}}}}\cdot\left[\int_0^{e_k} de_p \int_{e_k-e_p}^{\infty} de_{p_2}\cdot\min[\sqrt{e_{\vec{p}}},\sqrt{e_{\vec{p}_2}},\sqrt{e_{\vec{k}}},\sqrt{e_{\vec{k}_2}}]\right.$$
$$\left.+\int_{e_k}^{\infty} de_p \int_0^{\infty} de_{p_2}\cdot\min[\sqrt{e_{\vec{p}}},\sqrt{e_{\vec{p}_2}},\sqrt{e_{\vec{k}}},\sqrt{e_{\vec{k}_2}}]\right]$$
$$\times[\{N_{e_{\vec{p}}}N_{e_{\vec{p}_2}}(1+N_{e_{\vec{k}}})(1+N_{e_{\vec{k}_2}})\}-\{N_{e_{\vec{k}}}N_{e_{\vec{k}_2}}(1+N_{e_{\vec{p}}})(1+N_{e_{\vec{p}_2}})\}] \quad (11)$$

5.13 Equation for zero energy state

At k=0 the elastic scattering term is given by

$$\left(\frac{dN_{e_{\vec{k}}=0}}{dt}\right)_{elastic\_scattering} = \frac{4a_1^2 M_x}{\pi\hbar^3}\cdot\left[\int_0^{\infty} de_p \int_0^{\infty} de_{p_2}\cdot[\{N_{e_{\vec{p}}}N_{e_{\vec{p}_2}}(1+N_{e_{\vec{k}}=0})(1+N_{e_{\vec{k}_2}})\}\right.$$
$$\left.-\{N_{e_{\vec{k}}=0}N_{e_{\vec{k}_2}}(1+N_{e_{\vec{p}}})(1+N_{e_{\vec{p}_2}})\}\right] \quad (12)$$

5.14 Equations for in-scattering and out-scattering terms from k=0 state

If $\vec{k}_2 = \vec{0}$, we get [6]

$$\left(\frac{dN_{\vec{k}_2=0}}{dt}\right)_{out\_scattering\_zero} = \frac{2\pi}{\hbar}\cdot\frac{V^2}{(2\pi)^6}\cdot\left(\frac{4\pi\hbar^2 a_1}{M_x V}\right)^2\cdot\frac{N_{\vec{k}_2=0}}{V}\int_0^{e_{\vec{k}}} p^2 dp\cdot 8\pi^2\cdot\frac{M_x}{\hbar^2}\cdot\frac{1}{\vec{k}\,\vec{p}}$$

$$\times\{N_{\vec{p}}N_{\vec{p}_2} - N_{\vec{k}}(1+N_{\vec{p}_2}+N_{\vec{p}})\} \tag{13}$$

or,

$$\left(\frac{dN_{e_{\vec{k}_2}=0}}{dt}\right)_{out\_scattering\_zero} = \frac{2\pi}{\hbar}\cdot\frac{V^2}{(2\pi)^6}\cdot\left(\frac{4\pi\hbar^2 a_1}{M_x V}\right)^2\cdot\frac{N_{e_{\vec{k}_2}=0}}{V}\cdot 8\pi^2\cdot\left(\frac{M_x}{\hbar^2}\right)^2\cdot\int_0^{e_{\vec{k}}}\frac{1}{k}\,de_{\vec{p}}$$

$$\times\{N_{e_{\vec{p}}}N_{e_{\vec{p}_2}} - N_{e_{\vec{k}}}(1+N_{e_{\vec{p}_2}}+N_{e_{\vec{p}}})\} \tag{14}$$

or,

$$\left(\frac{dN_{e_{\vec{k}_2}=0}}{dt}\right)_{out\_scattering\_zero} = \frac{4a_1^2}{\pi\hbar}\cdot\frac{N_{e_{\vec{k}_2}=0}}{V}\left[\int_0^{e_{\vec{k}}}\frac{1}{k}\cdot de_p\cdot\{N_{e_{\vec{p}}}N_{e_{\vec{p}_2}} - N_{e_{\vec{k}}}(1+N_{e_{\vec{p}_2}}+N_{e_{\vec{p}}})\}\right] \tag{15}$$

with $e_{\vec{p}_2} = e_{\vec{k}} - e_{\vec{p}}$ and V is the volume.

Similarly if $\vec{p}_2 = 0$, we get [6]

$$\left(\frac{dN_{e_{\vec{p}_2}=0}}{dt}\right)_{in\_scattering\_zero} = \frac{4a_1^2}{\pi\hbar}\cdot\frac{N_{e_{\vec{p}_2}=0}}{V}\left[\int_{e_{\vec{k}}}^{\infty}\frac{1}{k}\cdot de_p\cdot\{N_{e_{\vec{p}}}(1+N_{e_{\vec{k}_2}}+N_{e_{\vec{k}}}) - N_{e_{\vec{k}}}N_{e_{\vec{k}_2}}\}\right] \tag{16}$$

with $e_{\vec{k}_2} = e_{\vec{p}} - e_{\vec{k}}$.

5.2 Numerical modeling

We discretize the energy $e_{\vec{k}} = (j_k - 1)\Delta e$ where $j_k = 1.....ne$, ne is an integer and $\Delta e = \frac{e_0}{M}$ with M is an integer. Analogously we discretize the energy $e_{\vec{p}} = (j_p - 1)\Delta e$, $e_{\vec{p}_2} = (j_{p_2} - 1)\Delta e$, $e_{\vec{k}_2} = (j_{k_2} - 1)\Delta e$.

$$\left(\frac{dN_{j_k}}{dt}\right)_{elastic\_scattering} = \frac{4a_1^2 M_x}{\pi\hbar^3}\cdot\frac{1}{\sqrt{j_k - 1}}\cdot\left(\frac{e_0}{M}\right)^2\cdot\left[\sum_0^{j_{\vec{k}}}\sum_{j_{\vec{k}}-j_{\vec{p}}}^{\infty}\min[\sqrt{j_p - 1},\sqrt{j_{p_2} - 1},\sqrt{j_k - 1},\sqrt{j_{k_2} - 1}]\right.$$

$$+\sum_{j_{\vec{k}}}^{\infty}\sum_{0}^{\infty}\min[\sqrt{j_p-1},\sqrt{j_{p_2}-1},\sqrt{j_k-1},\sqrt{j_{k_2}-1}]\Bigg]$$

$$\times[\{N_{j_p}N_{j_{p2}}(1+N_{j_k})(1+N_{j_{k_2}})\}-\{N_{j_k}N_{j_{k_2}}(1+N_{j_p})(1+N_{j_{p2}})\}] \quad (17)$$

We can write the equation (12), for $j_{\vec{k}}=1$ in the form

$$\left(\frac{dN_{j_k=1}}{dt}\right)_{elastic\_scattering}=\frac{4a_1^2M_x}{\pi\hbar^3}\cdot\left(\frac{e_0}{M}\right)^2\cdot\Bigg[\sum_{0}^{\infty}\sum_{0}^{\infty}[\{N_{j_p}N_{j_{p_2}}(1+N_{j_k=1})(1+N_{j_{k_2}})\}$$

$$-\{N_{j_k=1}N_{j_{k_2}}(1+N_{j_p})(1+N_{j_{p_2}})\}]\Bigg] \quad (18)$$

Similarly we can write the equations (15) and (16), for $j_{\vec{k}_2}=1$ and $j_{\vec{p}_2}=1$ in the form

$$\left(\frac{dN_{j_{\vec{k}_2}=1}}{dt}\right)_{out\_scattering\_zero}=\frac{4a_1^2}{\pi\sqrt{2M_x}}\cdot\frac{N_{j_{\vec{k}_2}=1}}{V}\cdot\left(\frac{e_0}{M}\right)^{1/2}$$

$$\times\Bigg[\sum_{j_{\vec{p}}=0}^{\vec{k}}\frac{1}{\sqrt{j_{\vec{k}}-1}}\cdot\{N_{j_{\vec{p}}}N_{j_{\vec{p}_2}}-N_{j_{\vec{k}}}(1+N_{j_{\vec{p}_2}}+N_{j_{\vec{p}}})\}\Bigg] \quad (19)$$

$$\left(\frac{dN_{j_{\vec{p}_2}=1}}{dt}\right)_{in\_scattering\_zero}=\frac{4a_1^2}{\pi\sqrt{2M_x}}\cdot\frac{N_{j_{\vec{p}_2}=1}}{V}\cdot\left(\frac{e_0}{M}\right)^{1/2}$$

$$\times\Bigg[\sum_{j_{\vec{p}}=\vec{k}}^{\infty}\frac{1}{\sqrt{j_{\vec{k}}-1}}\cdot\{N_{j_{\vec{p}}}(1+N_{j_{\vec{k}_2}}+N_{j_{\vec{k}}})-N_{j_{\vec{k}}}N_{j_{\vec{k}_2}}\}\Bigg] \quad (20)$$

Therefore the complete elastic scattering equation is [6]

$$\left(\frac{dN_{j_k}}{dt}\right)_{elastic\_scattering\_whole}=\left(\frac{dN_{j_k}}{dt}\right)_{elastic\_scattering}+\left(\frac{dN_{j_{\vec{k}_2}=1}}{dt}\right)_{out\_scattering\_zero}$$

$$+2\cdot\left(\frac{dN_{j_{\vec{p}_2}=1}}{dt}\right)_{in\_scattering\_zero} \quad (21)$$

5.3 Results in homogeneous system including phonon scattering and elastic scattering

The relaxation kinetics of excitons in Cu_2O due to phonon scattering and elastic scattering have been investigated in references [2, 4]. We have also investigated the Boltzmann kinetics of paraexcitons with phonon scattering and elastic scattering in Cu_2O in the homogeneous system.

After solving the phonon scattering and elastic scattering term of the Boltzmann equation we are getting the exciton occupation number as a function of energy *e*, and time *t*. We have used the initial distribution [7] which is Gaussian $N_e(t=0) = N_{\tilde{e}} \exp[-(e-\tilde{e})^2 / (\Delta e)^2]$ with the central energy $\tilde{e}$ and the width Δe.

The parameters, which we have used, are the exciton mass M_x=2.61 m_e, $m_e = 9.109\times10^{-31}\ kg$ is the electron rest mass, the longitudinal acoustic sound velocity v_s=4.5×10^3 m/s, the deformation potential energy D=1.68 eV, the crystal density $\rho = 6.11\times10^3\ kg/m^3$, the volume $V = 1\ \mu m^3$, the steepness constant $a = 0.5\mu eV\cdot\mu m^{-2}$ and the scattering length $a_1 = 2$ nm.

There have been several theoretical estimations of the exciton-exciton scattering for bulk systems [8-12] and quantum wells [13, 14] as well as calculations on biexciton-biexciton scattering [15]. These are generally in terms of scattering length a_1 which is related to the cross-section by the equation $\sigma = 4\pi a_1^2$. References [4, 9] have used the scattering cross section $\sigma = 50\ \text{nm}^2$. We have also used scattering cross section $\sigma = 50\ \text{nm}^2$.

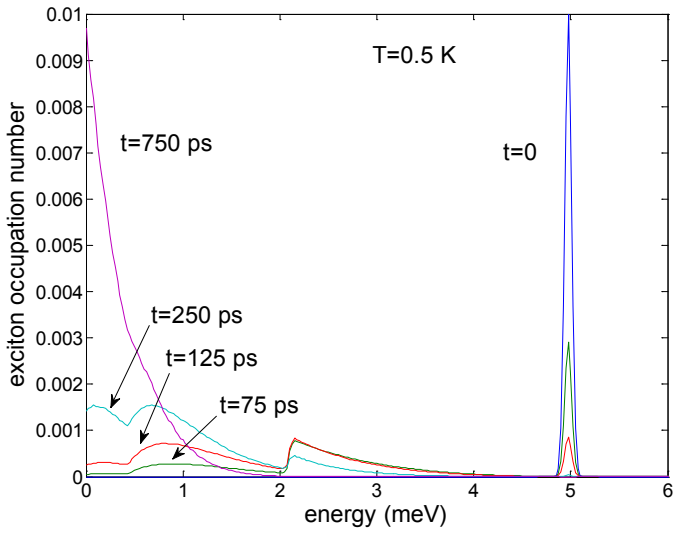

Figure 5.1: Exciton distribution in homogeneous system for 0.5 K from 0 to 750 ps. In this case exciton density is $1\times10^{3}\ \mu m^{-3}$.

Figure 5.1 represents the exciton distribution for 0.5 K at different times. We see at 750 ps the exciton distribution is taking the Boltzmann distribution. Figure 5.2 represents the exciton distribution for different temperatures at different times. We see for 3 K the exciton distribution is coming to the thermal equilibrium within 5 ns in contrast for 0.5 K it is taking 150 ns and for 0.3 K it is taking 400 ns to reach to the thermal equilibrium. For 0.1 K (see figure 5.2d) exciton distribution does not reach thermal equilibrium even at 5000 ns. The calculations, in the results for figure 5.2, are without including the equation for zero energy state, but the behaviour is same if we include the equation for zero energy state.

Figure 5.3 represents exciton's local effective temperature vs. time curve for different bath temperatures. We have calculated the local effective temperature T_{eff} by fitting the long energy tail of the exciton distribution using the equation $e^{-e/k_B T_{eff}}$.

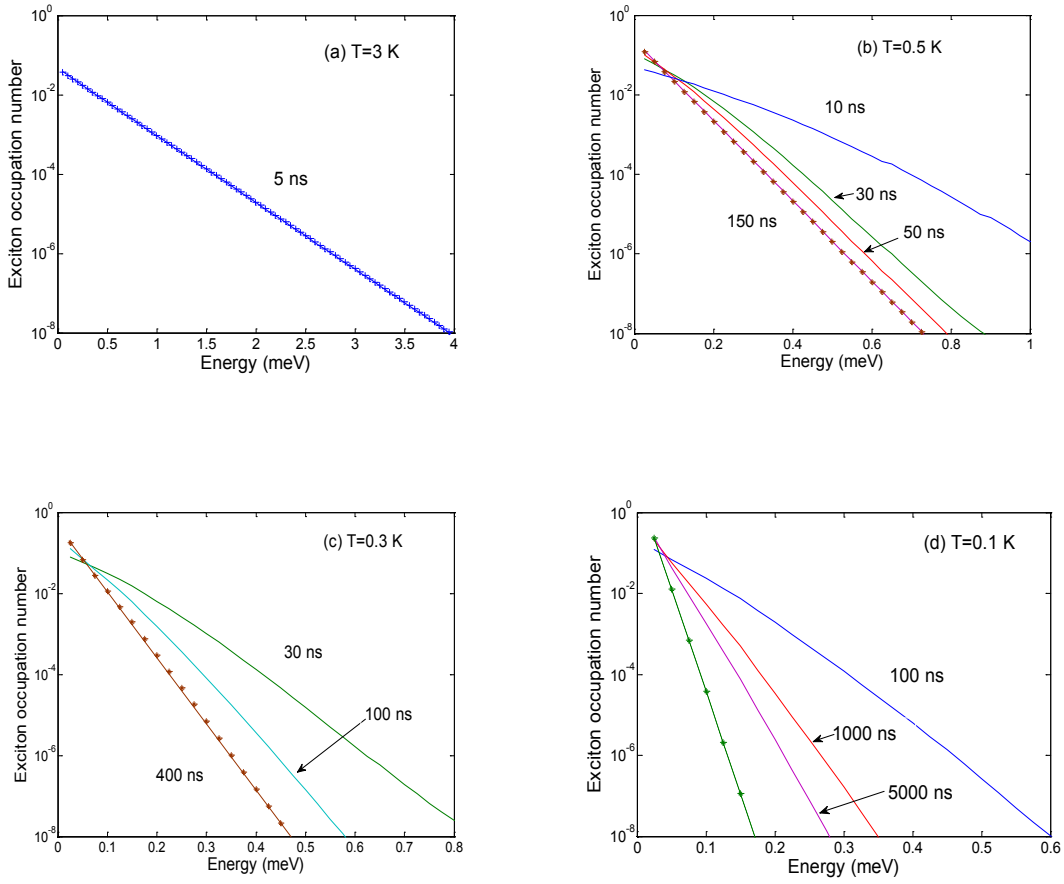

Figure 5.2: Exciton distribution in homogeneous system for different bath temperatures at different times. In these cases exciton densities are $1.7\times10^{3}\ \mu m^{-3}$ for 3 K and $1\times10^{3}\ \mu m^{-3}$ for 0.5 K, 0.3 K and 0.1 K. Full lines represents the results of the numerical simulations and markers represent the thermal equilibrium case for each temperature. In figure 5.2d, markers with dashed curve represents thermal equilibrium for 0.1 K where we see that the exciton distribution does not reach the thermal equilibrium even at 5000 ns.

We see that for 3 K the local effective temperature is coming down to the bath temperature within 5 ns, in contrast for 0.5 K it is taking around 100 ns and for 0.3 K it is taking 250 ns. But for 0.1 K the local effective temperature is coming down to 0.17 K at 5000 ns. For 0.05 K the relaxation behaviour is almost identical to that of 0.1 K, especially the excitons cool down to 0.17 K at 5000 ns.

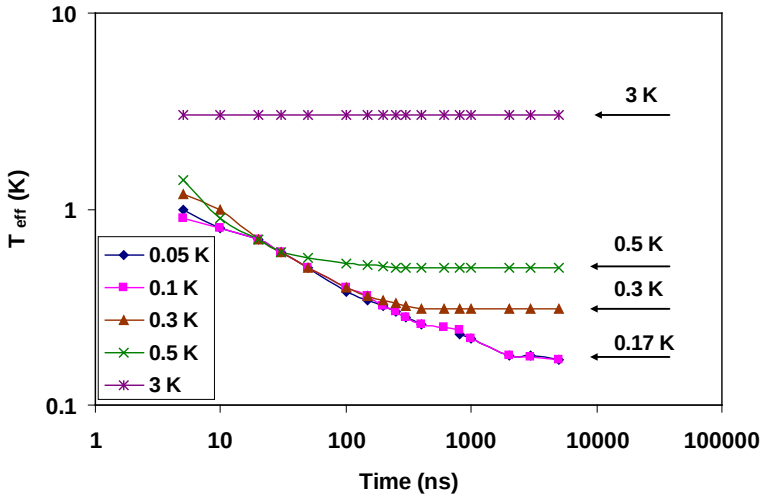

Figure 5.3: Local exciton temperature T_{eff} vs. time for different bath temperatures in the homogeneous system. Here we see that the effective temperature is changing with time for different bath temperatures. The arrows on the right hand side indicate the effective temperatures. For 3 K the exciton density is $1.8\times10^{3}\ \mu m^{-3}$ and for 0.05 K, 0.1 K, 0.3 K and 0.5 K the exciton density is $1\times10^{3}\ \mu m^{-3}$.

We know for constant potential energy, the critical density is given by

$$n_c = \left(\frac{M_x k_B T}{2\pi\hbar^2} \right)^{3/2} \tag{22}$$

In our numerical simulations, if we do not include the equation for in-scattering and out-scattering terms are equal to zero and increase the exciton density over the critical density then over 1.5 K, we see the high peak in the exciton distribution (see figure 5.4). Below 1.5 K simulations can not be performed over long time due to the excitons number at zero energy state is increasing with a high rate, which is an indication of BEC (see figure 5.5 for 0.5 K, which is almost same with and without including in-scattering and out-scattering terms are equal to zero).

If we include the equation for in-scattering and out-scattering terms are equal to zero, then for the all investigated temperatures excitons number at zero energy state is increasing with a high rate, which is an indication of BEC.

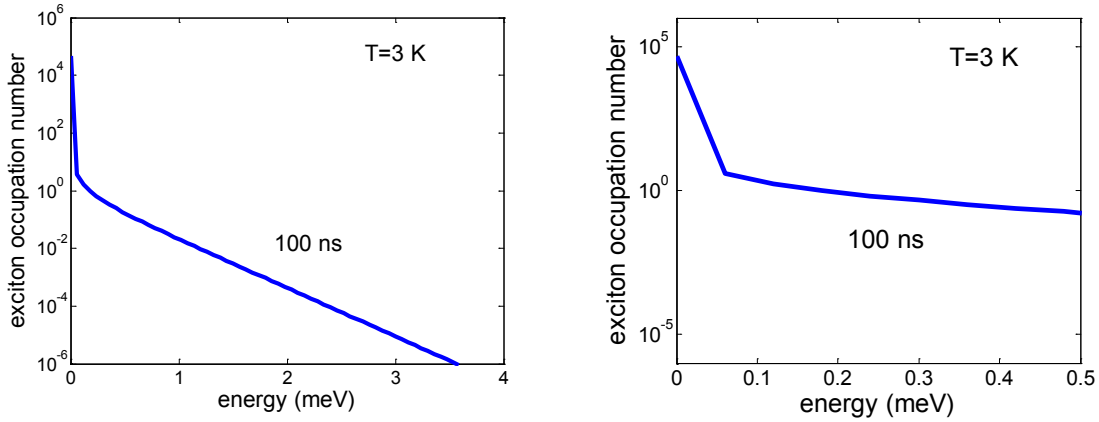

Figure 5.4: Exciton distribution in homogeneous system for 3 K when exciton density is $1.66\times10^{5}\ \mu m^{-3}$. Left hand side figure represents the exciton distribution between energy range zero to 4 meV whereas right hand side figure represents a close view of exciton distribution between energy range zero to 0.5 meV. The critical density of exciton for 3 K is $1.4\times10^{5}\ \mu m^{-3}$. Here exciton density is higher than the critical density.

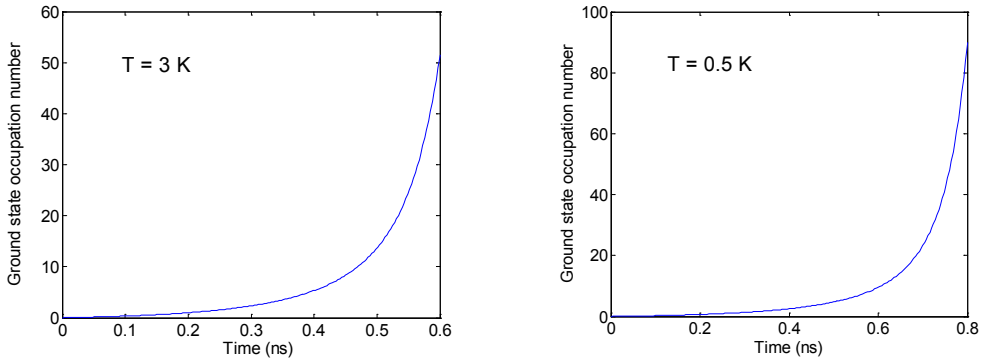

Figure 5.5: Ground state occupation number vs. time for different bath temperatures includes the equation for in-scattering and out-scattering terms are equal to zero. For 3 K and 0.5 K, exciton densities are $1.8\times10^{5}\ \mu m^{-3}$ and $1.2\times10^{5}\ \mu m^{-3}$ respectively. The critical densities of exciton for 3 K and 0.5 K are $1.4\times10^{5}\ \mu m^{-3}$ and $1\times10^{4}\ \mu m^{-3}$ respectively. Here the exciton densities are higher than the critical densities and we see that the ground state exciton number is increasing with a high rate with time.

Figure 5.4 shows the exciton occupation number vs. energy curve for 3 K, where the exciton density $1.66\times10^{5}\ \mu m^{-3}$ is higher than the critical density $1.4\times10^{5}\ \mu m^{-3}$ for 3 K. Left hand side figure of the figure 5.4 represents the exciton distribution between energy range zero to 4 meV whereas right hand side figure represents a close view of exciton distribution between energy range zero to 0.5 meV. Here we see that the high peak shows up at the zero energy. Figure 5.5 shows the ground state occupation number vs. time for different bath temperatures, where the exciton densities for 3 K and 0.5 K, are $1.8\times10^{5}\ \mu m^{-3}$ and $1.2\times10^{5}\ \mu m^{-3}$ respectively, which are over the critical density of exciton for 3 K and 0.5 K are $1.4\times10^{5}\ \mu m^{-3}$ and $1\times10^{4}\ \mu m^{-3}$, respectively. Here we see that the exciton number at zero energy state is increasing with a high rate [5]. Therefore numerical simulations can not performed over long time, but this is an indication of BEC.

5.4 Results within a potential trap including phonon scattering and elastic scattering

After solving the Boltzmann equation with phonon scattering and elastic scattering terms we are getting the exciton occupation number as a function of energy *e*, radius $\vec{r}$ and time *t*. We see that for a particular temperature, the excitons are going towards the bottom of the trap with increasing time, and after some time they are accumulated in a place near the bottom of the trap. In Fig. 5.6, this is demonstrated by an example at a bath temperature of T=0.1 K for t=0ns and t=10 ns.

From the exciton occupation numbers $N_e(r,e,t)$, one can calculate the interesting quantities like total excitons number N_{total} (eq. 21, chapter 3) and the excitons occupation (eq. 22, chapter 3) as usual. However, it has to be stressed, that these quantities refer only to the thermal excitons at e>0. To obtain the number of excitons in the condensate, we have to include the state at e=0 in the following way:

We approximate the number of particles at $k = 0$ by the number of excitons in the $\vec{k}$-space volume Δk^3 at $k = 0$. The condensed exciton density at the position $l \cdot \Delta R$ is $n_X(l,t) = \frac{N(l,0)}{\Delta R^3}$. The total number of condensed excitons is obtained by summing over the total volume as

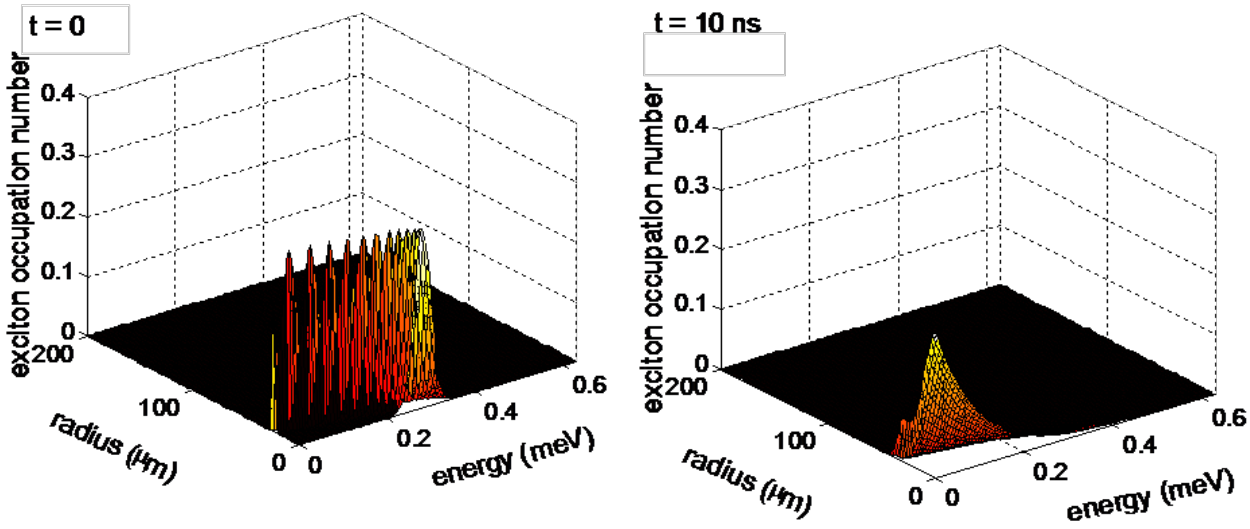

Figure 5.6: The result of the simulation with phonon and elastic scattering for T = 0.1 K. The left panel shows the initial distribution (t=0ns), the right panel shows the result for t = 10 ns. Initial exciton number within the trap is 1.1×10^8.

$$N_C(t) = \frac{1}{\Delta R^3}\sum_l N(l,0)\cdot 4\pi\cdot(l\cdot\Delta R)^2\cdot\Delta R = 4\pi\sum_l N(l,0)\cdot l^2 . \qquad (23)$$

5.4.1 Influence of quantization volume

In contrast to phonon scattering, the elastic scattering rates between thermal and condensed excitons depend explicitly on the quantization volume V (see eq. 19 and 20). To see its influence we have calculated for different volumes the exciton occupation n_r vs. energy curves for 0.5 K with different volume and different initial number of excitons (see figures 5.7, 5.8, 5.9). From these diagrams one can draw the conclusion that the exciton occupation n_r shows no influence of the volume on the relaxation behavior. Therefore, the following calculations will be always done with $V = 1\mu m^3$.

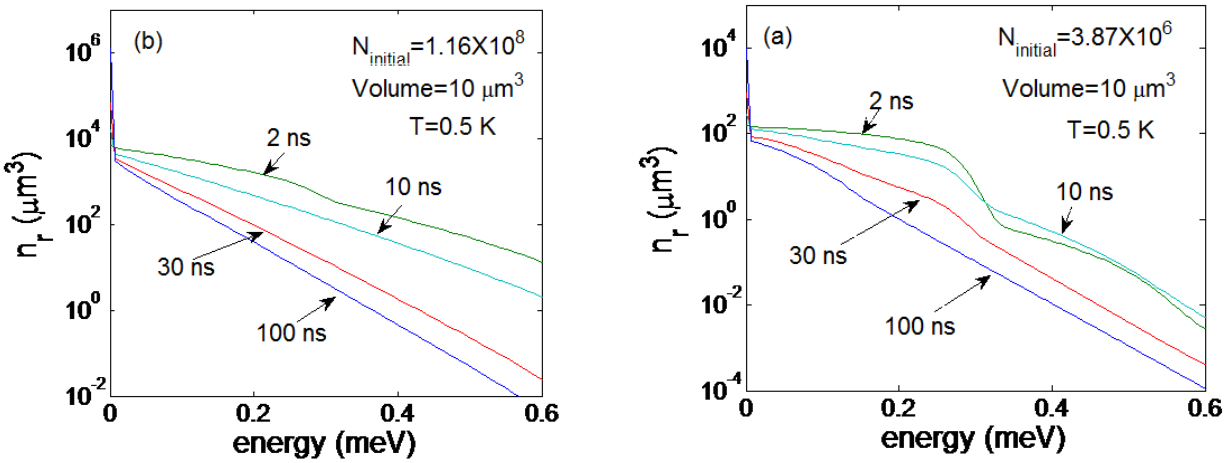

Figure 5.7: Exciton occupation n_r at 0.5 K by the summation of exciton number in r direction vs. energy for different times t for a volume $V = 10\ \mu m^3$. In figure (a) the initial exciton number is 3.87×10^6 and in figure (b) it is 1.16×10^8.

.

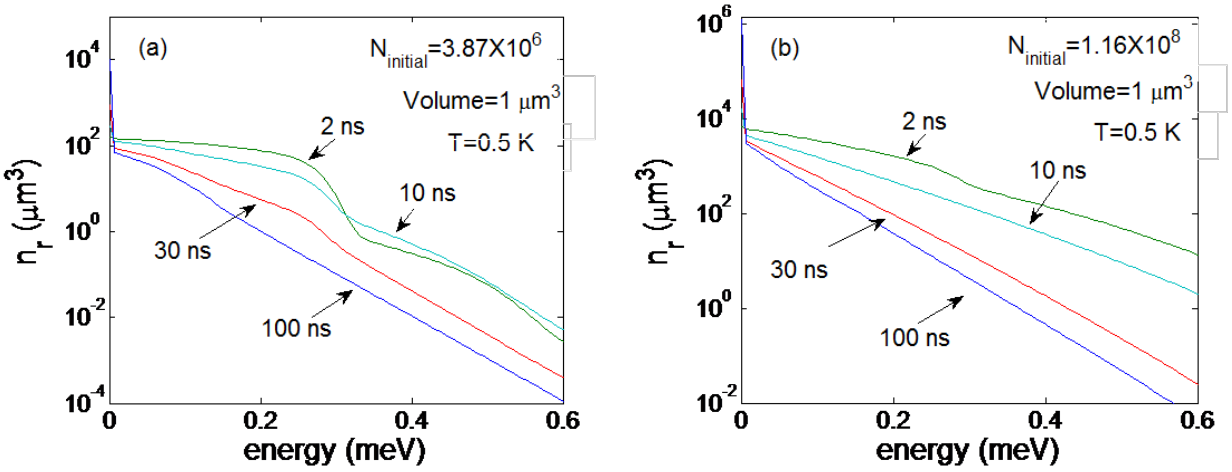

Figure 5.8: Exciton occupation n_r at 0.5 K by the summation of exciton number in r direction vs. energy for different times t for a volume $V = 1\ \mu m^3$. Figure (a): Initial exciton number 3.87×10^6; figure (b): Initial exciton number 1.16×10^8.

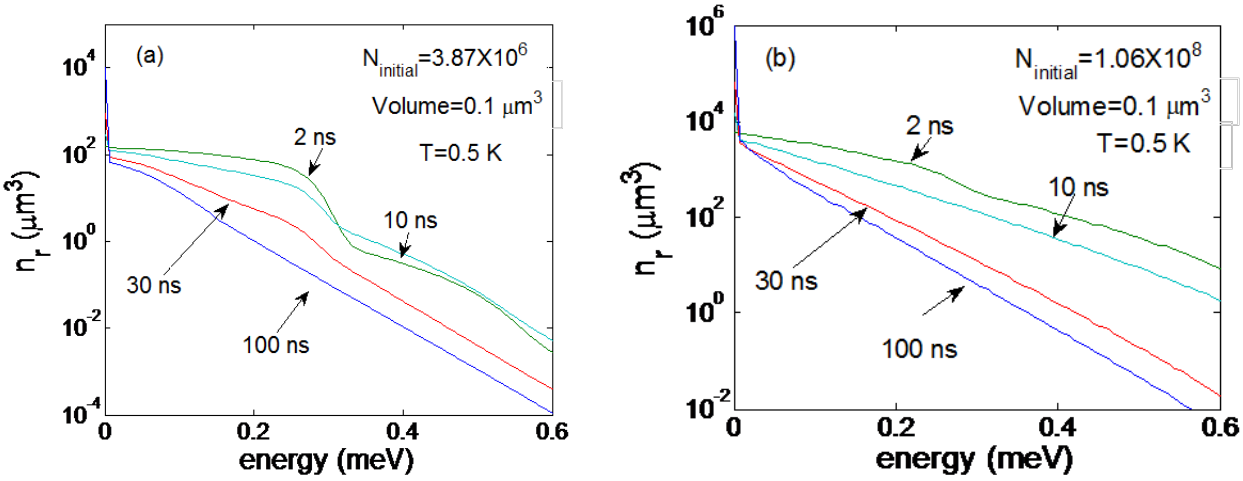

Figure 5.9: Exciton occupation n_r at 0.5 K by the summation of exciton number in r direction vs. energy for different times t for a volume $V = 0.1\ \mu m^3$. Figure (a): Initial exciton number 3.87×10^6; figure (b): Initial exciton number 1.06×10^8.

5.4.2. Numerical Stability

An important issue in the numerical simulation is a possible loss (or gain) of excitons due to the finite resolution and boundaries in real and momentum space. To check this, we have undertaken a series of simulations for T=0.5K and 0.1K and plotted the total exciton number as a function of time (figures 5.10 and 5.11).

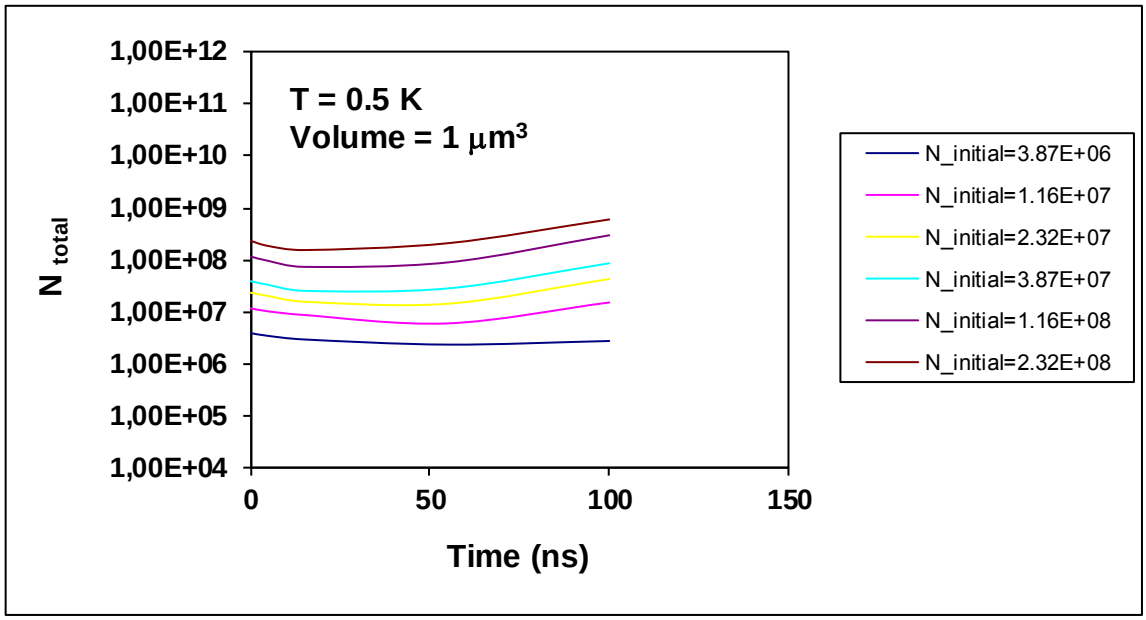

Figure 5.10: Total number of excitons vs. time for 0.5 K with the volume of 1 μm^3 including deformation potential phonon scattering and elastic scattering. The curves show how the total number of excitons is changing with time with different initial number of excitons.

Figure 5.10 represents the total number of excitons (N_{total}) vs. time curves for 0.5 K with the volume of 1 μm^3. Here we see that for the small initial exciton number N_{total} is

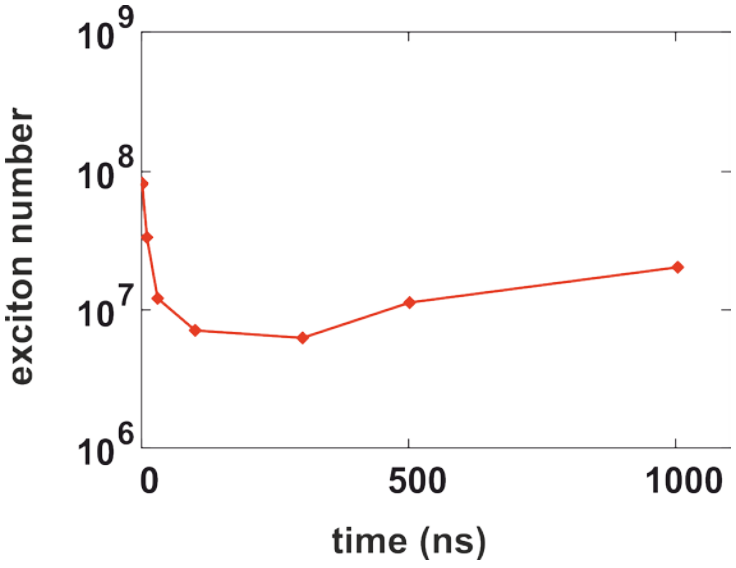

Figure 5.11: Total number of excitons vs. time for 0.1 K with the volume of 1 μm^3 including deformation potential phonon scattering and elastic scattering. Initial total number of excitons: 1.1×10^8.

almost constant with increasing time. But for large initial excitons numbers up to 2.32×10^8 the variation of N_{total} stays below a factor of 3. In fig. 5.11 we extended for T=0.1K the calculation to t=1000ns and plotted the actual total number of excitons $(N_{total}+N_c)$ including the condensate obtained from eq. (23) vs. time with 1.1×10^8 initial number of excitons (see chapter 5.4.5). Here we see that up to 10 ns, the exciton number is decreasing but after that it stays almost constant.

From the data we conclude that the calculation has sufficient numerical stability so that reliable results can be obtained.

5.4.3. Low number of excitons

For low number of excitons we expect no difference to the results including phonon scattering only. The question is from which exciton number the elastic scattering plays a significant role.

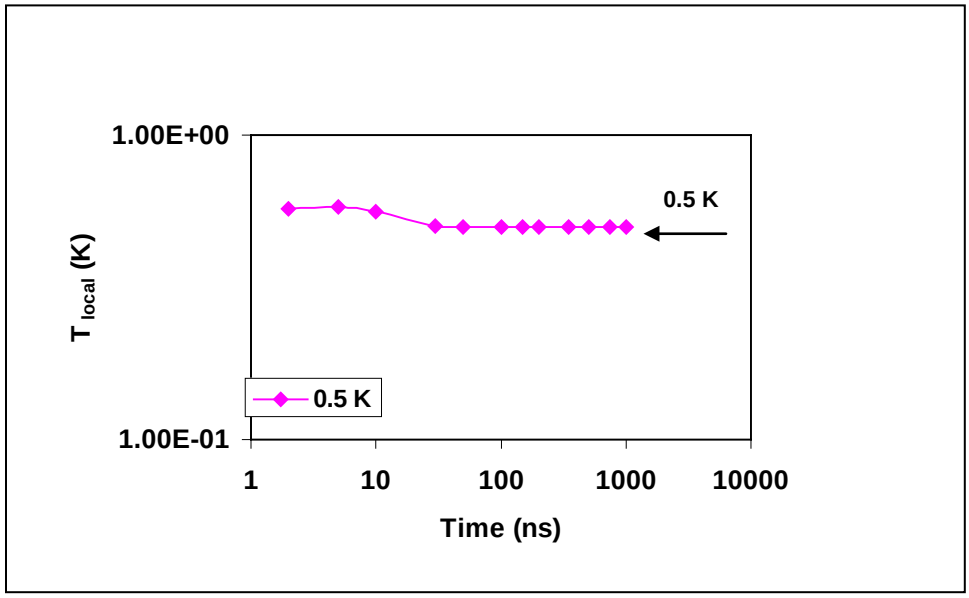

Figure 5.12: Local exciton temperature T_{local} vs. time for bath temperature of 0.5 K including elastic and phonon scattering. Number of excitons is 1×10^5. Curve serves as a guide to the eye.

In figure 5.12 we have plotted local exciton temperature T_{local} vs. time for the bath temperature of 0.5 K including elastic and phonon scattering at a exciton number of 1×10^5. We have calculated the local effective temperature T_{local} by fitting the long energy tail of the exciton distribution by a function proportional to $e^{-e/k_B T_{local}}$ and studied how it is changing with time. If we compare this figure with the figure 3.12 including phonon scattering only at an initial exciton number of 1.5×10^4 then we get no such differences. Therefore there is no effect of elastic scattering when the exciton number is 1×10^5.

5.4.4. High number of excitons

For high number of excitons we expect a strong effect of elastic scattering on the relaxation behavior. This shows up most significantly in the exciton occupation n_r. Data for T=0.5K have already been given in Fig.5.8, for T=0.1K the results are shown in Fig. 5.13.

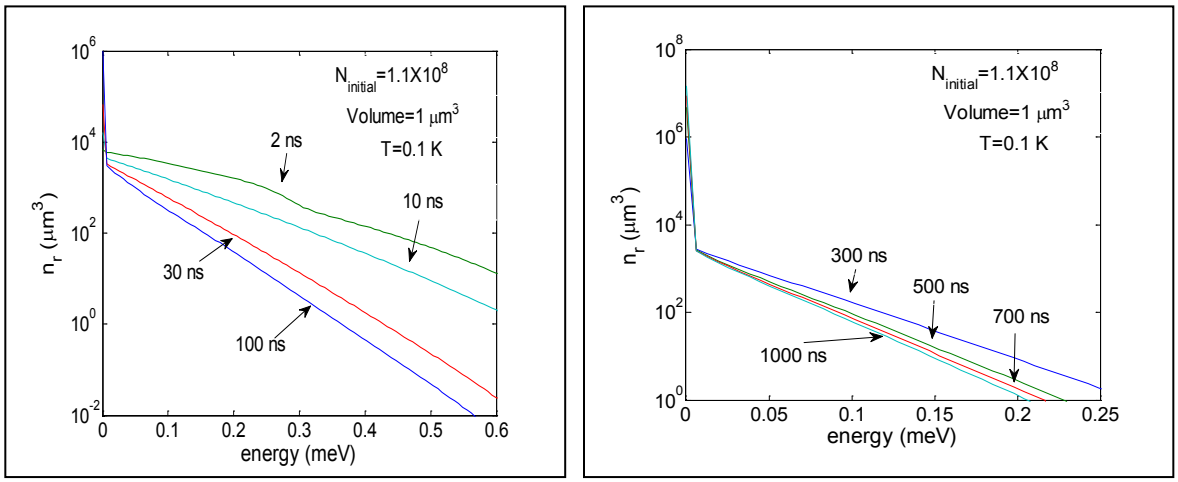

Figure 5.13: Exciton occupation n_r at 0.1 K by the summation of exciton number in *r* direction vs. energy for different times for the volume1 μm^3. Here the initial exciton number is 1.1×10^8.

For both temperatures we see that a thermal distribution is obtained for times larger than 10ns, so that we can compare the effective local temperatures for times larger than 10 ns for bath temperatures of 3K, 0.5K and 0.1K.

5.4.4.1. Local Temperature

Figure 5.14 represents the local effective temperatures vs. time curves for the bath temperatures 3 K, 0.5 K and 0.1 K. For 0.5 K and 3 K initially total number of exciton is 1.16×10^{8} and for 0.1 K initially total number of exciton is 1.1×10^{8}. We have calculated the local effective temperature T_{local} by fitting the long energy tail of the exciton distribution by a function proportional to $e^{-e/k_B T_{local}}$ and studied how it is changing with time. Here we see that the local effective temperature is coming down to the bath temperature for 3 K and 0.5 K, but for 0.1 K this is not the case. For 0.5K bath temperature is reached within 100 ns, but for 0.1 K the local effective temperature is not coming down to bath temperature even at 1000 ns.

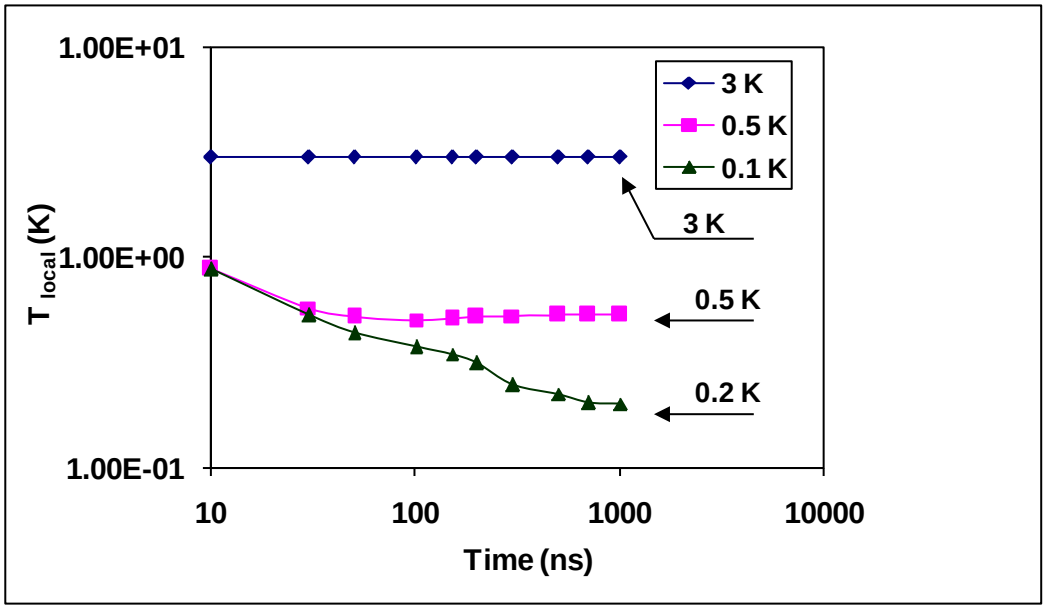

Figure 5.14: Local exciton temperature T_{local} vs. time for different bath temperatures including elastic and phonon scattering. Here we see that the effective temperature is changing with time for different bath temperatures. The arrows on the right hand side indicate the effective temperatures. For 0.5 K and 3 K initially total number of exciton is 1.16×10^{8} and for 0.1 K initially total number of exciton is 1.1×10^{8}. The curves serve as a guide to the eye.

5.4.4.2. Global temperature

To obtain information about the global distribution of excitons, we compare as in Sec. 5.2 and 5.3 the radial density distribution of excitons.

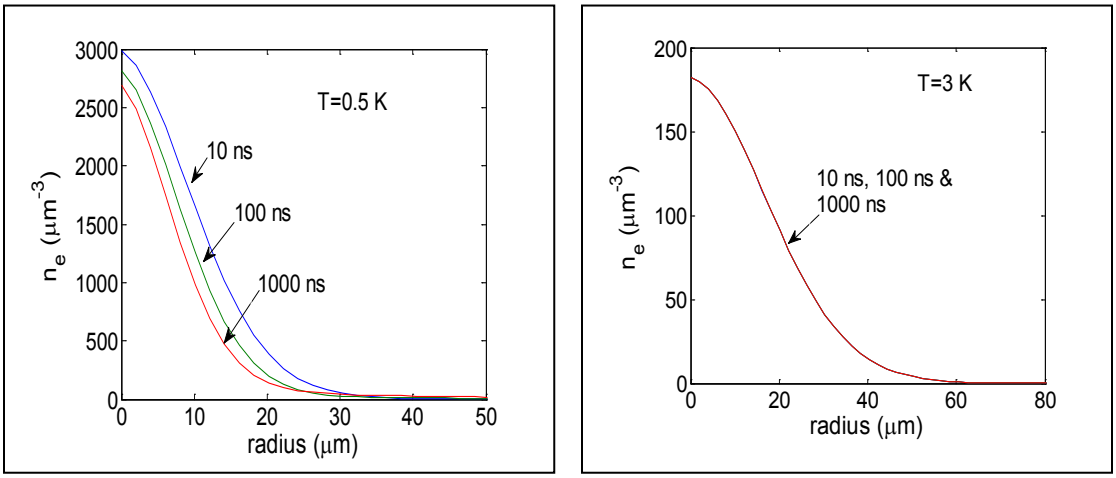

Figure 5.18: Spatial distribution n_e of excitons for different bath temperatures for 10 ns, 100 ns, and 1000 ns, i.e. the summation of exciton number over the direction of energy vs. radius r, with phonon and elastic scattering for different time. For 0.5 K and 3 K, initially total number of excitons is 1.16×10^8.

Figure 5.18 represents spatial distribution n_e of excitons, i.e. the summation of exciton number over the direction of energy vs. radius r, with phonon and elastic scattering for different time for the temperatures 0.5 K and 3 K.

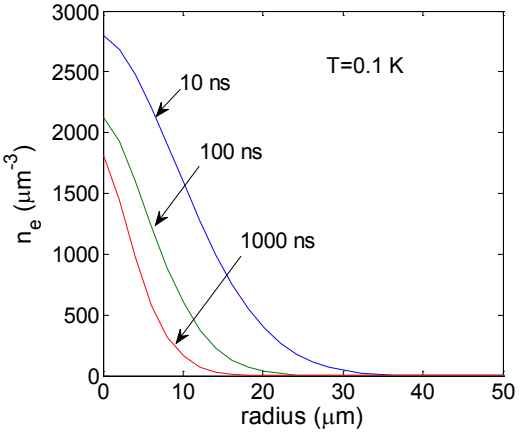

Figure 5.19: Spatial distribution n_e of excitons for a bath temperature of 0.1 K with 1.1×10^8 initial number of excitons, i.e. the summation of exciton number over the direction of energy vs. radius r, with phonon and elastic scattering for different times.

Figure 5.19 represents the spatial distribution n_e of excitons vs. radius r, with phonon and elastic scattering for different times for the temperature 0.1 K.

To calculate the global effective temperature we have plotted $n_e(r)$ vs. radius curves (see figures 5.18 and 5.19) by using the relation of the exciton distribution $n_e(\vec{r}) \sim e^{-\left(\frac{r}{\xi}\right)^2}$ with $\xi = \sqrt{\frac{k_B T_{global}}{a}}$ and the steepness constant $a = 0.5\mu eV \cdot \mu m^{-2}$. Therefore, we take the value of $\vec{r}$ at the half maximum of the exciton distribution, and determined the effective temperature.

In figure 5.20 we have plotted the global effective temperature T_{global} vs. time for the bath temperatures 0.1 K, 0.5 K and 3 K. Here we see that for the bath temperatures of 0.1 K both the local and global effective temperatures stay really a high value of 0.2 K even after 1000 ns.

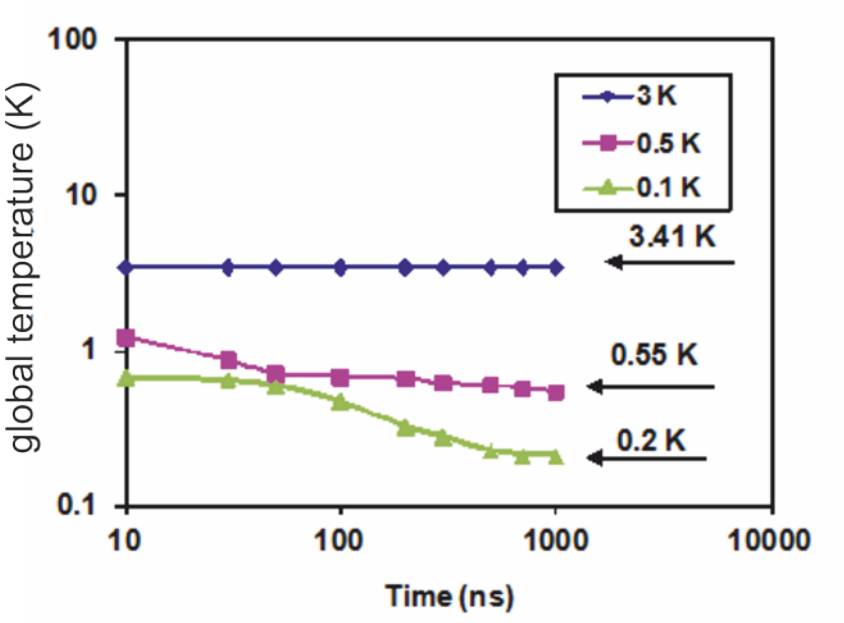

Figure 5.20: T_{global} vs. time for different bath temperatures including phonon scattering and elastic scattering. For 0.5 K and 3 K, initially total number of excitons is 1.16×10^8 and for 0.1 K, initially total number of excitons is 1.1×10^8. The arrows on the right hand side indicate the effective temperatures.

From the results we see that for the temperatures at and over 0.5 K the local effective temperature is coming down to the bath temperature but the global effective temperature is not coming down to the bath temperature staying about 10% larger. For the temperatures much below 0.5 K, as demonstrated for the temperature of 0.1 K both local and global temperatures are not coming down to bath temperatures and moreover seem to be the same.

However, a closer inspection of the radial distributions shows a remarkable behavior. While for T=3K, the distributions do not change at all, we find for the other temperatures a decrease in $n_e(r)$ with time, most prominent for T=0.1K. As one can easily check that the critical temperature for BEC for $N=10^8$ particles is 0.8K, we would expect that the loss of thermal excitons is due to condensation.

5.4.5. Exciton condensation at T=0.1K

The exact criterium for condensation, even for nonequilibrium systems, is that the chemical potential μ is reaching zero. This should occur first in the center of the trap, where the excitons density is highest. To obtain the temperature and chemical potential we therefore fitted the occupation number distribution at radius equal to zero N(0,e) with Bose-Einstein distribution [17] $f = \frac{1}{\exp(\frac{e-\mu}{k_B T})-1}$, where μ is the chemical potential.

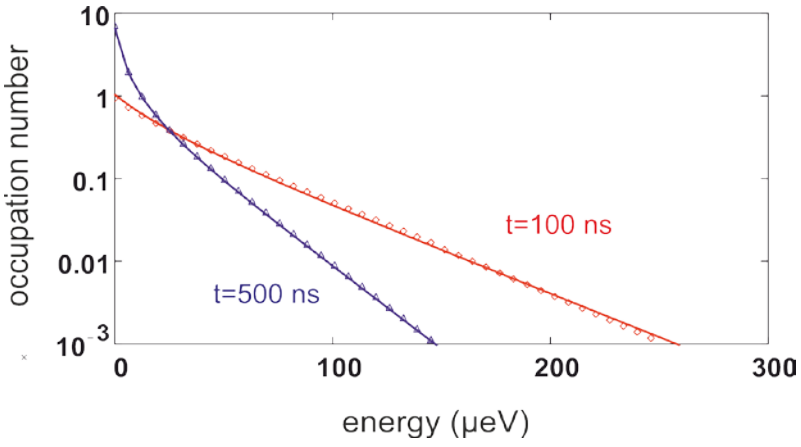

Figure 5.21: The exciton occupation number at r=0 versus kinetic exciton energy at different times t for the bath temperature of 0.1 K including elastic and phonon scattering. Initially total number of excitons is 1.1×10^8.

The results are shown in Fig. 5.21 for different times and demonstrate again the

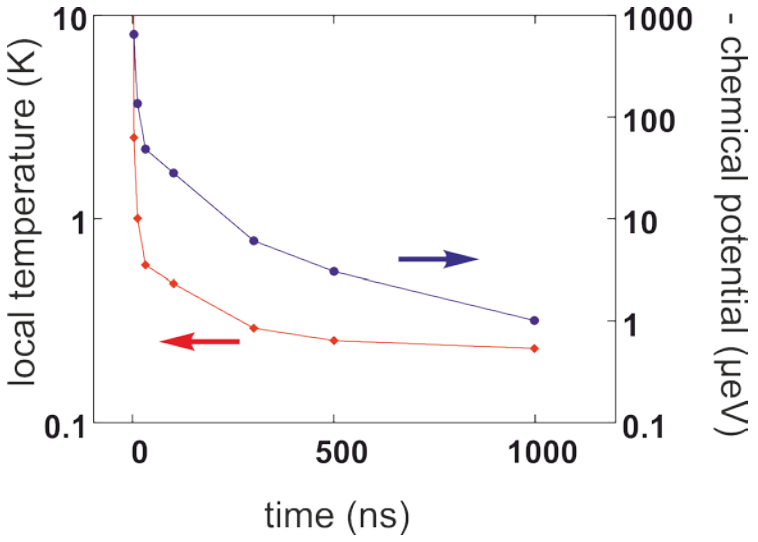

Figure 5.22: The exciton temperature T vs. time (red dots) and chemical potential vs. time (blue dots) for the bath temperature of 0.1 K including elastic and phonon scattering. Initially total number of excitons is 1.1×10^{8}.

quasiequilibrium distribution of the excitons in the trap. From these fits we have drawn the temperature vs. time and chemical potential vs. time curves (see figure 5.22) where we see that the temperature is decreasing with time and at 1000 ns it is coming down to 0.2 K. As well the chemical potential is increasing with time and for times larger than 300 ns it is zero within the numerical accuracy ($\pm5\mu eV$). This clearly demonstrates that for times larger than 300 ns the condition for condensation is fulfilled and we can observe the formation of a condensate.

This is substantiated by the dependence of the number of condensed excitons calculated from eq.(23) and shown in figure 5.23. Here we see a strong increase in the number of condensed excitons for times greater than 300 ns.

As the system is in local equilibrium, we expect that the condensate fraction $\eta_c = \frac{N_c}{N_{total} + N_c}$ follows the equilibrium result for the local temperature, which is given by [17]:

$$\eta_c = \left[1-1.202\left(\frac{k_B T}{\hbar\Omega}\right)^3\right].\phi\left[1-1.202\left(\frac{k_B T}{\hbar\Omega}\right)^3\right] \qquad (24)$$

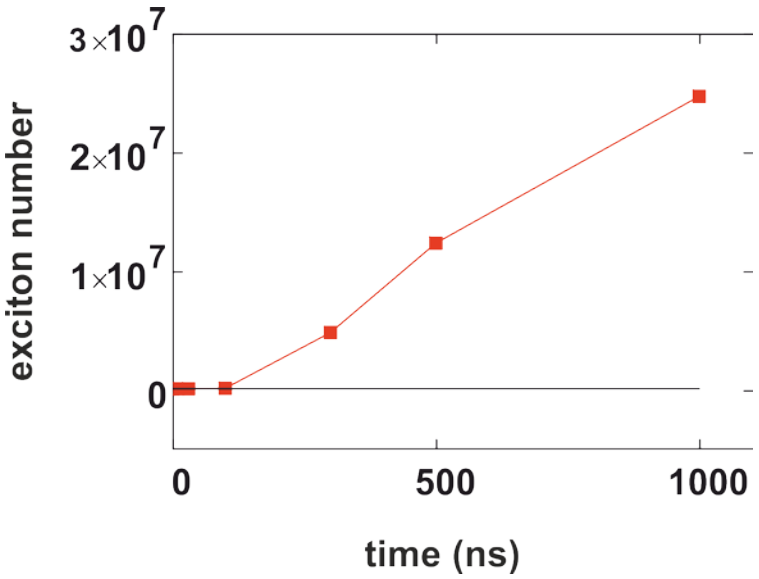

Figure 5.23: The condensed exciton number N_c vs. time for the bath temperature of 0.1 K including elastic and phonon scattering. Initially total number of excitons is 1.1×10^8. The curve is a guide to the eye.

Here ϕ is the Heaviside step function. Obviously, the condensate fraction η_c depends only on the local temperature and on the trap frequency. To obtain a continuous dependence, we interpolate the results for the temperature vs. time shown in Fig. 5.22 and those for the total number of excitons (Fig. 5.11) linearly and compare the resulting η_c

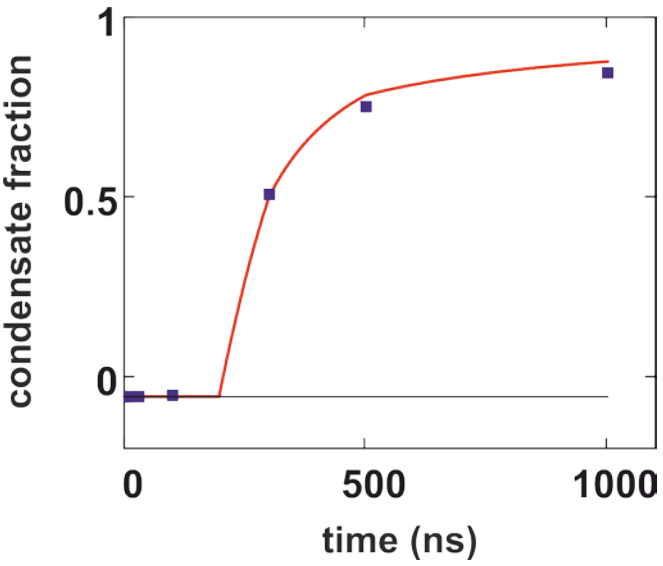

Figure 5.24: Time dependence of the condensate fraction η_c obtained from eq. 5.23 (full line) and the ratio $\frac{N_c}{N_{total}+N_c}$ (blue dots) obtained for a bath temperature of 0.1 K including elastic and phonon scattering and an initial total number of excitons of 1.1×10^8. vs. time.

with $\frac{N_c}{N_{total}+N_c}$ obtained from the calculations vs. time for the bath temperature of 0.1 K. Here we see that after 200 ns η_c is sharply increasing, indicating the sharp onset of condensation. For later times η_c is in very good agreement with the values of $\frac{N_c}{N_{total}+N_c}$ as obtained from the numerical simulation.

This clearly demonstrates that the numerical simulations give a consistent picture of the full relaxation dynamics including the condensate formation.

5.5 Summary

We have seen the relaxation behaviour of excitons in homogeneous system and also within a potential trap. In homogeneous system, over 1 K the effective temperatures are coming down to the bath temperatures within 5 to 10 ns whereas for 0.5 K it is taking 150 ns, for 0.3 K it is taking 400 ns. In the case of 0.1 K, the effective temperature is not coming down to the bath temperature even after 1000 ns.

Within the trap, with low number of excitons we see that for the temperatures between 0.5 K to 3 K excitons are thermalizing but for 0.3 K and below 0.3 K a non thermal distribution, a bending remains. With high number of excitons this bending has been removed. The local effective temperature is coming down to the bath temperature for 3 K and 0.5 K, but for 0.1 K this is not the case. For 0.5K bath temperature is reached within 100 ns, but for 0.1 K the local effective temperature is not coming down to bath temperature even at 1000 ns, rather it stays really a high value of 0.2 K. On a global scale, the global effective temperature is coming down to 3.41 K for the bath temperature of 3 K and the global effective temperature is coming down to 0.55 K for the bath temperature of 0.5 K, but for the bath temperatures of 0.1 K the global effective temperatures stay really a high value of 0.2 K even after 1000 ns.

For the temperature of 0.1 K, from the chemical potential vs. time curve (figure 5.22) we see that for times larger than 300 ns the condition of condensation is fulfilled and we can observe the formation of a condensate. Condensate fraction η_c vs. time curve (figure 5.24) shows that after 200 ns η_c is sharply increasing, which indicates condensation.

References

[1] Kadanoff L P and Baym G, 1989, "Quantum Statistical Mechanics" (Addison-Wesley Publishing Company, Inc.).

[2] Snoke D W and Wolfe J P, 1989, *Phys Rev B* **39**, 4030, "Population dynamics of a Bose gas near saturation".

[3] Snoke D W, Ruhle W W, Lu Y C, and Bauser E, 1992, *Phys Rev B* **45**, 10979, "Evolution of a nonthermal electron energy distribution in GaAs".

[4] O'Hara K E and Wolfe J P, 2000, *Phys. Rev. B* **62**, 12 909-921, "Relaxation kinetics of excitons in cuprous oxide".

[5] O'Hara K E, 1999, "Relaxation Kinetics of Excitons in Cuprous Oxide" Ph.D. Thesis (University of Illinois, Urbana, Illinois, USA).

[6] Semikoz D V and Tkachev I I, 1995, *Phys. Rev. Lett* **74,** 3093, "Kinetics of Bose Condensation".

[7] Ell C, Ivanov A L, and Haug H, 1998, *Phys. Rev. B* **57**, 9663-73, "Relaxation kinetics of a low-density exciton gas in Cu_2O".

[8] Hanamura E and Haug H, 1977, *Phys Lett C* **33**, 209, "Condensation effects of excitons".

[9] Haug H, 1976, *Z. Phys. B* **24**, 351, "On the Phase Transitions for the Electronic Excitations in Semiconductors".

[10] Elkomoss S G and Munschy G, 1981, *J Phys Chem Solids* **42**, 1, "Exciton-exciton elastic scattering cross sections for different semiconductors".

[11] Elkomoss S G and Munschy G, 1984, *J. Phys. Chem. Solids* **45**, 345, "Inelastic collisions between excitons in semiconductors—I: Collisions with excited final states".

[12] Shumway J and Ceperley D M, 2001, *Phys. Rev. B* **63**, 165209, "Quantum Monte Carlo treatment of elastic exciton-exciton scattering".

[13] Ciuti C, Savona V, Piermarocchi C, Quattropani A, and Schwendimann P, 1998, *Phys. Rev. B* **58**, 7926, "Role of the exchange of carriers in elastic exciton-exciton scattering in quantum wells".

[14] Koh T S, Feng Y P, and Spector H N, 1997, *Phys. Rev. B* **55**, 9271, "Elastic scattering of excitons by excitons in semiconducting quantum-well structures: Finite confining-potential model".

[15] Cam H N, 1997, *Phys. Rev. B* **55**, 10 487, "Biexciton-biexciton interaction in semiconductors".

[16] Shumway J B, 1999, "Quantum Monte Carlo Simulations of Electrons and Holes" Ph.D. Thesis (University of Illinois, Urbana, Illinois, USA).

[17] Pethick C J and Smith H, 2002, "Bose-Einstein Condensation in Dilute Gases" (Cambridge, UK: Cambridge University Press).

Chapter 6

Conclusions

In this thesis we have investigated the relaxation behaviour of excitons in cuprous oxide at ultra low temperatures when excitons are confined within a potential trap and also in a homogeneous system. It has been done numerically by solving the Boltzmann equation. Excitons behaviour under various conditions has been analysed. As relaxation processes, we have included the phonon scattering, Auger decay, radiative, non-radiative decay, and elastic scattering.

In chapter 2, we have modeled numerically a potential trap by using the force term in the Boltzmann equation. Then we set an initial condition and boundary conditions. We assumed that the excitons are confined in a stress induced parabolic potential trap with the potential energy $V(\vec{r}) = a\vec{r}^{\,2}$ with a the steepness constant and $\vec{r}$ the radius. The relation between the steepness constant a and the oscillator frequency Ω is $a = \frac{1}{2} M_x \Omega^2$, where M_x is the exciton mass.

In chapter 3, we have modeled numerically the phonon scattering term of the Boltzmann equation. Starting from the Boltzmann equation in momentum space, we transfer it into the energy space and solve it by MATLAB. In this case excitons behaviour has been analysed between 0.3 K to 5 K in a homogeneous system and also within a trap. Our aim

was to find the answer of two questions: first, how long time excitons take to thermalize and second, when does a BEC occurs. From the results we see that in a homogeneous system and also within the trap for both cases excitons are thermalizing between 0.5 K to 3 K but at 0.3 K and below 0.3 K a non thermal distribution remains. Local cooling behaviour is same in homogeneous system and within the trap. We see locally, that for the bath temperatures between 1 K to 5 K the local effective temperature T_{local} is coming down to the bath temperature very quickly within 10 nanoseconds, but for the bath temperatures below 1 K, the T_{local} is coming down to the bath temperature very slowly within 100 nanoseconds only. This effect can be related to the freezing out of phonons for very low temperatures. Within the trap on a global scale, exciton effective temperature T_{global} is not coming down to the bath temperature. For low temperatures, the global effective temperatures are almost a factor of 2 larger than the bath temperatures.

We see from our numerical simulations, that the BEC occurs for all observed temperatures. By comparing our results with the thermal equilibrium case, we see that for all temperatures the BEC comes at a higher number of excitons than in thermal equilibrium case. The effective temperature at the time of BEC has good agreement with the global effective temperature.

In the chapter 4, we have included the Auger decay, radiative and non-radiative decay with the phonon scattering. We see locally and globally that for both cases the effective temperatures are not coming down to the bath temperatures even after long times. In this case, no BEC occurs. The global effective temperatures are the same with and without Auger decay. However, there is a difference in local temperatures which is higher if we include the Auger decay. This is due to the local heating by the Auger decay which is the reason for the absence of BEC with the Auger decay. In the results with phonon scattering only we see the BEC occurs for all temperatures over and below 1 K. Therefore the Auger decay makes a barrier to get the BEC.

In the chapter 5, we have included the elastic scattering with the phonon scattering. We have seen the relaxation behaviour of excitons in a homogeneous system and also within

a potential trap between 0.05 K to 3 K. From the results we see that in a homogeneous system over 1 K the effective temperatures are coming down to the bath temperatures within 5 to 10 ns whereas for 0.5 K it is taking 150 ns, for 0.3 K it is taking 400 ns. In the case of 0.1 K and 0.05 K the effective temperature is not coming down to the bath temperature even after 1000 ns. This effect can be related to the freezing out of phonons for very low temperatures. Within the trap, the local cooling behaviour is almost same like in a homogeneous system. On a global scale, the excitons global effective temperatures T_{global} are not coming down to the bath temperatures. For the bath temperature of 0.1 K both the local and global effective temperatures stays really a high value of 0.2 K even after 1000 ns.

From the results with high number of excitons for the temperature of 0.1 K we get clear indication of condensation. Therefore these numerical simulations give a consistent picture of the full relaxation dynamics including the condensate formation.

Appendix A: Calculations of integration limits for the Stokes scattering part within the phonon scattering

For Stokes part delta function is given below (see equation (1), chapter 3)

$$\delta\left(e_{\vec{k}} - e_{\vec{p}} - \hbar\omega_{\vec{k}-\vec{p}}\right)$$

$$= \delta\left(e_{\vec{k}} - e_{\vec{p}} - \hbar v_s\left|\vec{k}-\vec{p}\right|\right) \qquad [\because \omega_{\vec{k}-\vec{p}} = v_s\left|\vec{k}-\vec{p}\right| \ ]$$

$$= \delta\left(e_{\vec{k}} - e_{\vec{p}} - \hbar v_s\sqrt{\vec{k}^2 + \vec{p}^2 - 2\vec{k}\vec{p}\cos\theta}\right)$$

$$= \delta\left(e - e_1 - \hbar v_s\sqrt{\frac{2M_x e}{\hbar^2} + \frac{2M_x e_1}{\hbar^2} - 2\sqrt{\frac{2M_x e}{\hbar^2}}\sqrt{\frac{2M_x e_1}{\hbar^2}}\cos\theta}\right)$$

$$= \delta\left(e - e_1 - \hbar v_s\sqrt{\frac{2M_x}{\hbar^2}}\sqrt{e + e_1 - 2\sqrt{e}\sqrt{e_1}\cos\theta}\right)$$

$$= \delta\left(e - e_1 - v_s\sqrt{2M_x}\sqrt{e + e_1 - 2\sqrt{e}\sqrt{e_1}\cos\theta}\right)$$

$$= \delta\left(e - e_1 - \sqrt{e_0}\sqrt{e + e_1 - 2\sqrt{e}\sqrt{e_1}\cos\theta}\right) \qquad [\because e_0 = 2M_x v_s^2] \qquad \text{(A.1)}$$

Now we have to find out the values of e_1 in terms of e, when delta function will be zero for $\cos\theta$ =1 and for $\cos\theta$ = -1.

When $\cos\theta$ =1

Putting delta function equal to zero, we get

$$e - e_1 - \sqrt{e_0}\sqrt{e + e_1 - 2\sqrt{e}\sqrt{e_1}} = 0 \qquad \text{(A.2)}$$

Or, $e - e_1 - \sqrt{e_0}\sqrt{\left(\sqrt{e} - \sqrt{e_1}\right)^2} = 0$

or, $e - e_1 - \sqrt{e_0}\left|\sqrt{e} - \sqrt{e_1}\right| = 0 \qquad \text{(A.3)}$

For Stokes $e > e_1$, so it should be

$$e - e_1 - \sqrt{e_0}\left(\sqrt{e} - \sqrt{e_1}\right) = 0 \qquad \text{(A.4)}$$

This is similar to step function $\Theta\left(q_s - \sqrt{e} + \sqrt{e_1}\right)$ for Stokes part.

Now dividing it by e_0, we get

$$\frac{e}{e_0}-\frac{e_1}{e_0}-\left(\frac{\sqrt{e}}{\sqrt{e_0}}-\frac{\sqrt{e_1}}{\sqrt{e_0}}\right)=0 \qquad \text{(A.5)}$$

Or, $\xi-\xi_1-\sqrt{\xi}+\sqrt{\xi_1}=0$ [where $\frac{e}{e_0}=\xi$ and $\frac{e_1}{e_0}=\xi_1$]

Or, $\sqrt{\xi_1}=\frac{1}{2}+\left|\sqrt{\xi}-\frac{1}{2}\right|$

Or, $\sqrt{\xi_1}=\frac{1}{2}\pm\left(\sqrt{\xi}-\frac{1}{2}\right)$ (A.6)

Now, if it is (-) means $\sqrt{\xi}<\frac{1}{2}$,

$$\sqrt{\xi_1}=\frac{1}{2}+\frac{1}{2}-\sqrt{\xi}=1-\sqrt{\xi}$$

This is invalid, because here $1-\sqrt{\xi}>\frac{1}{2}$ so, $\sqrt{\xi_1}>\frac{1}{2}$ or, $\sqrt{\xi_1}>\sqrt{\xi}$ or, $e_1>e$

But for Stokes it should be $e_1\le e$.

Now, if it is (+) means $\sqrt{\xi}>\frac{1}{2}$,

$$\sqrt{\xi_1}=\frac{1}{2}+\sqrt{\xi}-\frac{1}{2}=\sqrt{\xi}$$

Or, $e_1=e$

Or, p=j (A.7)

This is p_{max} for Stokes scattering, and here it should be greater than M/4. Because $\sqrt{\xi}>\frac{1}{2}$ or, $\frac{e}{e_0}>\frac{1}{4}$ or,

$j>\frac{M}{4}$.

When $\cos\theta$ = -1

Putting delta function equal to zero, we get

$$e - e_1 - \sqrt{e_0}\sqrt{e + e_1 + 2\sqrt{e}\sqrt{e_1}} = 0 \qquad \text{(A.8)}$$

Or, $e - e_1 - \sqrt{e_0}\sqrt{\left(\sqrt{e} + \sqrt{e_1}\right)^2} = 0$

Or, $e - e_1 - \sqrt{e_0}\left|\sqrt{e} + \sqrt{e_1}\right| = 0$

Or, $e - e_1 - \sqrt{e_0}\left(\sqrt{e} + \sqrt{e_1}\right) = 0 \qquad \text{(A.9)}$

This is similar to step function $\Theta\left(-q_s + \sqrt{e} + \sqrt{e_1}\right)$ for Stokes part.

Now dividing it by e_0, we get

$$\frac{e}{e_0} - \frac{e_1}{e_0} - \left(\frac{\sqrt{e}}{\sqrt{e_0}} + \frac{\sqrt{e_1}}{\sqrt{e_0}}\right) = 0 \qquad \text{(A.10)}$$

Or, $\xi - \xi_1 - \left(\sqrt{\xi} + \sqrt{\xi_1}\right) = 0 \qquad$ [where $\frac{e}{e_0} = \xi$ and $\frac{e_1}{e_0} = \xi_1$]

Or, $\sqrt{\xi_1} = -\frac{1}{2} + \left|\sqrt{\xi} - \frac{1}{2}\right|$

Or, $\sqrt{\xi_1} = -\frac{1}{2} \pm \left(\sqrt{\xi} - \frac{1}{2}\right) \qquad \text{(A.11)}$

Now, if it is (-) means $\sqrt{\xi} < \frac{1}{2}$,

$$\sqrt{\xi_1} = -\frac{1}{2} + \frac{1}{2} - \sqrt{\xi} = -\sqrt{\xi}$$

Or, $\sqrt{e_1} = -\sqrt{e}$ it is not possible.

Now, if it is (+) means $\sqrt{\xi} > \frac{1}{2}$,

$$\sqrt{\xi_1} = -\frac{1}{2} + \sqrt{\xi} - \frac{1}{2} = \sqrt{\xi} - 1$$

Or, $\sqrt{\frac{e_1}{e_0}} = \sqrt{\frac{e}{e_0}} - 1$

Or, $p_{\min} = \left(\sqrt{j} - \sqrt{M}\right)^2 \qquad$ [where $e = j\frac{e_0}{M}$ and $e_1 = p\frac{e_0}{M}$] $\qquad \text{(A.12)}$

This is the value of p_{min} for Stokes scattering.

For Stokes scattering, $e_1 \le e$. This is similar to step function $\Theta(e - e_1)$.

Appendix B: Calculations of integration limits for the anti-Stokes scattering part within the phonon scattering

For anti-Stokes part delta function is given below (see equation (1), chapter 3)

$$\delta\left(e_{\vec{k}} - e_{\vec{p}} + \hbar\omega_{\vec{p}-\vec{k}}\right)$$

$$= \delta\left(e_{\vec{k}} - e_{\vec{p}} + \hbar v_s \left|\vec{p} - \vec{k}\right|\right)$$

$$= \delta\left(e_{\vec{k}} - e_{\vec{p}} + \hbar v_s \sqrt{\vec{p}^2 + \vec{k}^2 - 2\vec{k}\vec{p}\cos\theta}\right)$$

$$= \delta\left(e - e_1 + \hbar v_s \sqrt{\frac{2M_x e}{\hbar^2} + \frac{2M_x e_1}{\hbar^2} - 2\sqrt{\frac{2M_x e}{\hbar^2}}\sqrt{\frac{2M_x e_1}{\hbar^2}}\cos\theta}\right)$$

$$= \delta\left(e - e_1 + \hbar v_s \sqrt{\frac{2M_x}{\hbar^2}}\sqrt{e + e_1 - 2\sqrt{e}\sqrt{e_1}\cos\theta}\right)$$

$$= \delta\left(e - e_1 + v_s \sqrt{2M_x}\sqrt{e + e_1 - 2\sqrt{e}\sqrt{e_1}\cos\theta}\right)$$

$$= \delta\left(e - e_1 + \sqrt{e_0}\sqrt{e + e_1 - 2\sqrt{e}\sqrt{e_1}\cos\theta}\right) \qquad \text{(B.1)}$$

Now we have to find out the values of e_1 in terms of e, when delta function will be zero for $\cos\theta$ =1 and for $\cos\theta$ = -1.

When $\cos\theta$ =1

Putting delta function equal to zero, we get

$$e - e_1 + \sqrt{e_0}\sqrt{e + e_1 - 2\sqrt{e}\sqrt{e_1}} = 0 \qquad \text{(B.2)}$$

Or, $e - e_1 + \sqrt{e_0}\left|\sqrt{e} - \sqrt{e_1}\right| = 0$ (B.3)

But in anti-Stokes, $e_1 > e$ so, it should be

$$e - e_1 + \sqrt{e_0}\left(\sqrt{e_1} - \sqrt{e}\right) = 0 \qquad \text{(B.4)}$$

This is similar to step function $\Theta\left(q_{as} + \sqrt{e} - \sqrt{e_1}\right)$ for anti-Stokes part.

Now dividing it by e_0, we get

$$\frac{e}{e_0}-\frac{e_1}{e_0}+\left(\frac{\sqrt{e_1}}{\sqrt{e_0}}-\frac{\sqrt{e}}{\sqrt{e_0}}\right)=0 \tag{B.5}$$

Or, $\xi-\xi_1+\left(\sqrt{\xi_1}-\sqrt{\xi}\right)=0$ [where $\frac{e}{e_0}=\xi$ and $\frac{e_1}{e_0}=\xi_1$]

Or, $\sqrt{\xi_1}=\frac{1}{2}+\left|\sqrt{\xi}-\frac{1}{2}\right|$

Or, $\sqrt{\xi_1}=\frac{1}{2}\pm\left(\sqrt{\xi}-\frac{1}{2}\right)$ (B.6)

Now, if it is (+) means $\sqrt{\xi}>\frac{1}{2}$,

$\sqrt{\xi_1}=\frac{1}{2}+\sqrt{\xi}-\frac{1}{2}=\sqrt{\xi}$

Or, $e_1=e$

Or, p=j (B.7)

Now, if it is (-) means $\sqrt{\xi}<\frac{1}{2}$,

$\sqrt{\xi_1}=\frac{1}{2}-\sqrt{\xi}+\frac{1}{2}=1-\sqrt{\xi}$

Or, $\xi_1=\left(1-\sqrt{\xi}\right)^2=\left(\sqrt{\xi}-1\right)^2$

Or, $\frac{e_1}{e_0}=\left(\sqrt{\frac{e}{e_0}}-1\right)^2$

Or, $p_{\min}=\left(\sqrt{j}-\sqrt{M}\right)^2$ (B.8)

So, there are two values of p_{min} for anti-Stokes part. These are $p1_{min}$=j and $p2_{\min}=\left(\sqrt{j}-\sqrt{M}\right)^2$. p_{min} is the maximum values between $p1_{min}$ and $p2_{min}$.

When $\cos\theta$ = -1

Putting delta function equal to zero, we get

$$e - e_1 + \sqrt{e_0}\sqrt{e + e_1 + 2\sqrt{e}\sqrt{e_1}} = 0 \tag{B.9}$$

Or, $e - e_1 + \sqrt{e_0}\left|\sqrt{e} + \sqrt{e_1}\right| = 0$

Or, $e - e_1 + \sqrt{e_0}\left(\sqrt{e} + \sqrt{e_1}\right) = 0$ (B.10)

This is similar to step function $\Theta\left(-q_{as} + \sqrt{e} + \sqrt{e_1}\right)$ for anti-Stokes part.

Now dividing it by e_0, we get

$$\frac{e}{e_0} - \frac{e_1}{e_0} + \left(\frac{\sqrt{e}}{\sqrt{e_0}} + \frac{\sqrt{e_1}}{\sqrt{e_0}}\right) = 0 \tag{B.11}$$

Or, $\xi - \xi_1 + \left(\sqrt{\xi} + \sqrt{\xi_1}\right) = 0$ [where $\frac{e}{e_0} = \xi$ and $\frac{e_1}{e_0} = \xi_1$]

$$\sqrt{\xi_1} = \frac{1}{2} + \left|\sqrt{\xi} + \frac{1}{2}\right|$$

Or, $\sqrt{\xi_1} = \frac{1}{2} \pm \left(\sqrt{\xi} + \frac{1}{2}\right)$ (B.12)

If (+), then

$$\sqrt{\xi_1} = \frac{1}{2} + \frac{1}{2} + \sqrt{\xi} = 1 + \sqrt{\xi}$$

Or, $\xi_1 = \left(1 + \sqrt{\xi}\right)^2$

Or, $\frac{e_1}{e_0} = \left(1 + \sqrt{\frac{e}{e_0}}\right)^2$

Or, $p_{\max} = \left(\sqrt{j} + \sqrt{M}\right)^2$ [where $e = j\frac{e_0}{M}$ and $e_1 = p\frac{e_0}{M}$] (B.13)

This is p_{max} for anti-Stokes part.

If (-), then

$$\sqrt{\xi_1} = \frac{1}{2} - \sqrt{\xi} - \frac{1}{2} = -\sqrt{\xi}$$

It is not possible.

Publications and Presentations

Publications

1. **Sunipa Som**, Frank Kieseling and Heinrich Stolz, "*Numerical Simulation of Exciton Dynamics in Cu_2O at Ultra Low Temperatures Within a Potential Trap*", Journal of Physics Condensed Matter (**In Press**).

2. Heinrich Stolz, Rico Schwartz, Frank Kieseling, **Sunipa Som**, Maria Kaupsch, Siegfried Sobkowiak, Dirk Semkat, Nobuko Naka, Thomas Koch, and Holger Fehske, "*Bose-Einstein Condensation of Excitons in Cu_2O at Ultracold Temperatures: Experiment and Theory*", New Journal of Physics (**arxiv 1206.7029**).

3. **Sunipa Som** and Heinrich Stolz, "*Numerical Simulation of Exciton Dynamics at Ultra Low Temperatures with Phonon and Elastic Scattering*" (**Manuscript in preparation**).

Presentations

1. 11^{th} International Workshop on "*Nonlinear Optics and Excitation Kinetics in Semiconductors*", September 23-27, 2012, Stuttgart, Germany.
   Poster (to be presented): "Numerical Simulation of Exciton Dynamics in Cu_2O at Ultra Low Temperatures Within a Potential Trap".

2. International Conference on "*Correlation Effects in Radiation Fields*", September 12-16, 2011, Rostock, Germany.
   Presented poster: "Numerical Simulation of Exciton Dynamics at Ultra Low Temperatures Within a Potential Trap".

3. 75^{th} Annual Meeting of the DPG and Combined DPG Spring Meeting, March 13- 18, 2011, Dresden, Germany.
   Presented poster: "Numerical Simulation of Exciton Dynamics at Ultra Low Temperatures".

4. In-house seminar on semiconductor physics, Institute of Physics, University of Rostock, April, 30, 2010, Rostock, Germany.
   Presented talk: "Numerical Simulation of Exciton Dynamics at Ultra Low Temperatures due to Phonon Scattering".

Acknowledgements

First of all, I would like to thank my supervisor, Prof. Heinrich Stolz for guiding me during my time as a PhD student at the University of Rostock. His continuous encouragement and interest have been essential in completing this work. It was one of the greatest experiences in my life to work with Prof. Stolz and to have him as an advisor.

I would like to give thanks to the members of Prof. Stolz's group. I would like to express my gratitude to Dr. Gerd Rudlof, Dr. Frank Kieseling, Michael Petzold, and Christine Schoof for valuable help and support. Many thanks to Rico, Martin, Stephan, Thomas, Karsten and Dietrich for their valuable help and support. I wish to thank to the Institute of Physics, University of Rostock for giving me opportunity to study here.

I am grateful to my husband, Anup Som, for his constant encouragement, support and help. I also thank my wonderful son, Krishanu, a great source of joy in my life. Finally, I would like to give thanks to my parents and sister who have always supported and encouraged me throughout my life.